DAA/Langley

Hampton University
Hampton VA. 23668

IN-36

Semiannual Progress Report

P.98

Submitted to: National Aeronautics and Space Administration
Langley Research Center
Hampton, Va 23665

Institution: Hampton University
Dept. of Physics

Title of Research: Direct Solar-Pumped Iodine Laser Amplifier

NASA Grant Number: NAG-1-441

Period Covered: Sept. 1, 1986 - Feb. 28, 1987

Principal Investigator: Dr. Kwang S. Han

Research Associates: Dr. K. H. Kim
Mr. L. V. Stock

Direct Solar-Pumped Iodine Laser Amplifier

Contents

Abstract

This semiannual progress report covers the period from September 1, 1986 to February 28, 1986 under NASA grant NAG-1-441 entitled "Direct Solar-pumped Iodine Laser Amplifier". During this period the improvement on the collection system of the Tarmarack Solar-Simulator beam has been attemped. On the other hand the basic study of evaluating the solid state laser materials for the solar-pumping and also the work to construct a kinetic model algorithm for the flashlamp-pumped iodine lasers have been carried out.

It was observed that the collector cone worked better than the lens assembly in order to collect the solar simulator beam and to focus it down to a strong power density. The study on the various laser materials and their lasing characteristics shows that the neodymium and chromium-co-doped gadolinium scandium gallium garnet (Nd:Cr:GSGG) may be a strong candiate for the high-power solar-pumped solid state laser crystal. On the other hand the improved kinetic modeling for the flashlamp-pumped iodine laser provides a good agreement between the theoretical model and the experimental data on the laser power output, and predicts the output parameters of a solar-pumped iodine laser.

I. Fesibility Study of the Solar-Pumped Dye Laser

A. Introduction

The parametric study of a dye laser amplifier pumped by a solar-simulator and a flashlamp, and the amplifier gain measurement at various pump-beam irradiances on a dye cell were reported in the previous semiannual report [Ref. 1]. From the previous work it has been shown that a solar concentration of 20,000 is required to reach the threshold of the rhodamine 6G dye laser. About maximum 5,000 solar constants was previously achieved at the focus of a cone-shaped collector of the front diameter of 9.6 cm with the Tarmarack solar simulator. Thus, a different approach to focus the solar-simulator beam has been carried out in this research period.

An assembly of a couple of lenses was used instead of the conical collector to place the focus of the solar simulator, which is located in the shutter position, into the work region where the laser or laser amplifier can be assembled [refer to Fig. 1]. Because of the reflection of the solar simulator beam on the lens surfaces, the solar simulator beam concentration, which was less than 1,000 solar constants, was not improved as compared to that obtained with the conical collector. Therefore, it was concluded that a solar simulator, which provides a higher power than the present Tarmarack solar-simulator does, or a larger solar furnace is necessary to provide an optical power density of at least 20,000 solar constants (=2,706 W/cm^2) in order to attempt to make a solar-pumped dye laser.

B. Experiment and Results

Figure 1 shows the assembly of the several lenses to focus the solar simulator beam down to a small spot. The solar simulator beam at the focus of the lens assembly was reflected by the diffuse surface, which was made of a Taflon bar. The reflected beam was focused down by a f=12.5 cm lens onto the mochromator whose dial was set at 530 nm with a grating of 1180 grooves/mm and with a less than 5Å linewidth. Then, the spectral intensity was detected by a photomultiplier tube. A silicon photodiode was used to pick up a reference signal and to trigger the oscilloscope.

After the spectral irradiance of the solar simulator beam was measured,

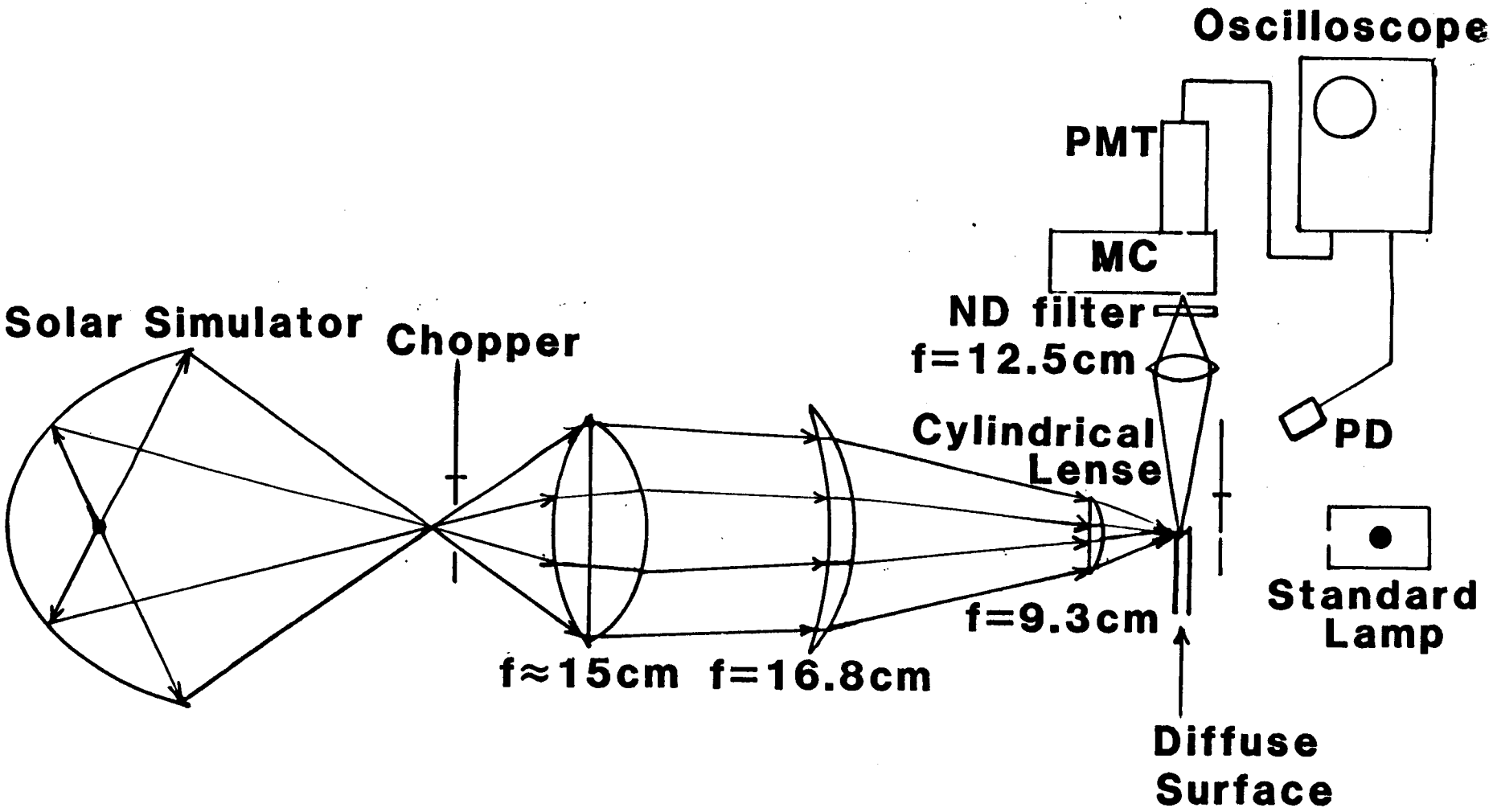

Figure 1 Experimental setup to focus down the solar-simulator bam to a small cylindrical spot with the use of lenses. MC: monochrometer, PMT: photodiode.

the diffuse surface was turned by 180^0 and the standard lamp signal was observed in order to calibrate the solar simulator's intensity. Figures 2 and 3 show the typically observed signals of the standard lamp and the solar-simulator beams, respectively, on a Nicolet oscilloscope. The observed spectral irradiance of the standard source was 1.45×10^{-3} solar constants (=0.268 w/cm^2 nm), and those of the solar simulator at various input currents are shown in Graph 1. The maximum intensity at the input current 600 A was about 777 solar constants.

With an experimental setup as shown in Fig. 4 the intensity of the light at the focus (F3) of the three lens assembly was observed to be about 14% of that at F1. The light intensity at the focus (F2) of the first two lens assembly without the cylinderical lens was about 68% of that at F1. This results show that the more lens we use the more optical loss will be caused.

In Fig. 5 the solar simulator beam collection was tried without the cylindrical lens. The observed intensity at the focus was about 512 solar constants which is lower than that obtained with the cylindrical lens. The focusing of the solar simulator beam became poor without the cylindrical lens.

The spatial distribution of the solar-simulator beam along the focal line of the 9.6-cm conical collector was remeasured with the experimental setup shown in Fig. 6. The absolute intensity calibration was done in a two-step process. A sun-gun (UL model:SG-63A) was placed instead of the standard lamp in Fig. 6 at a distance of 43.2 cm from the diffuser. The intensity of the sun-gun was calibrated with the standard lamp and a small number of neutral density filter. Then, this sun-gun was used to calibrate the intensity of the solar-simulator beam instead of using the standard lamp, because the standard lamp intensity was very weak to directly calibrate the solar simulator beam intensity and required a large number of ND filter. Possibly this may cause a large error. The measured absolute spectral irradiance of the sun-gun at λ= 530 nm was 1.08 solar constants, and that of the solar simulator 5,204 solar constants at the maximum focus.

In conclusion, the conical collector provides the higher concentration of the solar simulator beam than any other lens assembly does. The observed maximum concentration is still much lower than the required threshold for the dye laser, which is 20,000 solar constants. The study on the solar-pumped dye laser will be closed at this point until a large solar furnace or a high power solar-simulator is available.

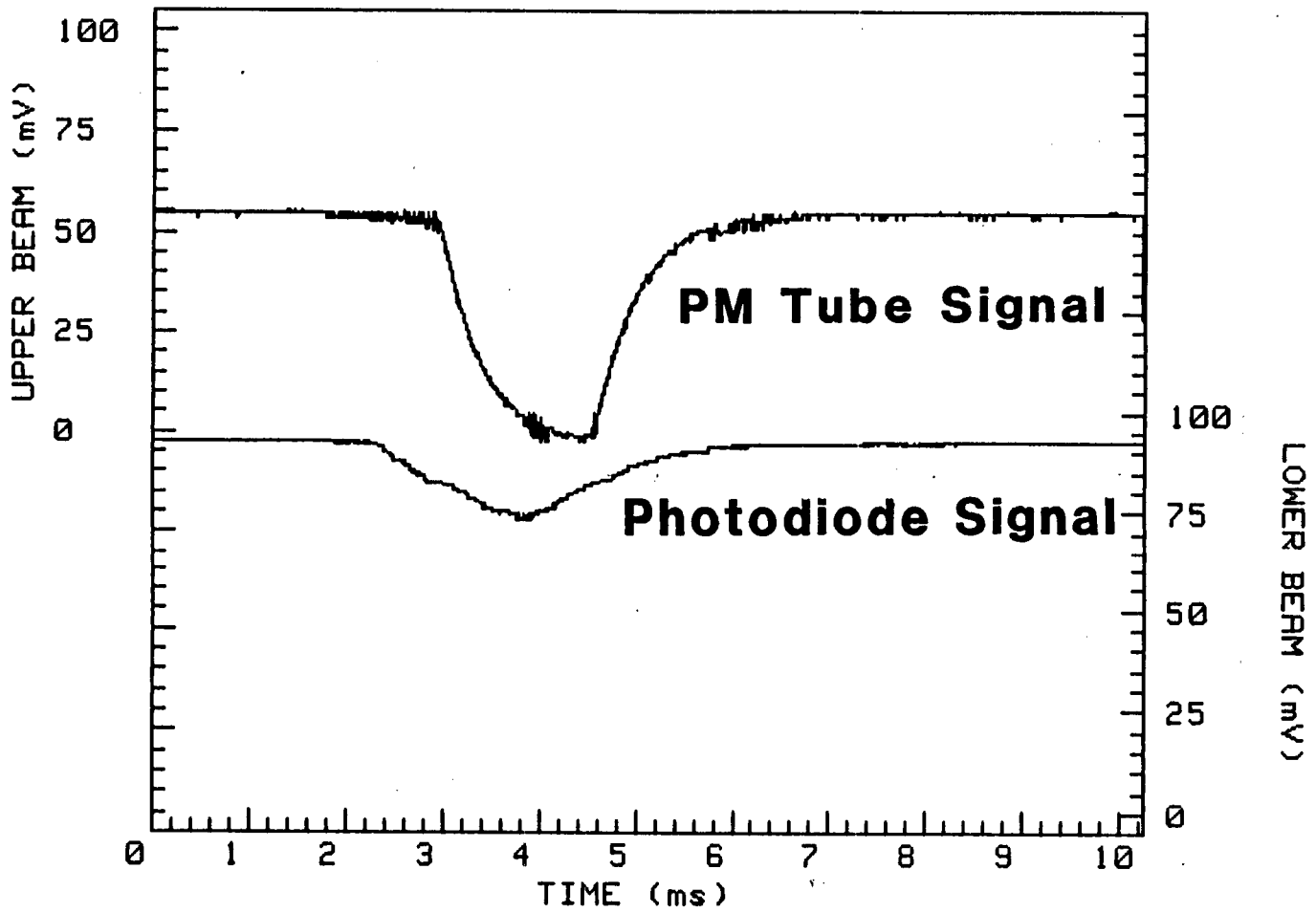

Figure 2 A typical oscillogram of the standard lamp signal observed with the experimental setup shown in Fig. 1 at the monochrometer dial setting at 530nm.

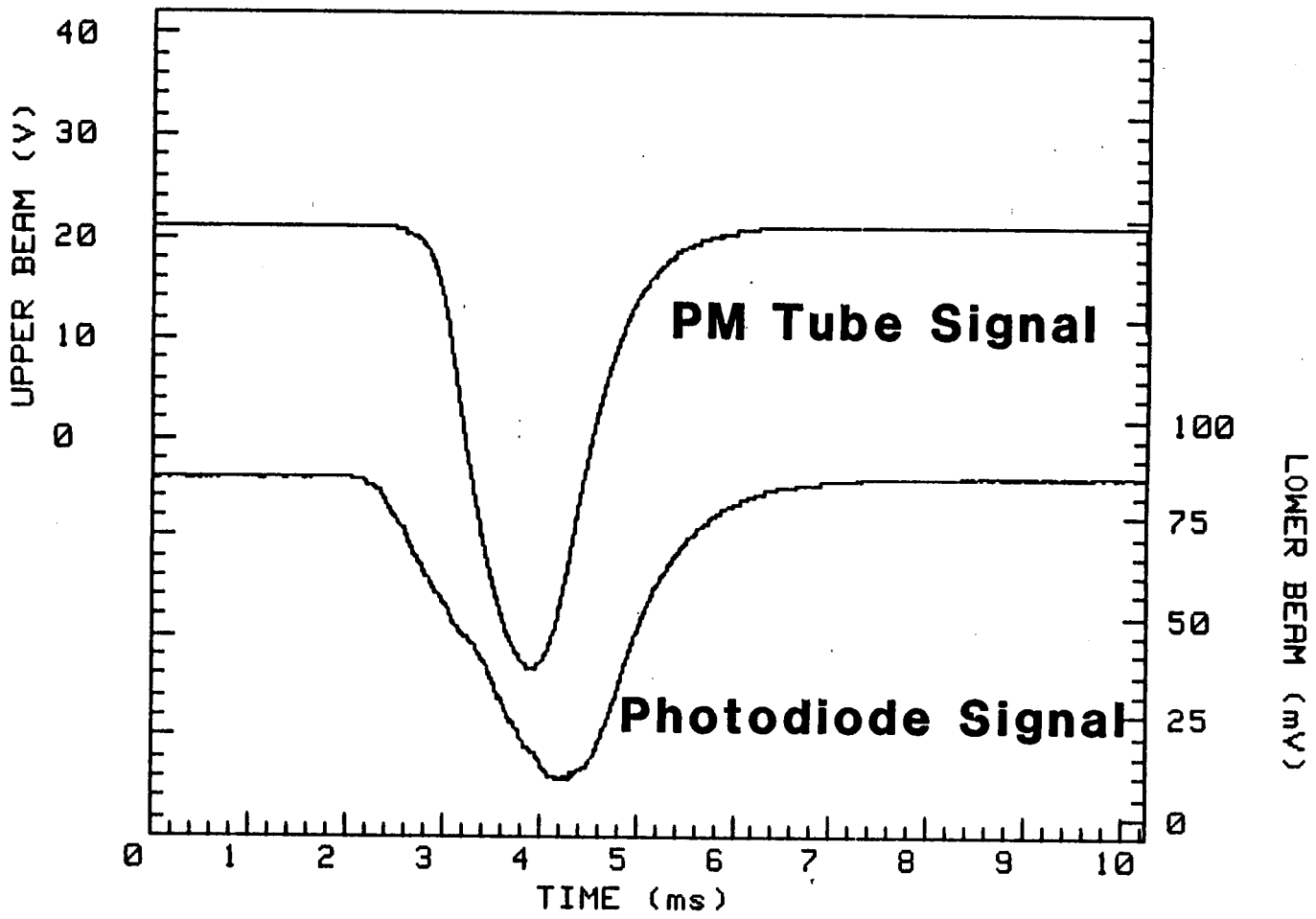

Figure 3 A typical oscillogram of the solar simulator signal observed with the experimental setup shown in Fig. 1 at the monochromater dial setting at 530nm. The ND filter used was 5.0, and the solar-simulator input current 600A.

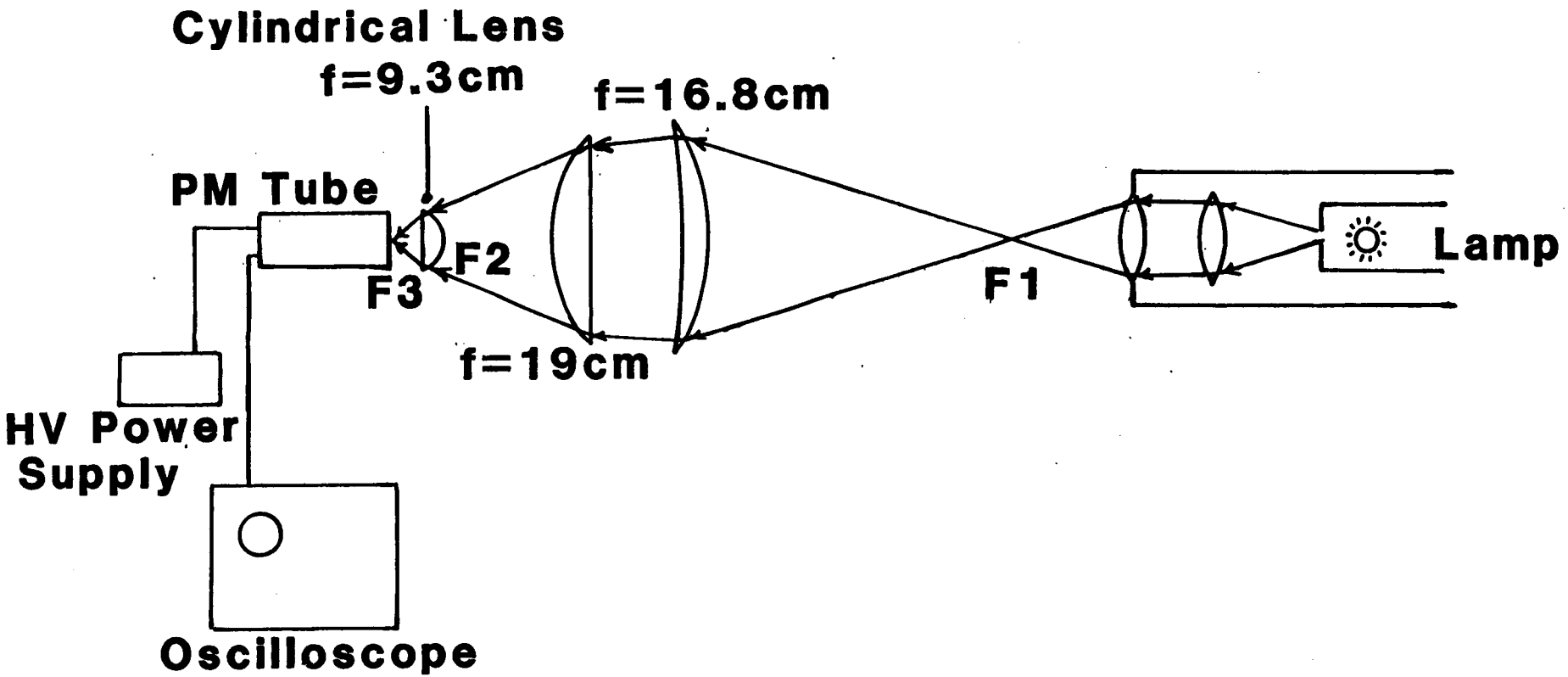

Figure 4 Experimental setup to test the light transmission through the lenses which are used to collect the solar simulator beam.

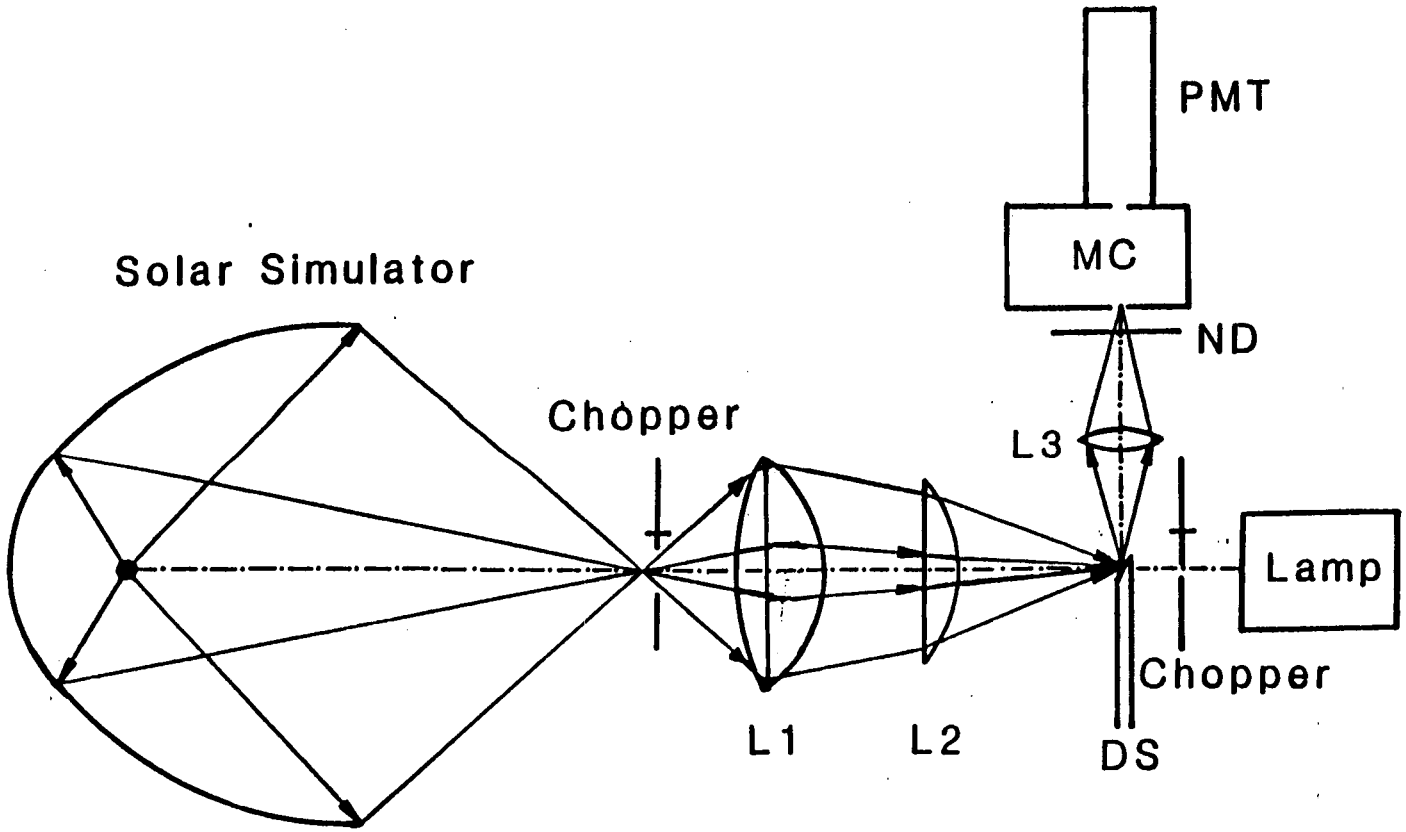

Figure 5 Two-lens assembly to collect the solar-simulator beam.

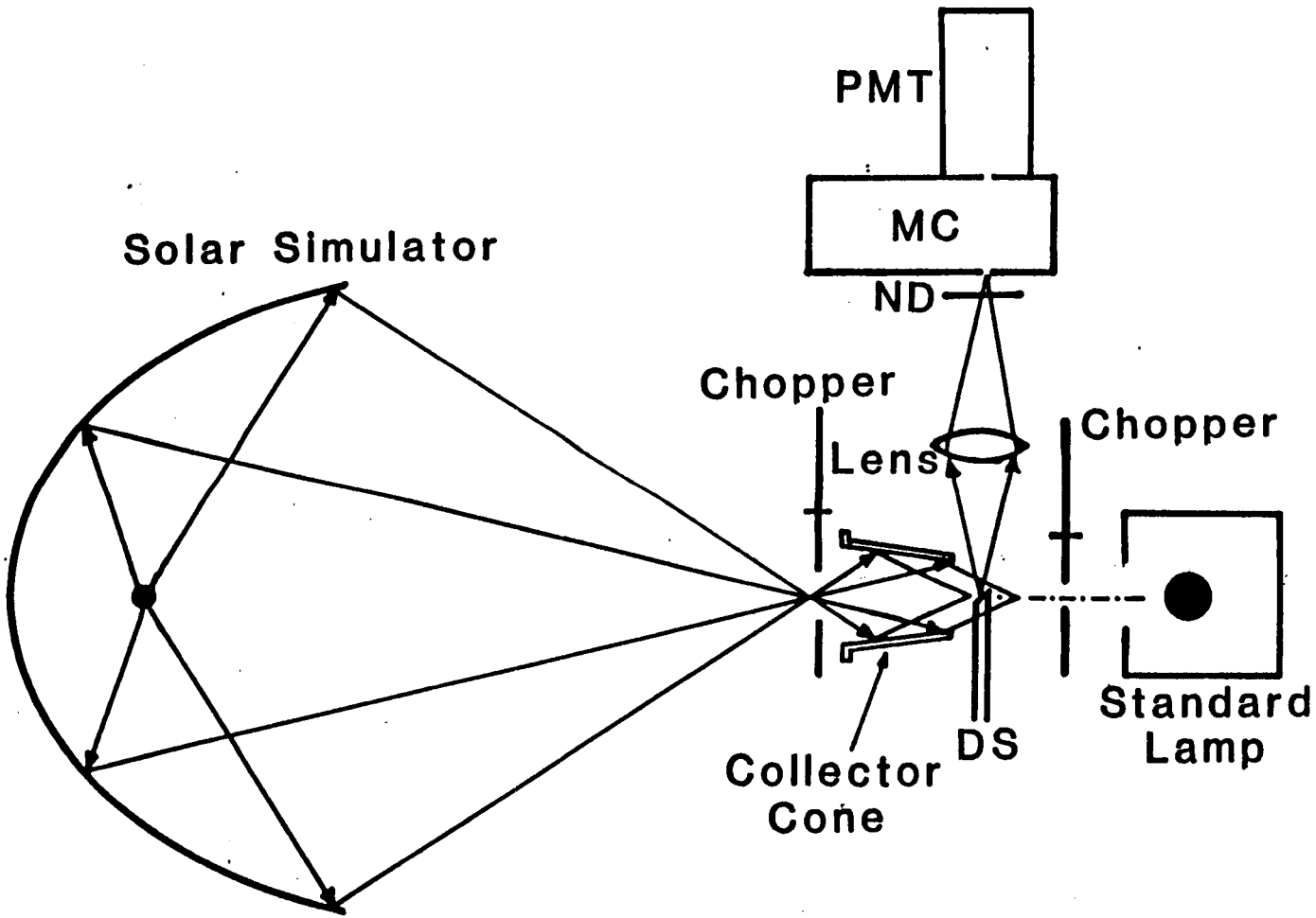

Figure 6 Experimental setup for the intensity measurement of the solar-simulator beam at the focus of a conical collector. The conical collector's size = 9.6 cm front I.D. x 5.6 cm rear I.D. x 8.9 cm width.

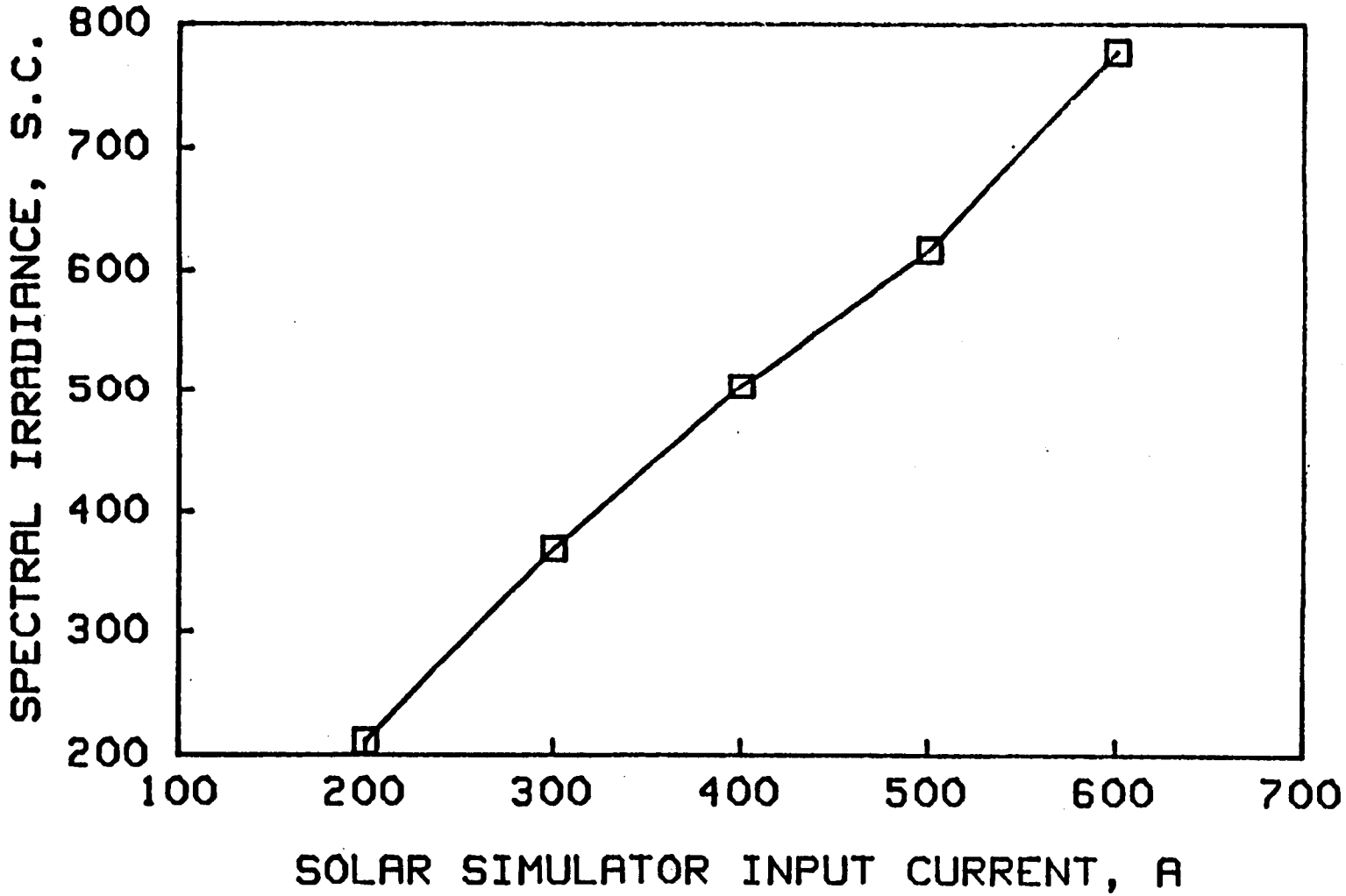

Graph 1 The specral irradiances at various solar-simulator input currents at the focus of the solar-simulator beam collecting system shown in Fig. 1.

C. References

1. K.S. Han, K.H. Kim and L.V. Stock
"Direct Solar-Pumped Iodine Laser Amplifier"
Semiannual Progress Report, NASA, NAG-1-441, Sept. 1986.

II. Evaluation of the Solid State Laser Materials for the Solar-Pumping

A. Introduction

Since the first observation of the optical maser action with the $CaF_2:Dy^{2+}$ crystal by Kiss, Lewis and Duncan [Ref.1] in 1963, several kinds of the solid state materials, such as Nd_2O_3-doped barium crown glass, Nd:YAG, Nd:Cr:YAG, Ruby and $Nd:CaWO_4$, have been used for the solar-pumped lasers. Among them, the Nd:YAG crystal has been known as an efficient laser materials, so far. Its highest laser output power observed is 100W with a solar pumping [Ref. 10]. However, the laser output power of at least an order of 1kW cw is required for the space power transmission. In order to satisfy the demand, the improvement of the solar-pumped Nd:YAG laser or the search of new laser material has to be carried out. This report shows the evaluation of the laser crystals such as Ruby, Nd:YAG, Nd:Glass, Nd:YLF, Nd:Cr:GSGG, Alexandrite and Emerald for the high power solar pumping.

Section B will describe the historical background of the solar-pumped solid state lasers. In section C, the characteristics of the various solid state materials will be summarized. The temperature distribution in the crystals and the coolant flowrate will be determined in section D. Section E will show the experimental setup and the results on the spectral and spatial distribution of the Tarmarack solar-simulator beam at the focus of a conical collector. Finally, the laser system and the expected laser output will be discussed in section F.

B. Historical Background of the Solar-Pumped Solid State Lasers.

1963: Z.J. Kiss, H.R. Lewis, and R.C. Duncan in RCA Laboratories. [Ref.1]
- Observed the first solar-pumped optical maser action with the $CaF_2:Dy^{2+}$ crystal at the liquid neon temperature of $27^{o}K$ and at the wavelength of 2.3um.

1964: G.R. Simpson in American Optical Company [Ref.2]
- Observed the laser action at the wavelength of 1.06μm and the temperature of $30^{o}C$ with a 6.25 wt% Nd_5O_3-doped barium crown glass of 0.1 mm diameter and 30 mm long.

- pumping source = sun and carbon arc sun-simulator.
- Flashlamp threshold = 1 Joule
- Observed the laser oscillation at the input energies of 1.15J(= 144 w/cm^2 = 1,062 solar constants) with sun-pumping and of 1.50J (= 188 w/cm^2 = 1,386 solar constants) with the carbon arc sun-simulator pumping.

1966: C.W. Reno in RCA Defense Electronics Products [Ref. 3]
- Measured the threshold input power of 100 W (= 35 w/cm^2 = 259 solar constants) for a solar-pumped Nd:YAG laser, and observed the laser output of 100 mW with a 25-W coupled power to the crystal.
- Observed the same results for the Nd:Cr:YAG laser as those for the Nd:YAG laser. The Cr-ions did not improve the laser action because of the slow Cr - Nd transfer time (=1 ms) compared to the fluorescence lifetime of the neodymium ions.

1966: C.G. Young in American Optical Company [Ref. 4]
- Observed that the threshold powers for the Ruby and Nd:$CaWO_4$ cyrstals are larger than those for the Nd:YAG and Nd:Glass.
- Observed a 1-W cw laser output from a Nd:YAG crystal of 3-mm diameter and 30-mm long and of 1 at % doping density with a solar-pumping.
- Observed a 1.25-W pulse laser output from a sun-pumped Nd:Glass with a pulse width of 7 ms.

1972: L. Huff in GTE Sylvania Inc. [Ref. 5]
- Observed a 4.85 W multimode laser output from a Nd:YAG crystal with a 24-inch diameter solar collector.
- Used a conductive cooling of the laser rod with a copper heat sink.
- Observed a TEM_{oo} output of 0.8-W.

1976: J. Falk, L. Huff and J.D. Taynai in GTE Sylvania Inc. [Ref. 6]
- Observed the mode-locked and internally frequency-doubled laser output from a Nd:YAG crystal

λ	Multimode	TEM_{oo} CW	TEM_{oo} mode locked
1.06 μm	5.6 W	2.05 W	0.4 W
0.53 μm	--	0.5 W	0.16 W

- Used an end pumping on the crystal with a 24-inch diameter solar collector and with the use of a UV cut-off-filter.

1978: D. Radick, E. Reed, and C. Chadwick in GTE Sylvania [Ref. 7]

- Developed a pulsed Nd:YAG laser for the space communication purpose with a 24-inch diameter collector.
- Observed a TEM_{oo} mode laser output of 400 mW.

1981: V.M. Batenin, A.L. Golger, and I.I. Klimovski in USSR [Ref. 8].

- Theoretical study on the feasiblity of a solar-pumped color-center crystal laser.
- The expected values for a waveguide-type crystal with a solar-pumping of $\approx 10^2$ solar constants:
  Gain $\simeq 10^{-3}$ cm^{-1}
  efficiency $\simeq$ 1-6%
  output power $\simeq$ 10-60 W from an 1-m active medium.

1984: H. Arashi, Y. Oka, and N. Sasahara in Japan [Ref. 9].

- Observed an 18-W cw laser output from a Nd:YAG crystal of 4-mm diameter and 75-mm long and of 0.9 at % doping density with a 10-m aperture solar collector.
- Effective pump power = 1.1 kW(= 117 w/cm^2 = 863 solar constants).
- Conversion efficiency (pump power → laser power) = 1.64%.

1986: M. Weksler, J. Shartz, and Weizmann in Israel [Ref. 10].

- Observed a 100-W laser output from a Nd:YAG crystal with a solar furnace.

1986: L. Zapata at NASA Langley Research Center [Ref. 11]

- Observed a 28-W laser output from a Nd:Glass fiber bundle with a solar-simulator pumping.

C. Laser Crystals for the High-Power Solar Pumping.

(1). Ideal Laser Crystals.

The characteristics which an ideal laser crystal for the high-power solar pumping should have are listed as below:

(a) Efficient pumping (or absorption) bands near the peak of the solar spectrum.

(b) Long fluorescent lifetime to lower the threshold input power for a cw operation and to provide a high energy storage.

(c) High operation temperature at least higher than the room temperature to facilitate the rejection of heat.

(d) Good thermal conductivity and high thermal resistance for a cw operation.

(e) Mechanically strong.

(2). Characteristics of various laser crystals.

Table 1 shows the list of the characteristics of the various crystals obtained from Refs. 12-35. The advantage and disadvantage of each crystal are discussed as follows:

Ruby

(i) Disadvantages

- 3-level laser system
  : requires a high threshold input power
  : gives a poor quantum efficiency
- Small gain coefficient

(ii) Advantages

- Broad absorption bands
- Visible laser output
- High thermal conductivity
- Long fluorescence lifetime
- The lowest doping concentration is possible.

Table 1. CHARACTERISTICS OF LASER CRYSTALS

	Ruby	Nd:YAG	Nd:Glass*	Cr:Nd:GSGG	Nd:YLF	Alexandrite	Emerald
λ laser (nm)	694.5	1064.1	1062.3	1061.2	1053 (σ) 1047 (π)	700-800	720-842
Doping	.05 wt % Cr_2O_3	.725 wt%	3.1 wt %	Cr:1.18 at %	1.0 at %	0.1 at % Cr	
Density	1.58×10^{19} $\frac{Cr^{3+}}{cm^3}$	1.38×10^{20} $\frac{Nd^{3+}}{cm^3}$ 1.0 at %	2.83×10^{20} $\frac{Nd^{3+}}{cm^3}$	Nd:1.56 at % 1.8×10^{20} $\frac{Nd^{3+}}{cm^3}$	1.3×10^{20} $\frac{Nd^{3+}}{cm^3}$	3.51×10^{19} $\frac{Cr^{3+}}{cm^3}$	
Fluorescense Lifetime (μs)	3000	240	300	256**	480	260	22
Fluorescence Linewidth	.55 nm 330 GH_z	.40 nm 120 GH_z	26.0 nm 7500 GH_z		1.38 nm 375 GH_z	100 nm	
Refractive Index at λ = 1.06 μm	1.7262 (E⊥C) 1.755 (E//c)	1.815	1.555	1.95	1.46	1.737 (E//a) 1.742 (E//b) 1.735 (E//c)	1.57
Thermal Conductivity (w/cm K)	.42	.14	.0135	.08	.06	.23	.055 (//c) .044 (⊥C)
Stimulated Emission Cross Section (cm^2)	2.5×10^{-20}	$2.7\text{-}8.8\times10^{-19}$	3.03×10^{-20}	4.2×10^{-19}	1.2×10^{-19} (σ) 1.8×10^{-19} (π)	$1\text{-}5\times10^{-20}$	3.3×10^{-20}
Thermal Expansion Coeff. ($x10^{-6}/^oC$)	5.8	7.5	7.5	7.8	13 (A axis) 8 (C axis)	5.9 (//a) 6.1 (//b) 6.7 (//c)	1.35 (//C) 1.00 (⊥C)
Heat Capacity (J/gK)	--	.59	.88	.40	.79	--	--
Specific Heat (J/gK)	.18	.6		.4			
Thermal Resistance Parameter (w/m)	3400	770-7700	230	660-6600	140	2350	--

CHARACTERISTICS OF LASER CRYSTALS (concluded)

	Ruby	Nd:YAG	Nd:Glass*	Cr:Nd:GSGG	Nd:YLF	Alexandrite	Emerald
Density(g/cm^3)	--	4.56	2.547	6.46	3.99	3.69	2.66
Scatter Losses at 1.06 μm (cm^{-1})	0.001	0.002	0.005		0.033+		
Breaking Strength (Kg/mm^2)		~ 20		15-20	33500		
Inversion for 1% gain/cm(ions/cm^3)	$4x10^{17}$	$1.1x10^{16}$	$3.3x10^{17}$			$2 \sim 10x10^{17}$	
Gain Coeff. for 1J stored energy (cm^{-1})	0.087	4.73	0.160			0.038-0.19	
Slope Efficiency (%)	<0.51>	3.7		7	2.0	<1.4>	

* ED-2 Silicate Glass

** Cr → Nd transfer time = 17 μs (compared to 6.2 ms in Nd:Cr:YAG)

\+ This value is for 1.1% Nd concentration

In the same paper $\alpha_{sc} = 0.030\ cm^{-1}$ for 0.9% Nd:YAG

Nd:YAG (Neodymium-doped Yittrium Aluminum Garnet)

(i) Advantages

- 4-level laser system
- Good thermal conductivity
- Good Quantum efficiency
- High gain coefficient
- Low threshold input power required
- Commercially well developed (600 Watts laser output)
- Relatively good slope efficiency
- 100 Watts cw laser operation with the solar-pumping has been achieved already

Nd:Glass

(i) Advantages

- 4-level laser system
- Cheap! easy to fabricate to a high doping density
- Relatively low threshold input power required
- Large absorption of the solar beam at high doping densities

(ii) Disadvantages

- Poor thermal conductivity
  : but still good for a short pulse laser operation at a low repetition rate
- Broad fluorescence line width
  : increases the laser threshold
  : permits a good energy storagy and shorter light pulses

Nd:YLF (Neodymium-doped Yittrium Lithium Fluoride)

(i) Advantages

- 4-level laser system
- Long fluorescence lifetime (Twice of Nd:YAG)
  : requires a low threshold input power
  : provides a good energy storage
- Low emission cross section
  : provides a good energy storage
- Low thermal lensing effect. (smaller than Nd:YAG)

Nd:Cr:GSGG (Neodymium-and chromium-codoped Gadolinium Scandium Gallium Garnet)

(i) Advantages

- 4-level laser system
- Broad absorption bands over the solar spectrum due to the Cr^{3+} ions
- Effective energy transfer from the Cr^{3+}-ions to the Nd^{3+}-ions
- Low threshold input power required
- High slope efficiency
- A strong candidate for the high power laser

Alexandrite

(i) Advantages .

- Tunability (700-800 nm)
- Good thermal conductivity

(ii) Disadvantages

- Broad fluorescence linewidth
  : Require a high threshold input power

Emerald

(i) Advantage

- Tunability (720-842 nm)

(ii) Disadvantage

- Short fluorescence time and broad fluorescence linewidth
  : Requires a high threshold input power

(3) Absorption of the Solar Spectrum by the Laser Crystals

The absorption spectrum of various laser crystals are shown in Fig. 1 through 5, and compared with the spectral irradiance of the air-mass-zero solar spectrum. The amount of absorption of the solar beam per unit area by laser crystals has been calculated for the input solar spectrum of 1 solar constant

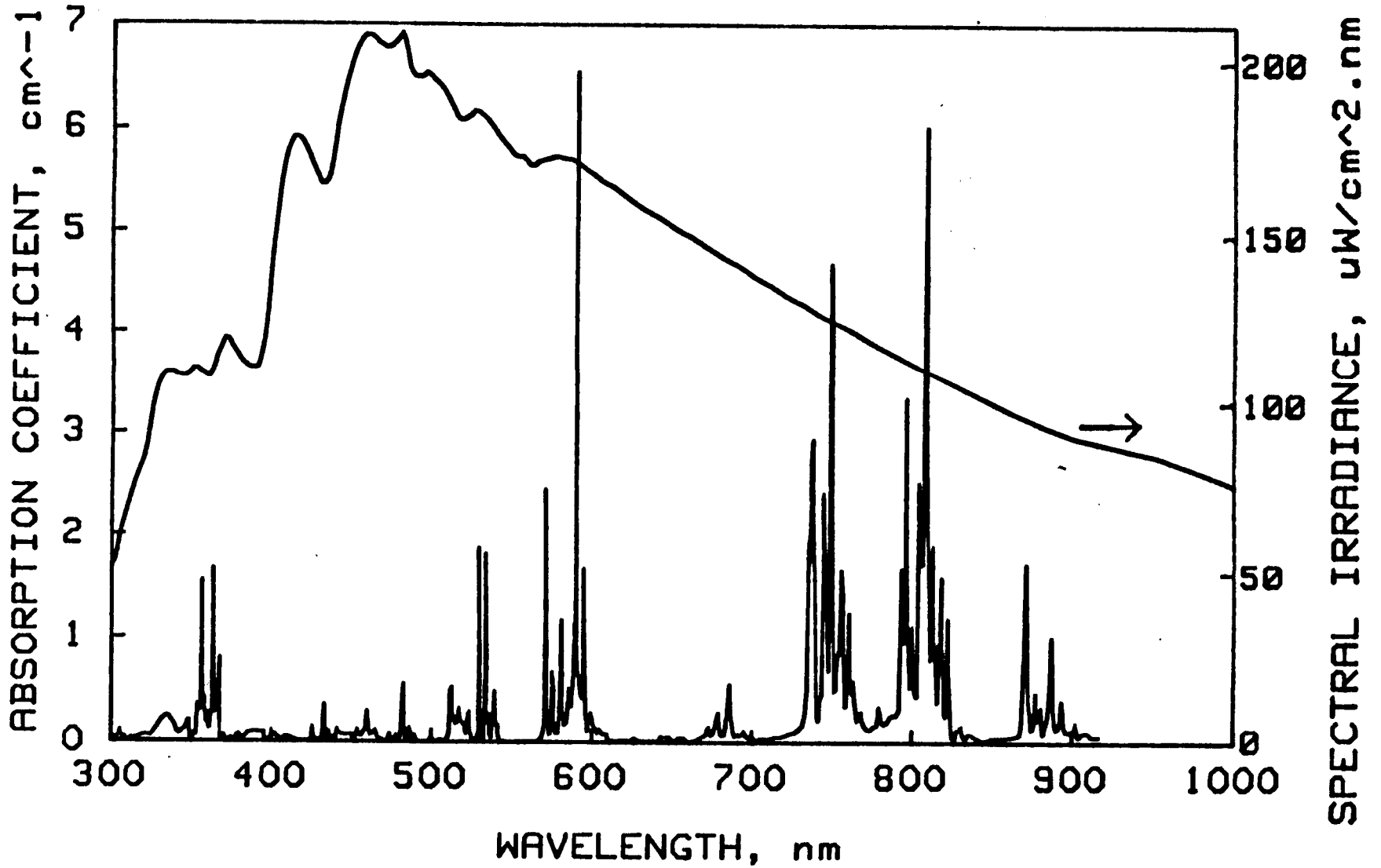

Figure 1 The absorption spectrum of the Nd:YAG crystal at a doping density of 1 at% compared to the spectral irradiance of the air-mass-zero solar spectrum.

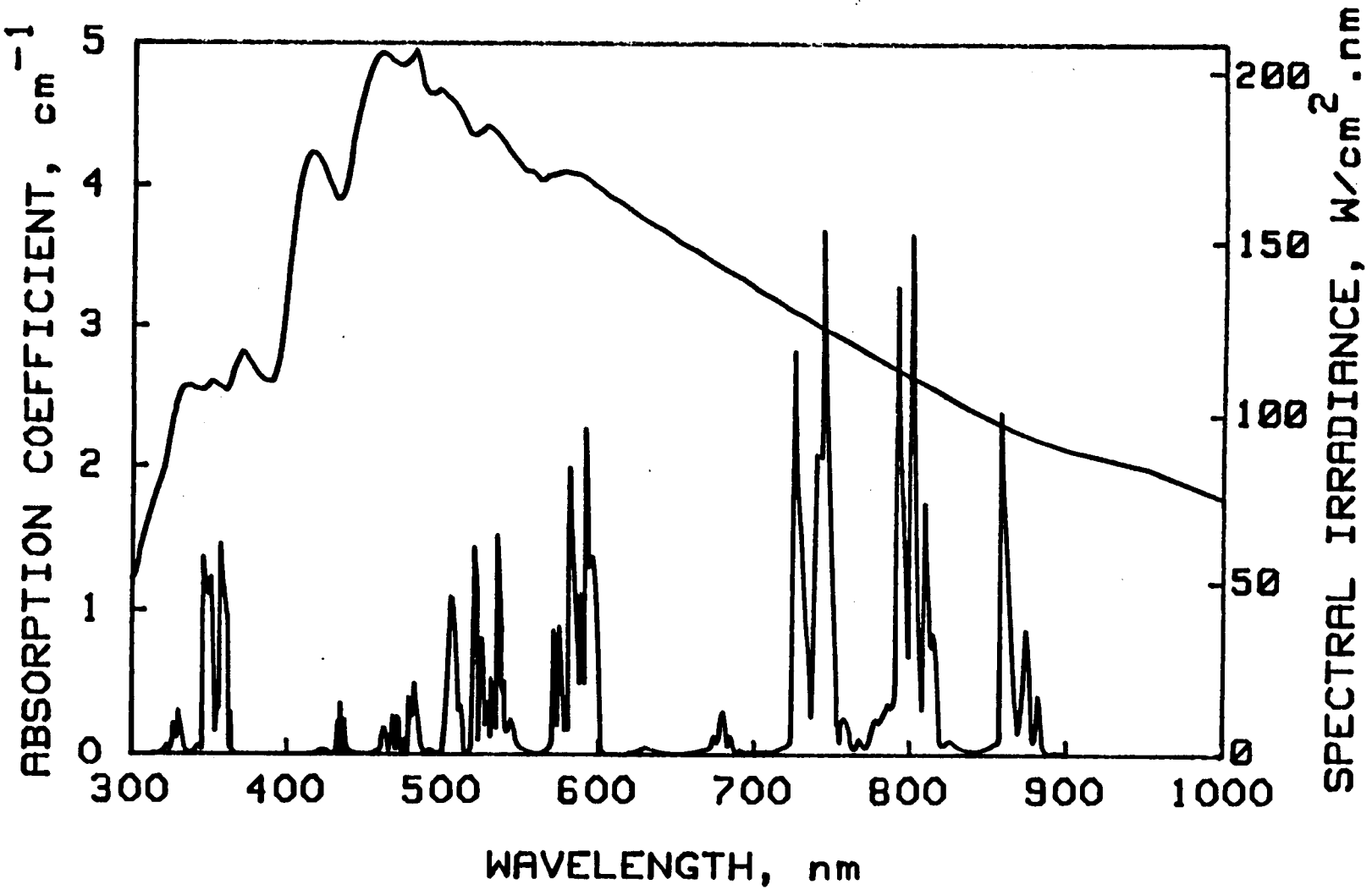

Figure 2 The absorption spectrum of the Nd:YLF (π-polarized) crystal with a doping density of 2 at% compared to the spectral irradiance of the air-mass-zero solar spectrum.

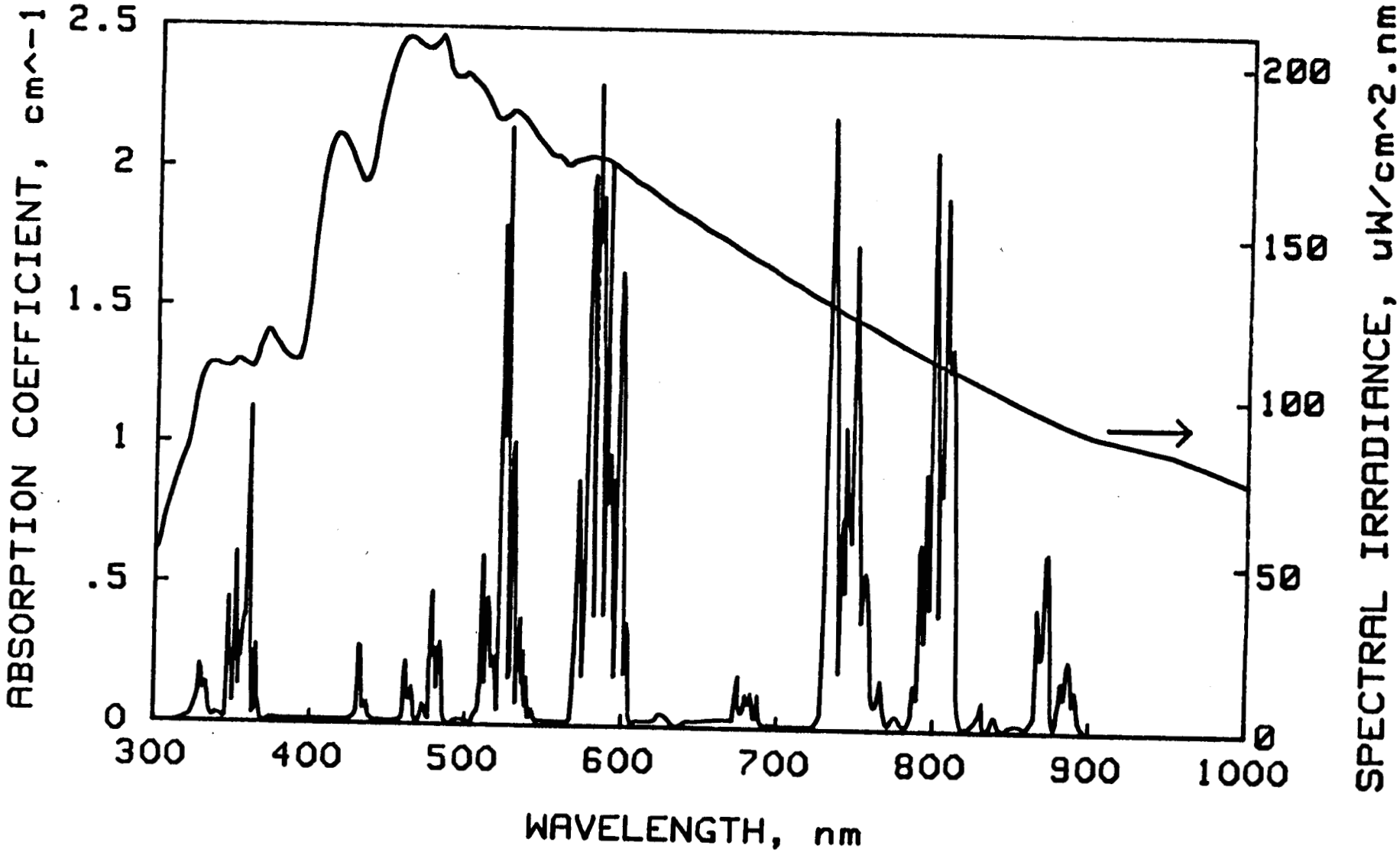

Figure 3 The absorption spectrum of the Nd:YLF (σ-polarized) crystal with a doping density of 2 atomic percent compared to the spectral irradiance of the air-mass-zero solar spectrum.

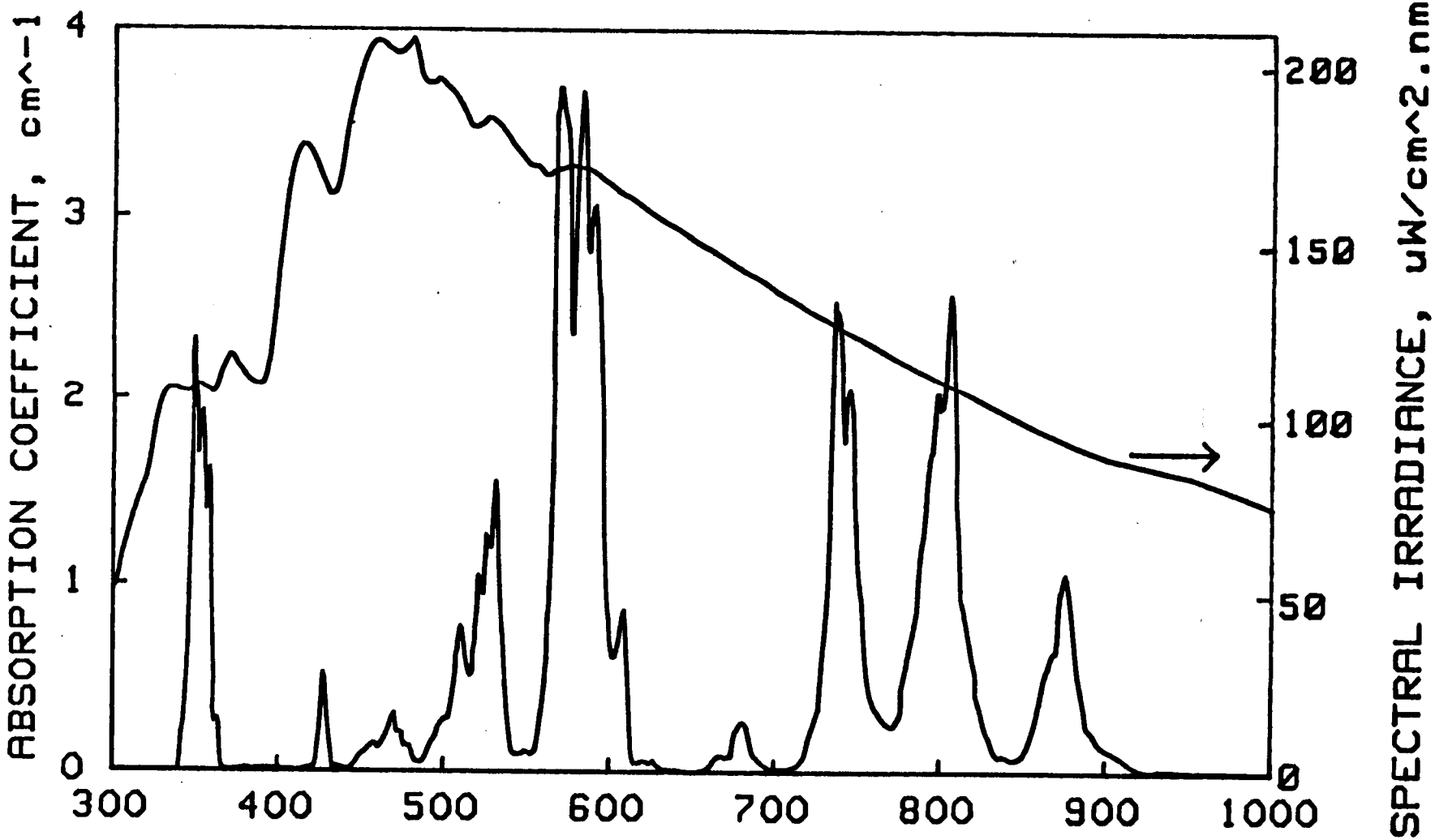

Figure 4 The absorption spectrum of a Nd:Glass compared to the air-mass-zero solar spectrum. The glass composition: SiO_2 = 66wt%, Nd_2O_3 = 5wt%, Na_2O_3 = 16wt%, BaO = 5wt%, Al_2O_3 = 2wt%, and Sb_2O_3 = 1wt%.

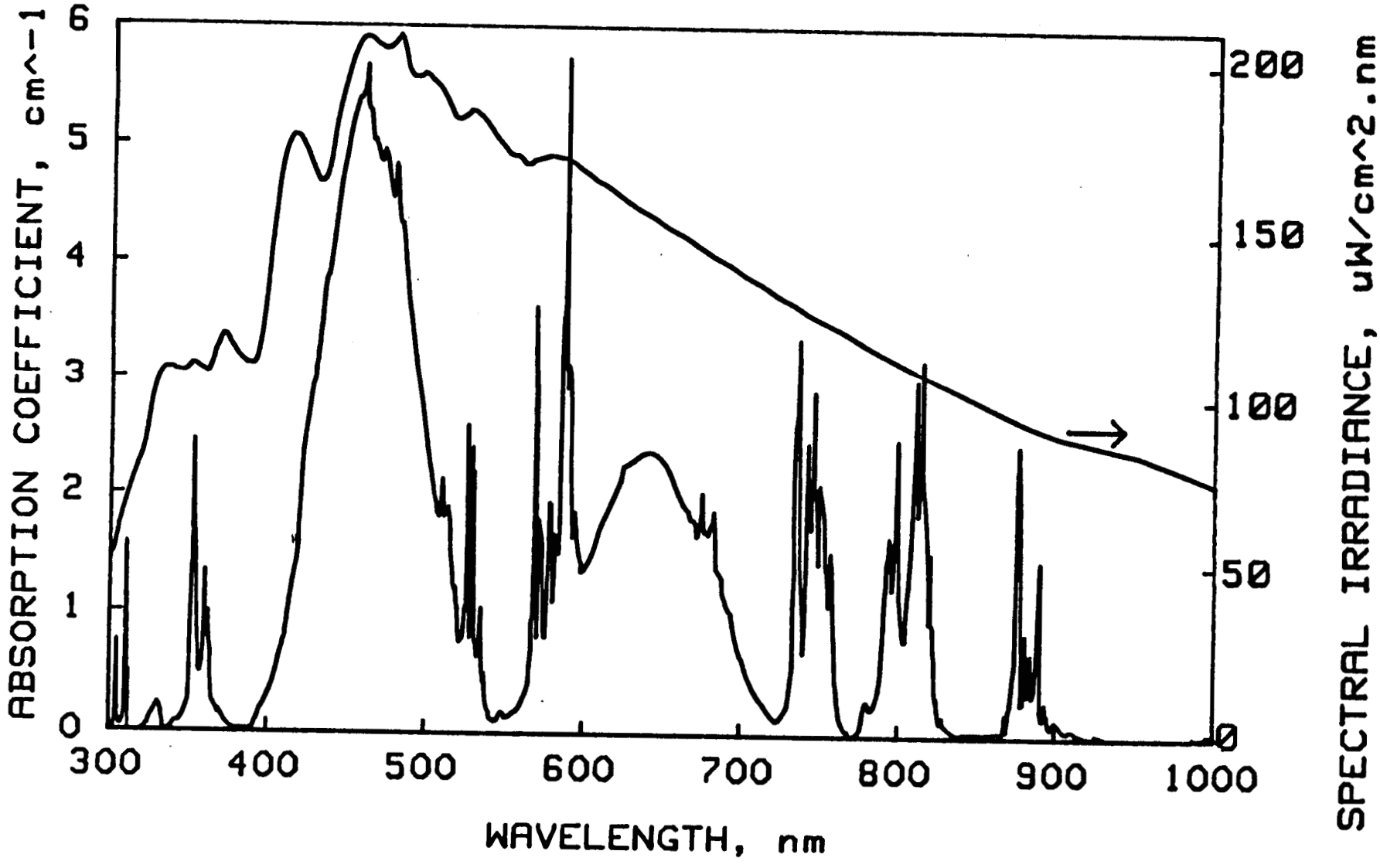

Figure 5 The absorption spectrum of the Nd:Cr:GSGG crystal at a doping density of Cr = 1 x10^{20}ions/cm^3 and Nd = 2 x 10^{20} ions/cm^3 compared to the air-mass-zero solar spectrum.

with an incident angle of 45^{o} as shown in Fig. 9. The absorbed solar beam intensity, I_{abs}, in the crystal at a given spectral range from λ_1 to λ_2 is obtained from

$$I_{abs} = \int_{\lambda_1}^{\lambda_2} I_o(\lambda)\ (1 - e^{-N\sigma(\lambda)\cdot d})d\lambda \qquad (1)$$

or

$$I_{abs} = \int_{\lambda_1}^{\lambda_2} I_o(\lambda)\ (1 - e^{-\varepsilon_{abs}(\lambda)\cdot d})\cdot d\lambda$$

where $I_o(\lambda)$: Spectral irradiance of the incident light (W/cm^2)
N : Absorbing molecules (or ions) per cm^3
$\sigma(\lambda)$: Molecular absorption cross section (cm^2)
d : Pass length of the pump beam in the crystal (cm)
$\varepsilon_{abs}(\lambda)$: Absorption cefficient (cm^{-1}) = $N\sigma(\lambda)$.

Then the ratio of the absorbed solar beam intensity to the total incident solar beam becomes

$$R = \frac{\int_{\lambda_1}^{\lambda_2} I_o(\lambda)(1 - e^{-\varepsilon_{abs}(\lambda)d})\cdot d\lambda}{\int_{o}^{\infty} I_o(\lambda)\cdot d\lambda}$$

The absorbed solar beam intensity in the central portion of the crystal rod within a 1.0-mm diameter is calculated from

$$I_{center} = \int_{\lambda_1}^{\lambda_2} I_o(\lambda)\ e^{-N\sigma(\lambda)(d/2 - 0.5mm)}(1 - e^{-N\sigma(\lambda)\cdot 1mm})d\lambda.$$

The sample data and calculated results are listed in appendix A, and Graph 1 shows the results on the absorbed solar beam intensity by the various crystals at the various doping densities according to Eq. (1). The amount of the solar beam absorption is the largest in the Nd:Cr:GSGG crystal. The absorption is larger in the Nd:YAG crystal than in the Nd:Glass at the same doping density. However, a Nd:glass of a high doping density can be easily fabricated compared to any other crystals, and the solar beam absorption can be increased with a high doping density. Nevertheless, the doping density can not be increased too high because of the collisional quenching effect which reduces the fluorescence lifetime at high doping densities.

Graph 2 shows the absorbed solar beam intensity at the rod center of the Nd:YAG within a 1.0-mm diameter for various doping densities and for various

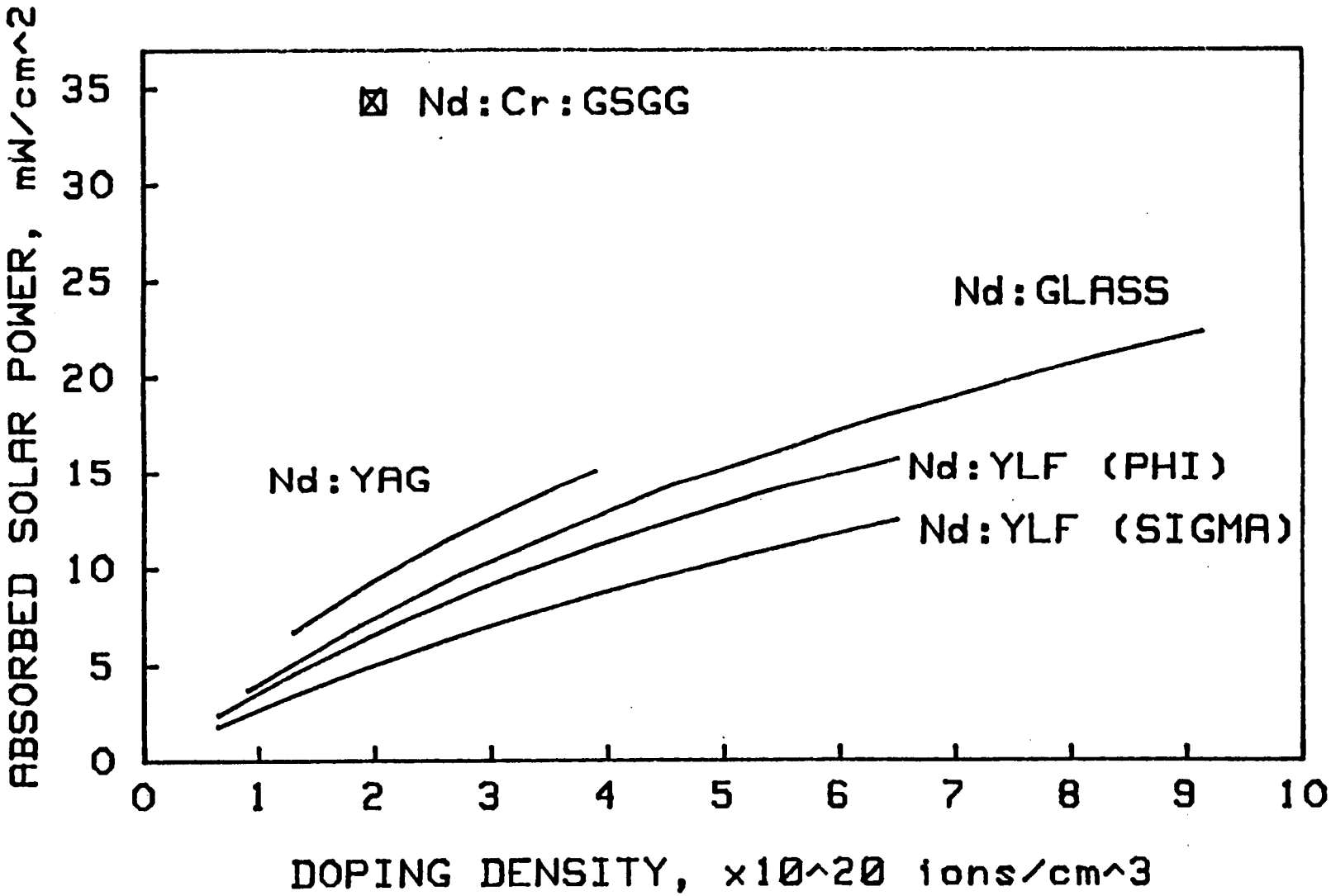

Graph 1 The absorbed solar beam by various laser crystals in an absorption thickness of 4.2 mm as a function of the Nd-ion doping density for the input pump-power of 1 solar constant (= 135.3 mW/cm^2).

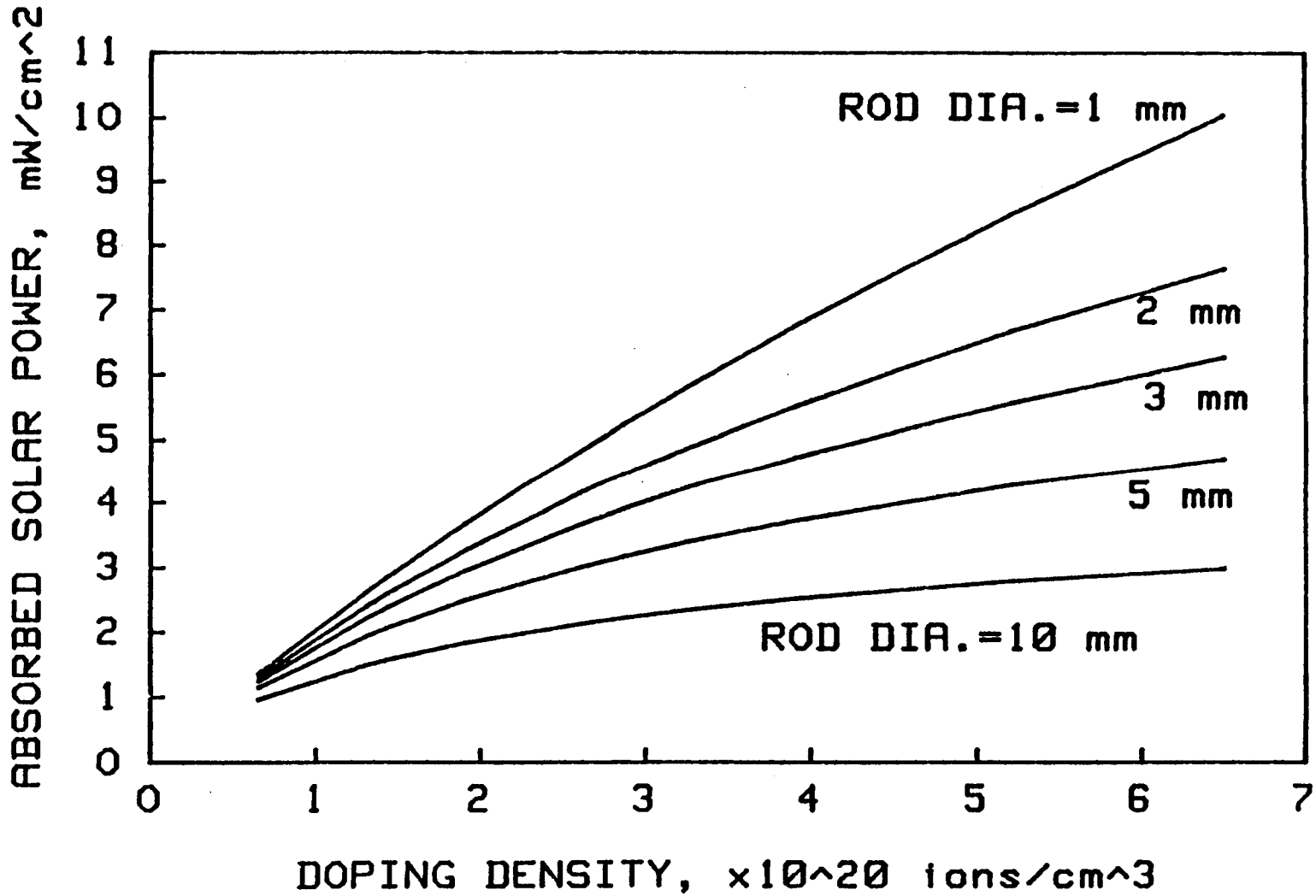

Graph 2 The absorbed solar beam intensity within the 1-mm diameter center of the various sizes of the Nd:YAG crystal as a function of the Nd-ion doping denisty.

rod diameters. The amount of the solar beam absorption at the rod center decreases as the rod diameter increases. Thus, the rod size is limited by the threshold pump power requirement at the rod center.

(4) Threshold Input Power and Slope Efficiency

Table 2, which is cited from Ref. 31, shows the population inversion densities at the threshold and the threshold input-power densities of various laser crystals. The Nd:YAG has the lowest values among Ruby, Nd:Glass, Alexandrite and Emerald. However, it has been recently observed [Ref. 36] that the threshold of the Nd:Cr:GSGG is about one half of that of the Nd:YAG for a flashlamp pumping, and its slope efficiency is twice of the Nd:YAG's [Ref. 30].

In Ref. 17, the threshold of the Nd:YLF was observed to be 510W and that of the Nd:YAG to be 600W with a tungustan lamp pumping. These values correspond to 251 solar constants (=340W/cm^2) and 295 solar constants (=40W/cm^2), respectively. This means that the Nd:YLF laser crystal can be easily pumped with a low power solar simulator beam.

D. Crystal Temperature and Coolant Flowrate

For a cylindrical laser rod and cooling system as shown in figure 6, the radial temperature distribution can be determined by solving an one-dimensional heat conduction equation [Ref. 37]:

$$T(r) = T(r_o) + (A_o/4K)(r_o^2 - r^2)$$

where $A_o = P_a / r^2 L$: rate of heat generated per unit volume in the crystal rod.

$P_a = I_{abs}$ (solar constant) (rod surface area) (1- rod surface reflectance): rate of heat dissipated by the rod.

k: Thermal conductivity of rod.

In steady state,

P_a = (Heat removed from the crystal surface by the coolant).

Thus,

$$P_a = h\, D_1 L (T_R - T_F)$$

where h : Surface heat transfer coefficient,

D_1 : Rod diameter.

$T_R = T(r_o)$: Rod surface temperature.

T_F : Mean fluid temperature.

Table 2. Population inversion densities and thresholds of various laser crystals.

Lasing Material	$N_{th}^{(4)} = \frac{8\pi\tau_0\eta^3\Delta\nu}{c\tau_c\lambda^2}$ $N_{th}^{(3)} = N_0/2$	$P_c = \frac{N_{th}h\nu}{\tau_0}$ [W/cm^3]	$E_{min} = \frac{N_{th}h\nu}{\eta}$ [J/cm^3]
Ruby 3-level λ = 694.3 nm $\Delta\nu$ = 11 cm^{-1} τ_0 = 3.10^{-3} sec	10^{19}	960	4600
Nd^{3+}:glass 4-level λ = 1.06 $\Delta\nu$ = 200 cm^{-1} τ_0 = 3.10^{-4} sec	9.10^{15}	5.6	2.7
Nd^{3+}:YAG 4-level λ = 1.064 $\Delta\nu$ = 6 cm^{-1} τ_0 = 5.5.10^{-4} sec	2.10^{15}	0.7	0.6
Alexandrite 4-level λA_{ve} = 720 nm $\Delta\nu$ = 1000 cm^{-1} τ_0 = 3.2.10^{-4} sec	1.6×10^{17}	140	70
Emerald 4-level λA_{ve} = 740 nm $\Delta\nu$ = 1500 cm^{-1} τ_0 = 6.5.10^{-5} sec	4.1×10^{16}	170	17

$N_{th}^{(4)}$ = population inversion density at threshold in the metastable state for a 4-level system.
$N_{th}^{(3)}$ = population inversion density at threshold for a 3-level system.
τ_0 = decay time associated with radiative laser transition.
η = refractive index.
$\Delta\nu$ = the width of the gain linewidth at room temperature.
τ_c = cavity lifetime — the time at which the energy is lost in the laser cavity.
c = speed of light.
λ = lasing wavelength.

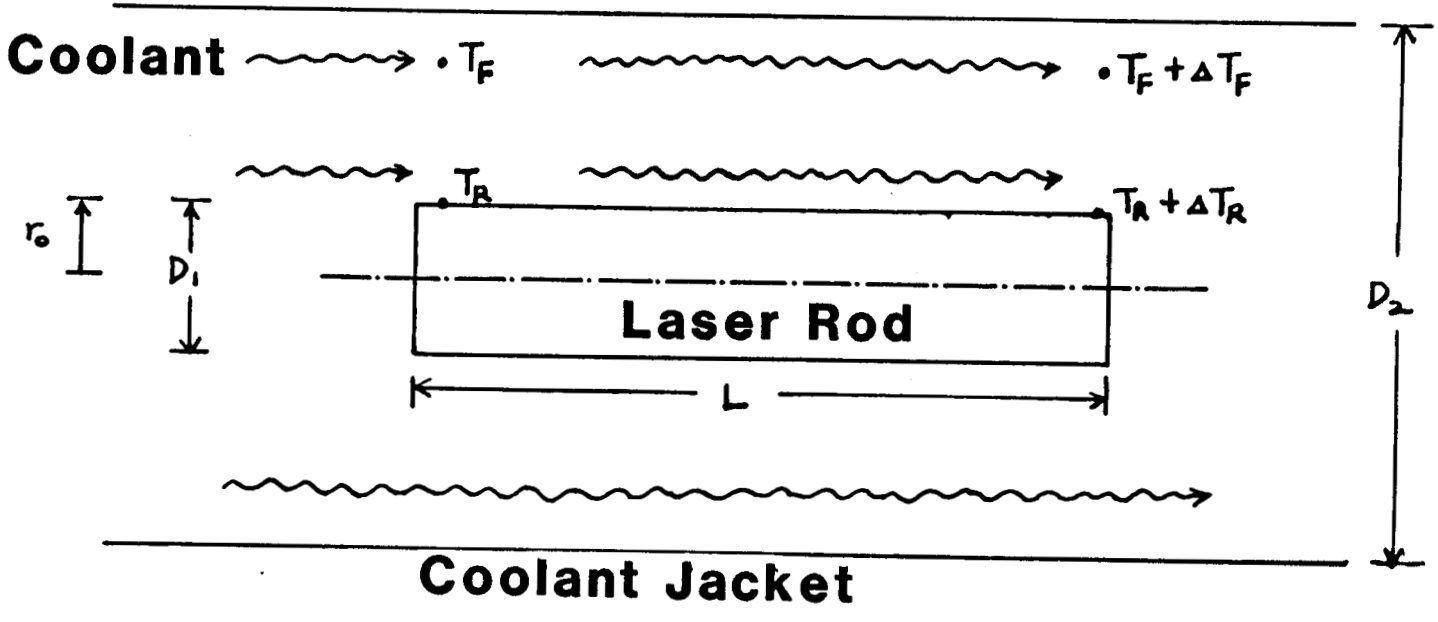

Figure 6 A model diagram for a laser crystal rod and a coolant jacket for the calculation of the temperature distribution in the rod.

The surface heat transfer coefficient can be determined as follows:

(i) for a laminar flow (900 N_{Re} 2,000)

$$h_e = 0.02 \frac{K_w}{D_2 - D_1} N_{Re}^{0.45} N_{Pr}^{0.5} N_{Gr}^{0.05} \left(\frac{D_2 - D_1}{L}\right)^{0.4} \left(\frac{D_2}{D_1}\right)^{0.8}$$

(ii) for a turbulant flow ($12{,}000 < N_{Re} < 220{,}000$)

$$h_t = 0.02 \frac{K_w}{D_2 - D_1} N_{Re}^{0.8} N_{Pr}^{0.33} \left(\frac{D_2}{D_1}\right)^{0.53}$$

where $N_{Re} = 4m^*/\pi\mu(D_2 + D_1)$: Reynolds number,

$N_{pr} = C_p\mu/K_w$: Prandtl number,

$N_{Gr} = [(D_2 - D_1)^3 \rho_w^3 g \cdot \gamma (T_R - T_F)]/\mu^2$: Grashof number,

K_w : Thermal conductivity of the coolant,

D_2 : Inside diameter of the coolant jacket,

μ : Viscosity of the coolant,

C_p : Specific heat of the coolant

m^* : Mass flow rate

ρ_w : Density of coolant,

γ : Volumetric thermal expansion coefficient,

g : Gravitational constant.

The axial temperautre gradient along the laser crystal can be approximated as

$$\Delta T_R = \Delta T_F = P_a/m^*C_p.$$

The sample data and calculations are listed in Appendix B. Graph 3 shows the radial temperature distribution of the various cyrstals with a rod shape of 3.2mm diameter x 75mm long for an input solar beam intensity of 4,000 solar constants and for a water flowrate of 0.5 galon per minute. The rod temperature of the Nd:Cr:GSGG crystal is the highest among the four crystals because of its largest absorption of the solar spectrum. Since the thermal conductivity of the Nd:Cr:GSGG is higher than that of the Nd:YLF, the actual temperature of the GSGG crystal will be very low for the same laser output as the Nd:YAG's or Nd:YLF's. Graph 4 shows the radial temperature distribution of the Nd:YAG of an 1.0 atomic percent doping density for various coolant flowrates. There is not a significant temperature difference at the coolant flowrates above 0.5 galon/minute. Graph 5 shows the axial temperature distribution of the Nd:YAG crystal of an 1.0 atomic percent doping density for various coolant flowrates. The flowrates below 0.5 galon/minute are the laminar flows and those above 2.0 galon/minute are the turbulent flows. The temperature difference is not significant at the flowrates above 0.5 galon/minute.

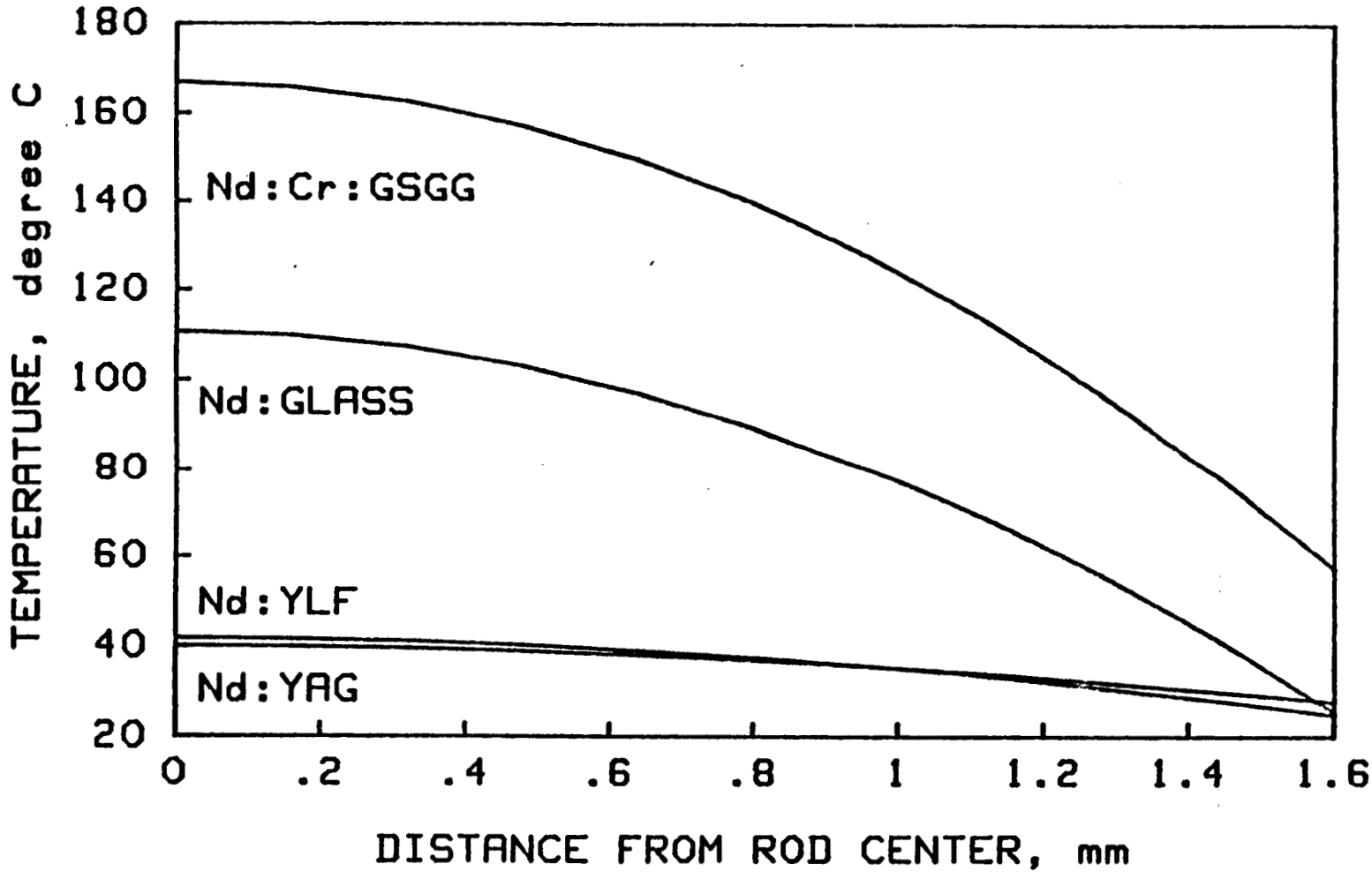

Graph 3 Radial temperature distribution of various laser crystals at a water flowrate of 1.5 gal/min. The laser rod size considered was 3.2 mm (diameter) x 75 mm (long), and the input power density was 1 solar constant.

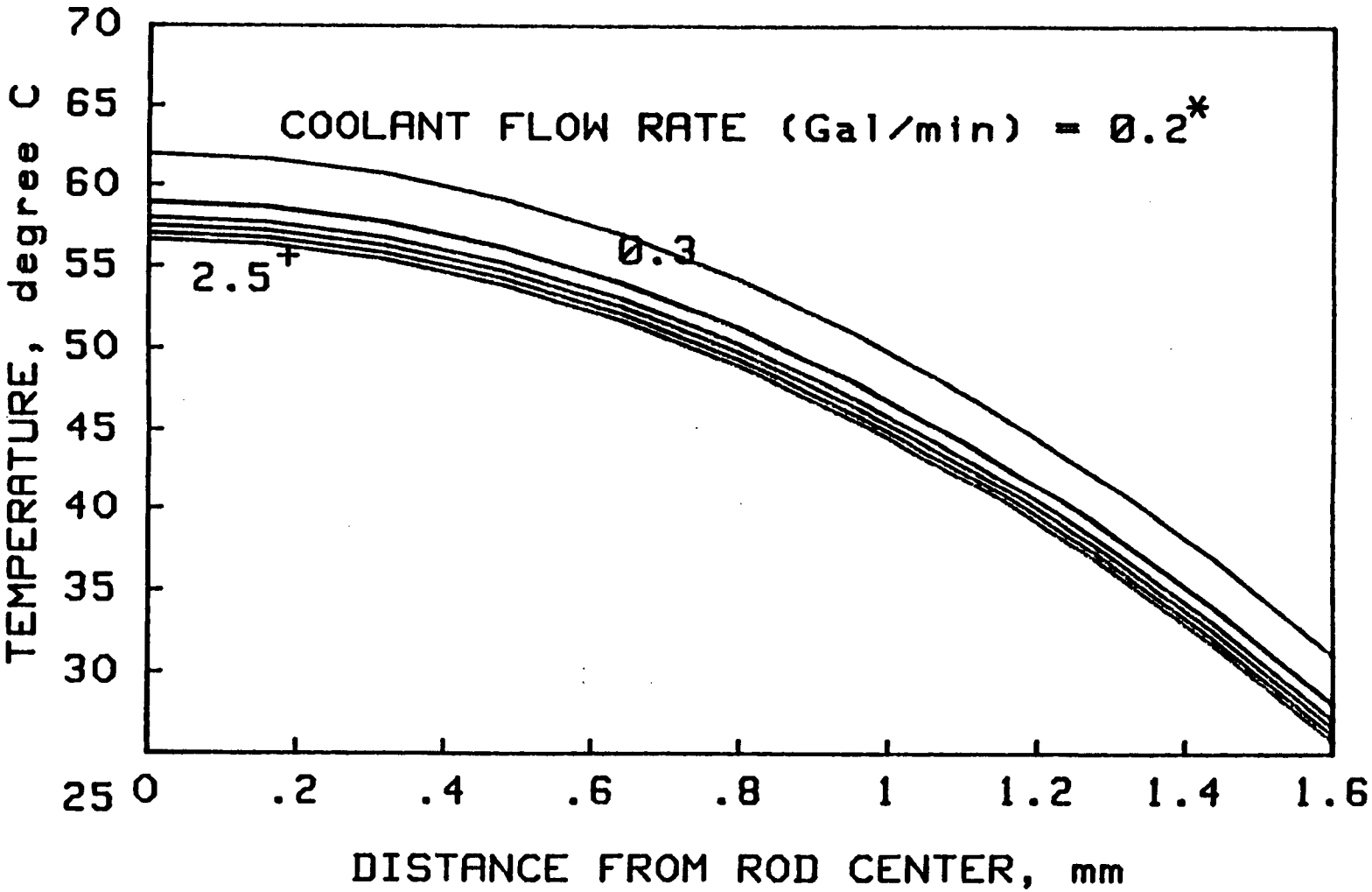

Graph 4 Radial temperature distribution of a Nd:YAG crystal at various water flowrates. The conditions considered were the same as those in Graph 3.

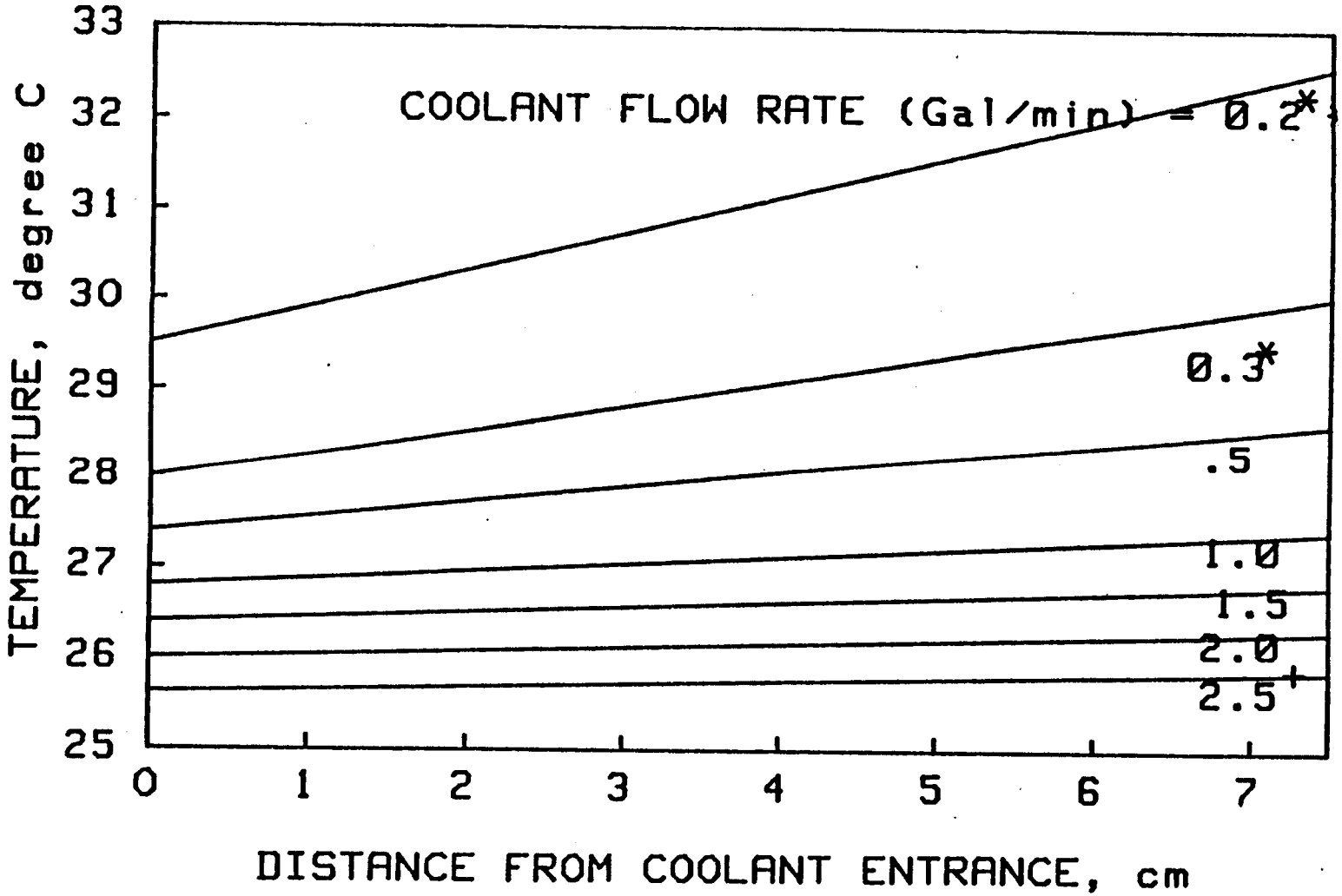

Graph 5 Axial temperature distribution of a Nd:YAG crystal at various water flowrates. The same conditions as shown in Graph 3 were considered.

E. Spectral and Spatial Distribution of the Tarmack Solar-Simulator Beam

The experimental setup used to measure the spatial distribution of the solar-simulator beam at the focus of a conical collector is shown in figure 7. The dimensions of the conical collector and the coordinates for the spatial distribution are shown in figure 8. Graphs 6, 7 and 8 show the three dimensional intensity distribution of the solar-simulator beam and the location of the laser crystal.

The experimental setup used to measure the spectral distribution of the solar-simulator beam at the focus of the conical collector is basically same as the one shown in figure 7 except the use of a lens between the spectrometer and the diffuse surface instead of the fiber optics. A quartz lens was used for the UV transmission. Graph 9 shows the absolute intensity of the Tarmarack solar-simulator at the simulator input current of 200 A. The intensity at the focus of the conical collector is about 1,000 times higher than that of the air-mass-zero solar spectrum. At the wavelength of about 830nm there appear the line spectra of the xenon gas.

Graph 10 shows the spectral intensities of the solar-simulator beam at the various solar-simulator input currents. The peak intensity at I = 600 A is about 6 times higher than that at I = 200 A.

F. Laser System and Expected Laser Output

Figure 9 shows the schematic diagram of the experimental setup for the laser system, and figure 10 shows the detailed diagram of the laser crystal holder and the cooling water jacket. The mirror M_1 has a reflectivity of 99.5% at = 1.06 m and a curvature of 0.3 m. The reflectivity of the mirror M_2, which has a curvature of 0.3 m, is changed to several values for the maximum laser output.

The Tamarack solar-simulator provides 4-kW optical beam power [Ref. 38] at the electrical input power of 45 kW which is obtained with the input current of 600 A and the DC voltage of 75 volts. Assuming that there is no loss on the conical reflector and using the same optical conversion efficiency as the one achieved by H. Arash, et al [Ref. 9], the expected maximum laser output power can be calculated for a Nd:YAG crystal as follows:

$$P_{Nd:YAG} = (0.0164)(4kW) = 65.6\ W.$$

The slope efficiency of the Nd:Cr:GSGG crystal can be assumed to be twice

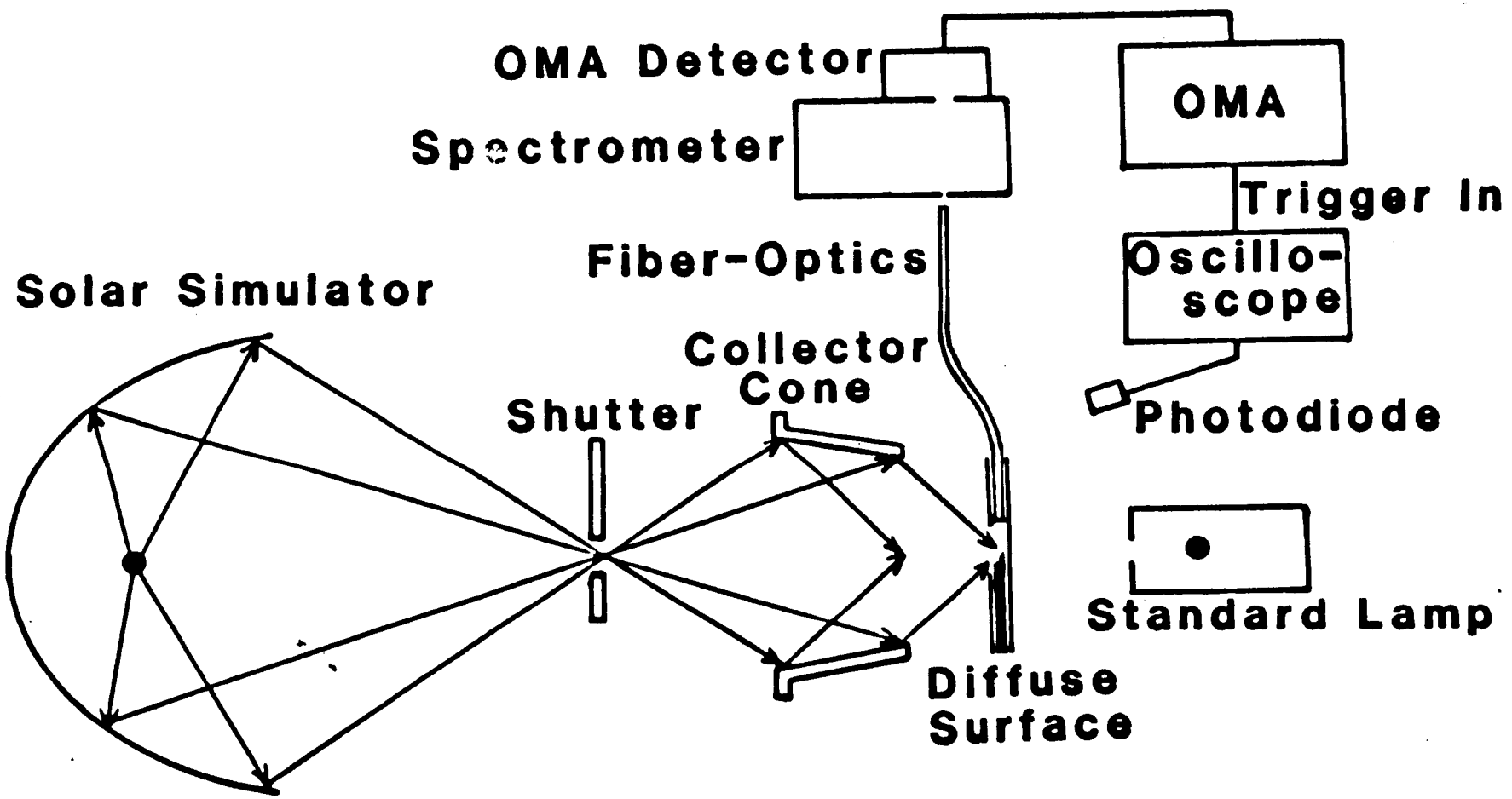

Figure 7 The systematic diagram for the spatial and spectral measurements of the solar-simulator beam at the focus of a conical collector.

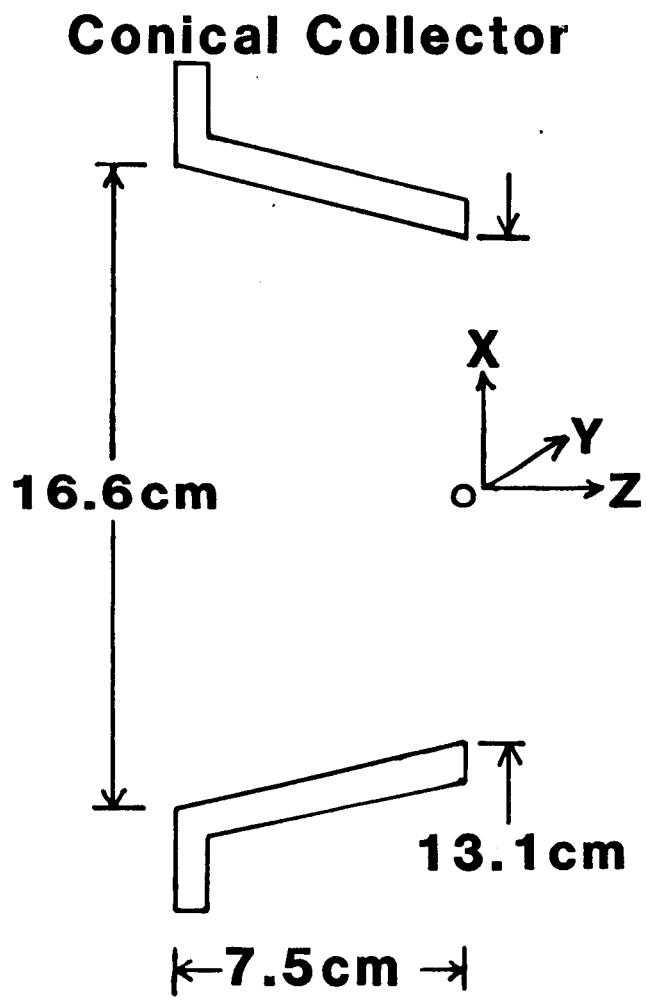

Figure 8 Dimensions of the conical collector used to focus down the solar-simulator beam, and the coordinates for the spatial distribution measurement of the beam at its focus.

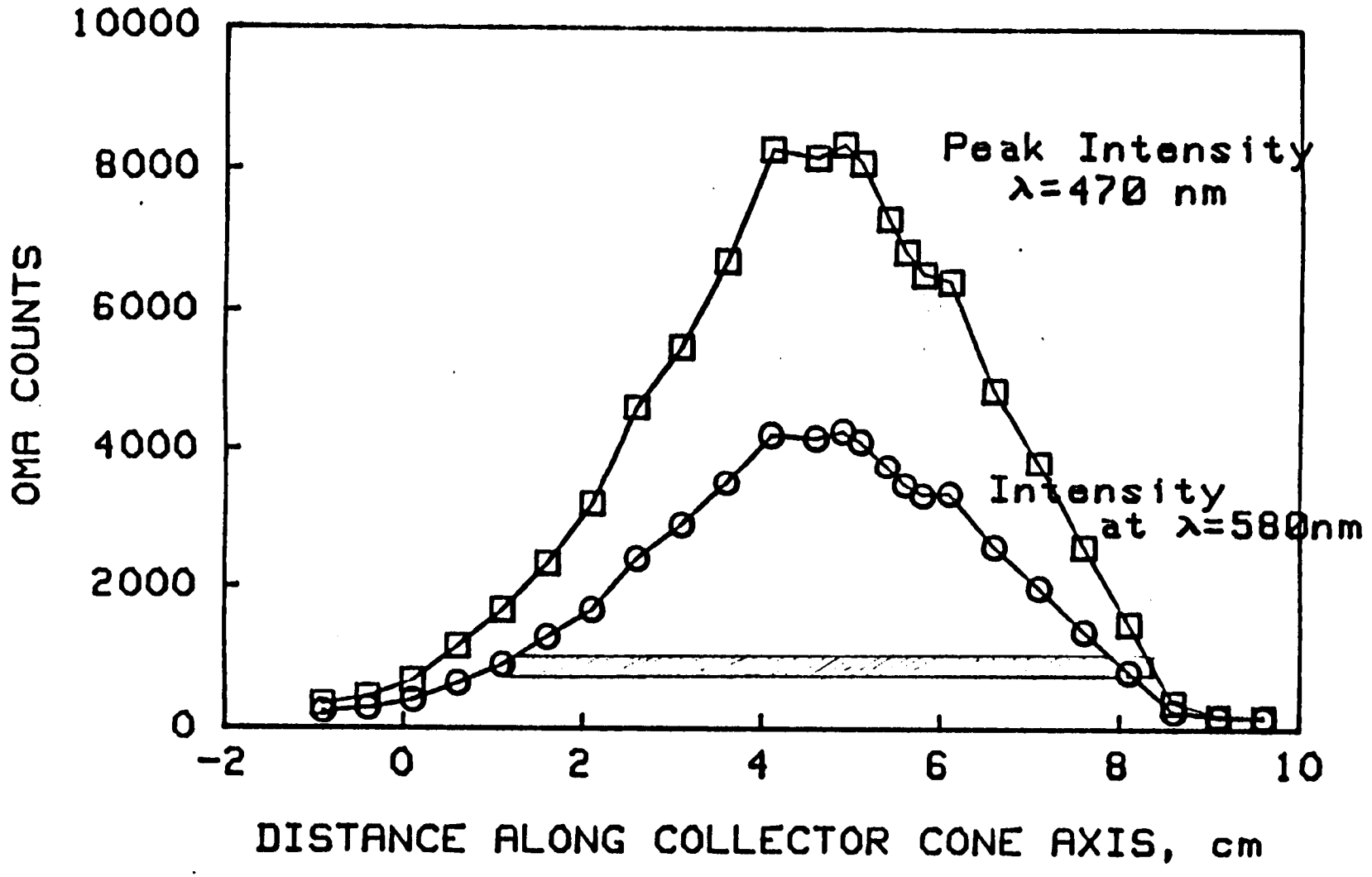

Graph 6. Spatial Distribution of the Solar-Simulator Beam at the Focus of the Collector Cone

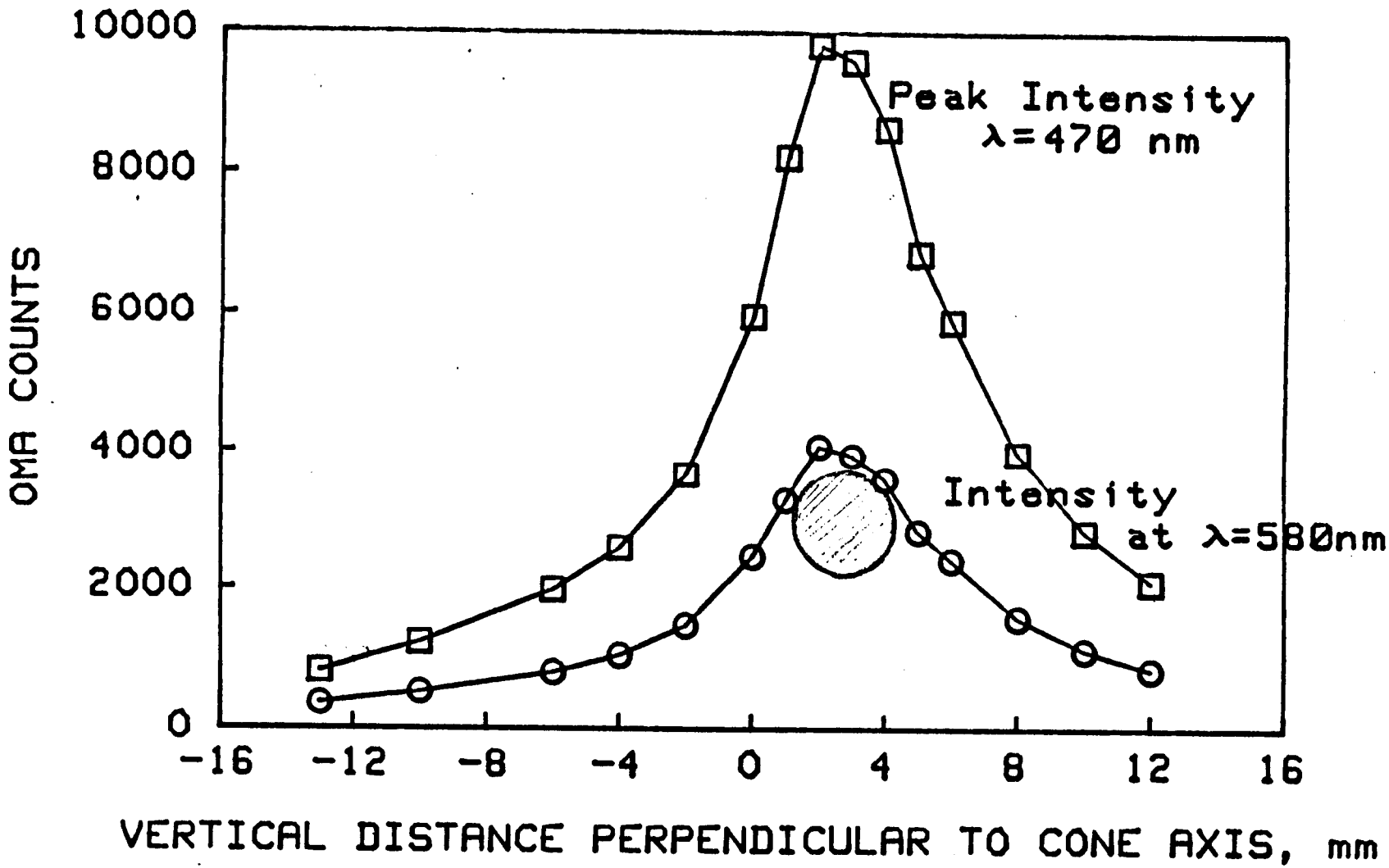

Graph 7. Spatial Distribution of the Solar-Simulator Beam at the Focus of the Collector Cone.

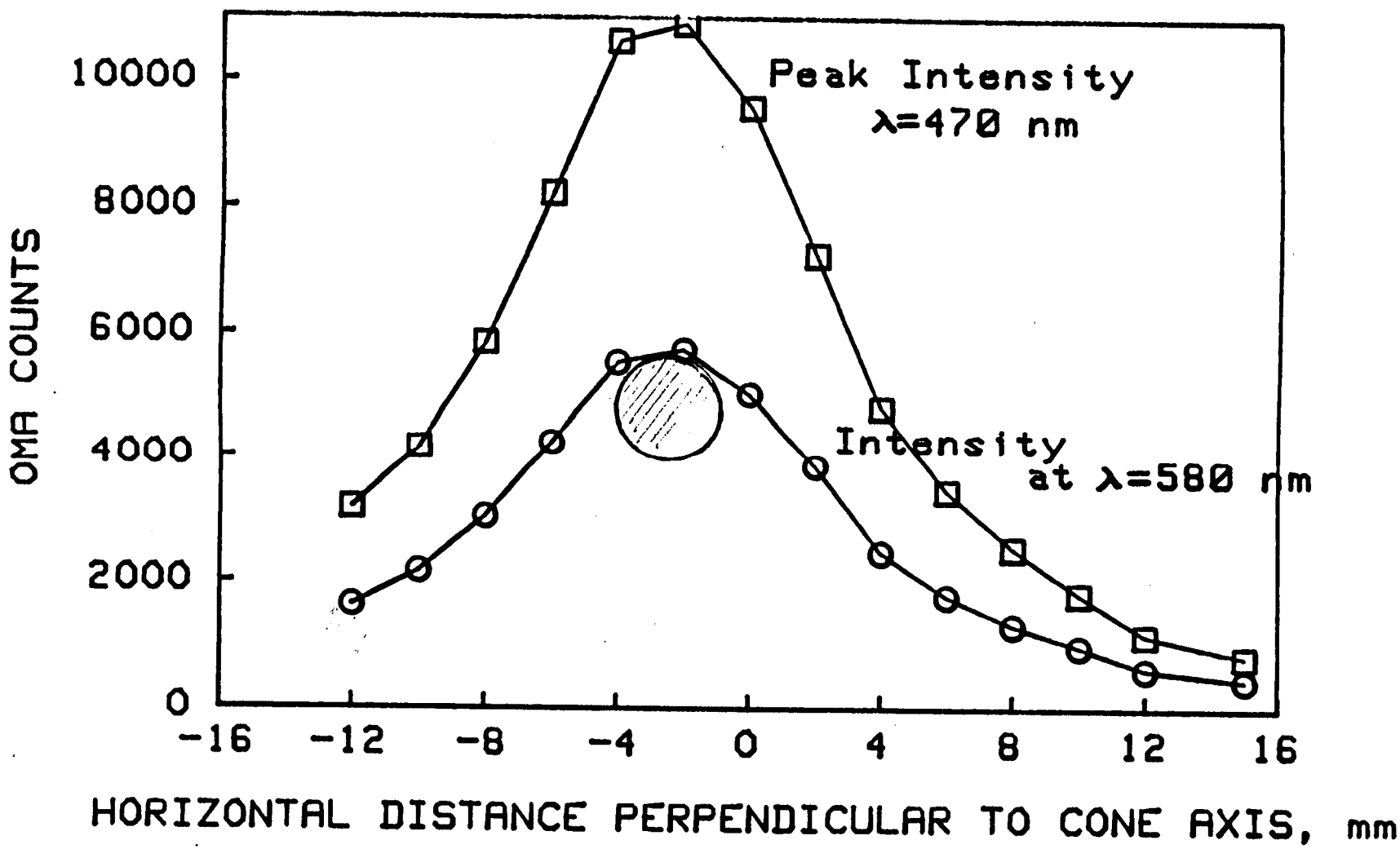

Graph 8. Spatial Distribution of the Solar-Simulator Beam at the Focus of the Collector Cone.

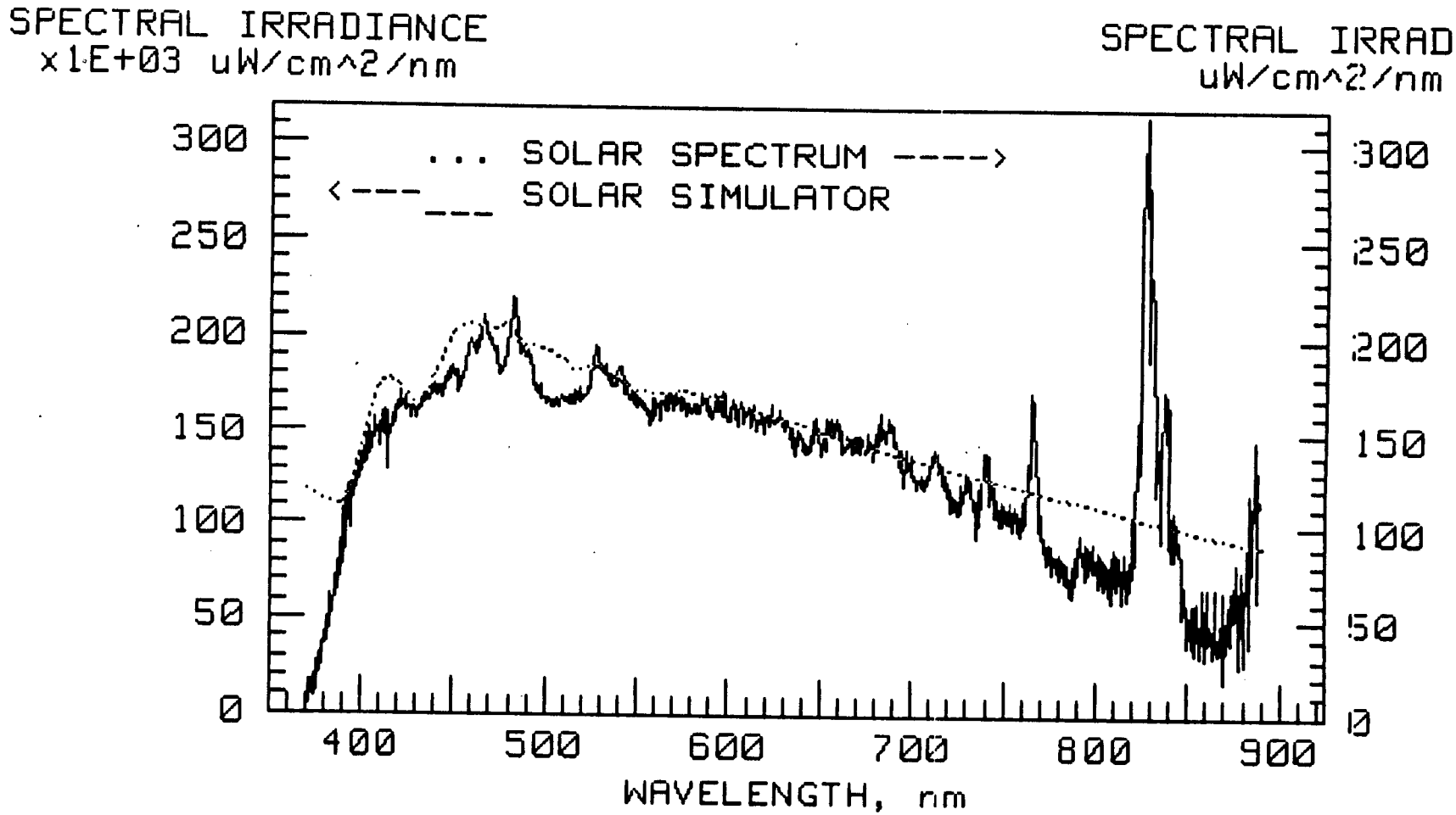

Graph 9 The absolute intensity of the solar-simulator spectrum at the input current of 200 A compared with the air-mass-zero solar spectrum.

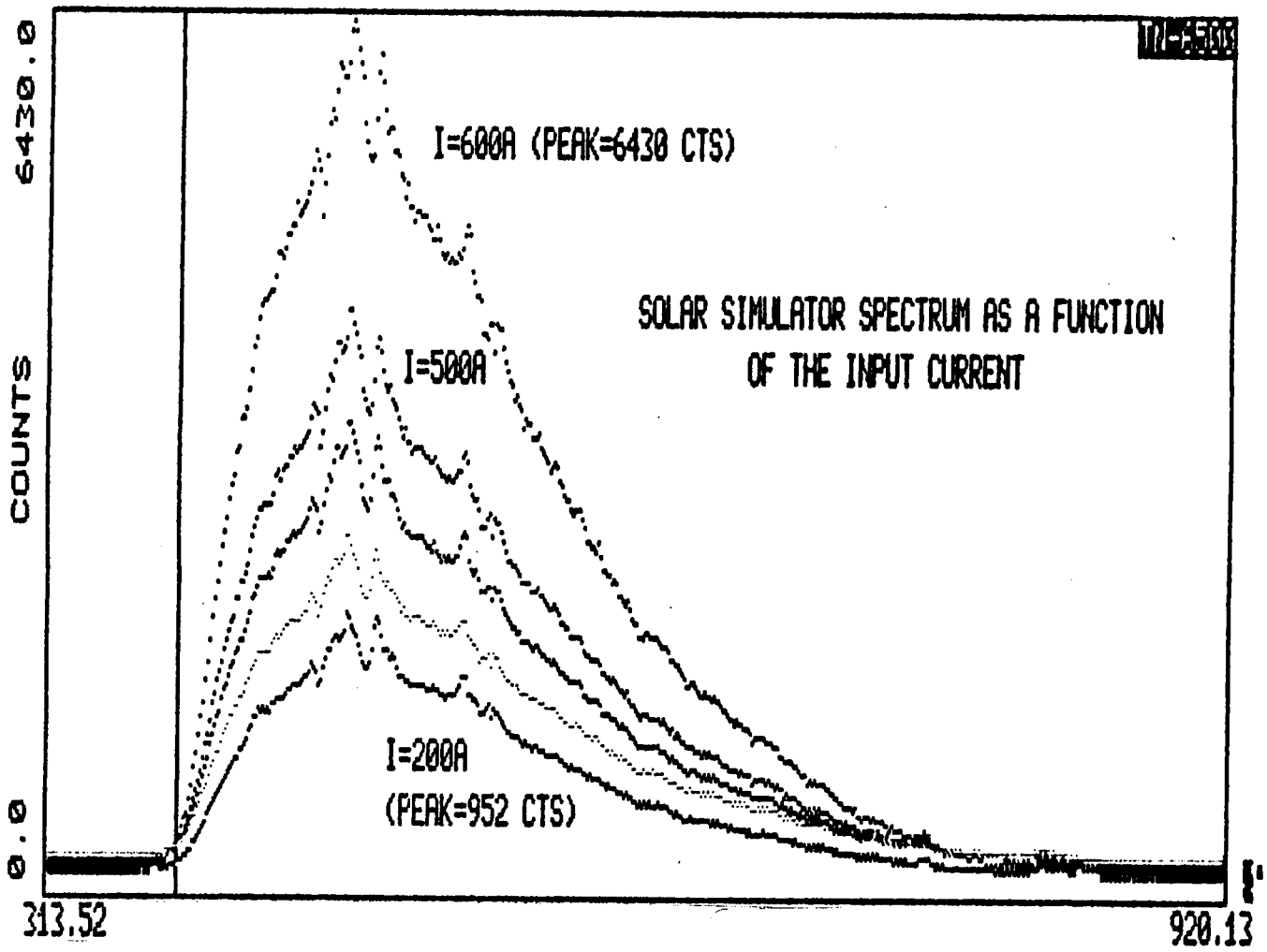

Graph 10 The spectral irradiances of the solar simulator beam measured with an OMA at various solar-simulator input currents.

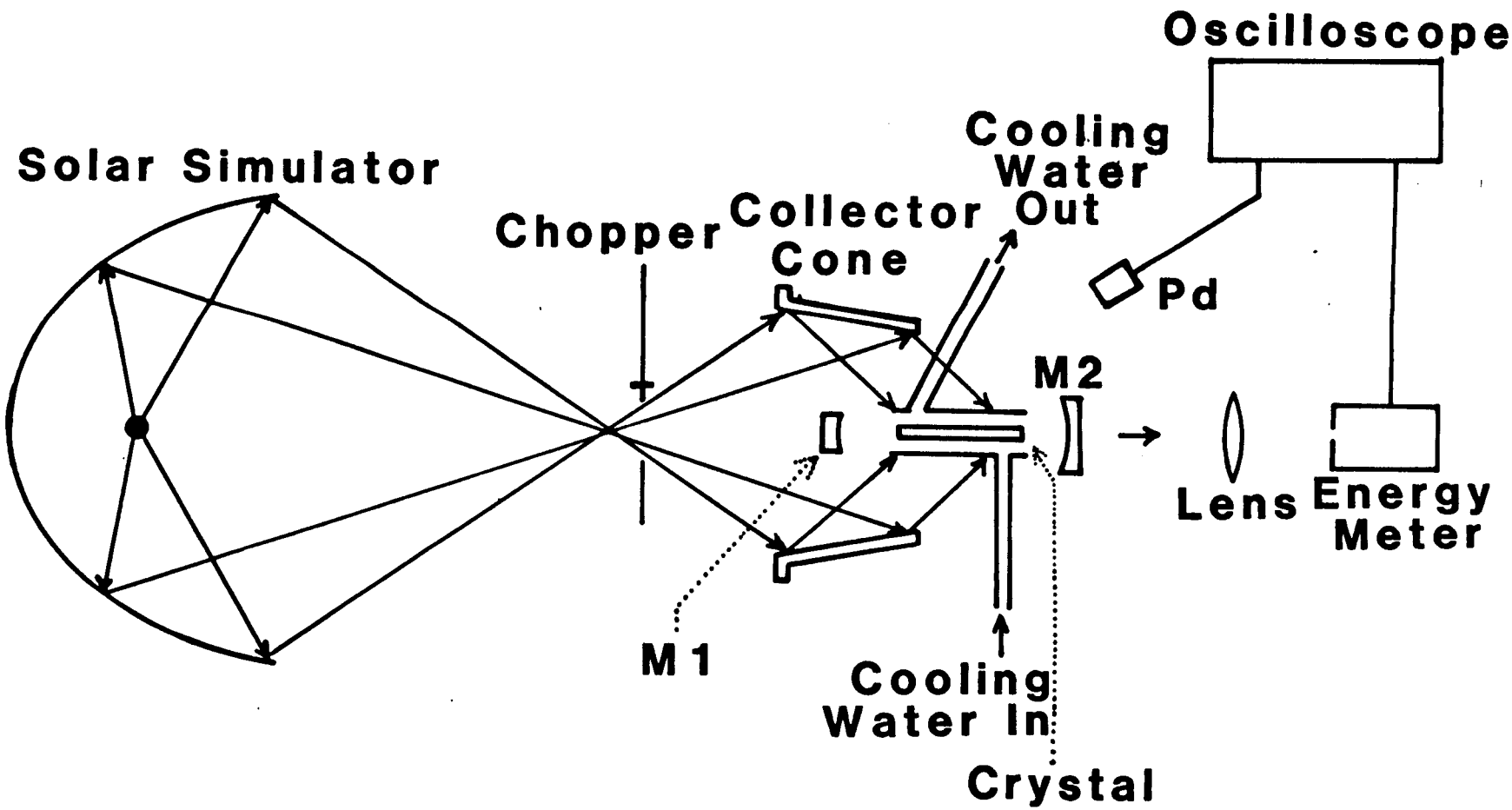

Figure 9 Setup for the solid state laser experiments with a Tarmarack solar-simulator pumping.

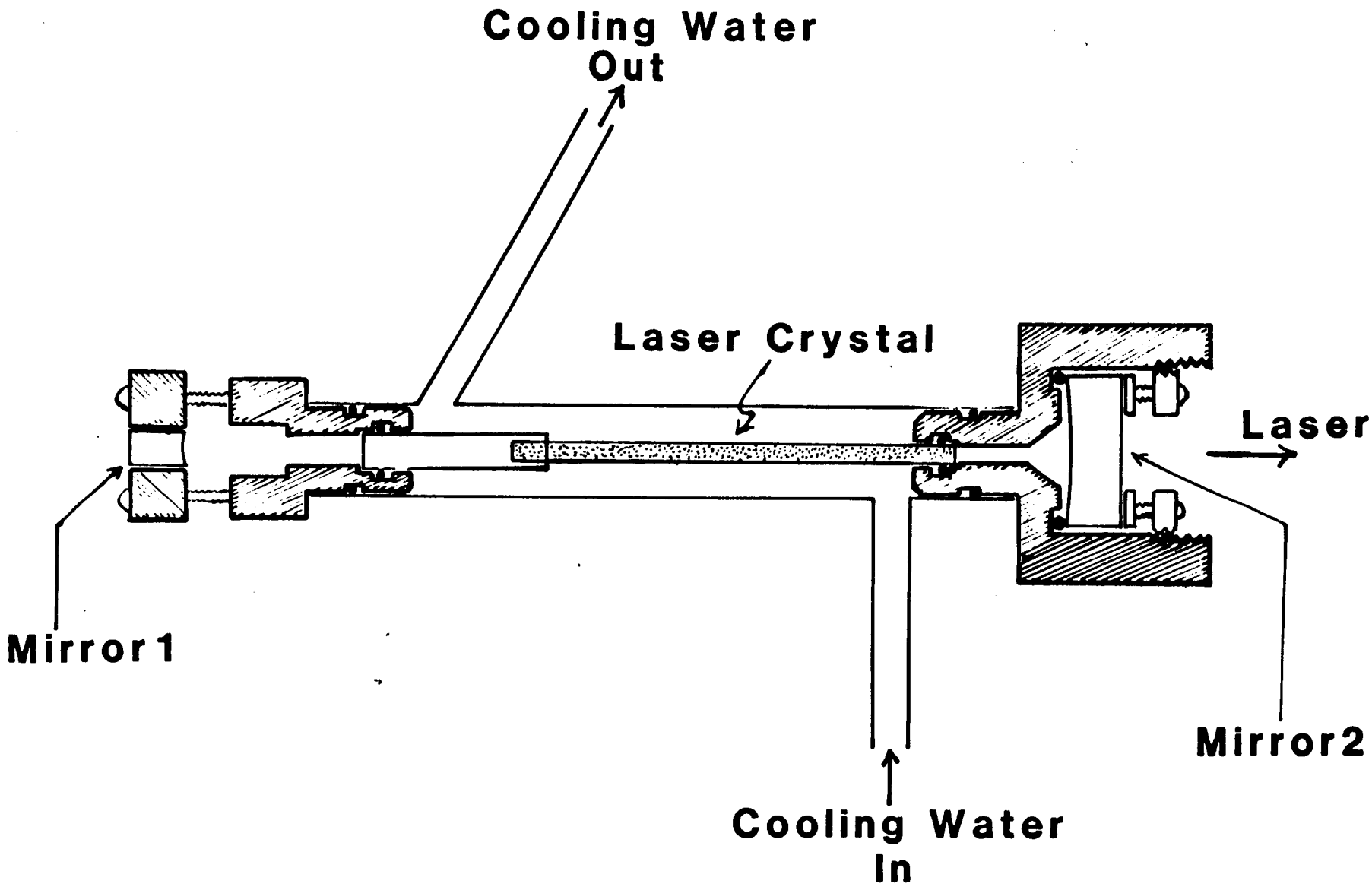

Figure 10 Laser crystal holder and water-jacket with the mirrors attached to both ends.

higher than that of the Nd:YAG crystal according to Refs. 30 and 36. Then the expected laser output with a Nd:Cr:GSGG crystal will be

$$P_{Nd:Cr:GSGG} = 2 \times 65.6 \text{ W} = 131.2 \text{ W}.$$

G. Conclusion

Nd:YAG, Nd:Cr;GSGG and Nd:YLF crystals are good candidates for the solar-pumped CW laser material. Among them, Nd:Cr:GSGG has the largest absorption of the solar spectrum, and possibly can be scaled up to a high power laser. The thermal problem is not significant for the crystals except the Nd:Cr:GSGG up to 4,000 solar constants pump power with a flowrate less than 2 galon/minute. The detailed calculation and experimental measurements should be done during the next project period to determine the maximum pump power for each crystal before the thermal problem becomes significant.

Appendix A. Absorption of the solar beam by various laser crystals.

Nd:YAG

	RANGE (nm)
SOLAR SPECTRUM	115.0 - 1000000.0
ABSORPTION SPECTRUM OF LASANT	300.0 - 910.0
INCIDENT ANGLE (in degree) =	45

* *

INTEGRATED SOLAR INTENSITY (mW/cm^2) = 135.3

ROD DIA. (cm)	PUMPING LENGTH (cm)	DOPING DENSITY (ions/cm^3)	ABSORBED SOLAR INTENSITY (mW/cm^2)	RATIO (Abs. S.I./ Integ. S.I.)(%)	ABSORBED POWER AT CENTER dia=1mm,(mW/cm^2)
.10	.14	6.50E+19	1.363	1.01	1.363
		1.30E+20	2.607	1.93	2.607
		1.43E+20	2.843	2.10	2.843
		1.90E+20	3.668	2.71	3.668
		2.60E+20	4.819	3.56	4.819
		2.86E+20	5.225	3.86	5.225
		3.25E+20	5.816	4.30	5.816
		3.90E+20	6.753	4.99	6.753
		5.20E+20	8.481	6.27	8.481
		6.50E+20	10.047	7.43	10.047
.20	.28	6.50E+19	2.607	1.93	1.300
		1.30E+20	4.819	3.56	2.391
		1.43E+20	5.225	3.86	2.589
		1.90E+20	6.613	4.89	3.259
		2.60E+20	8.481	6.27	4.146
		2.86E+20	9.125	6.74	4.447
		3.25E+20	10.047	7.43	4.874
		3.90E+20	11.483	8.49	5.528
		5.20E+20	14.050	10.38	6.664
		6.50E+20	16.304	12.05	7.626
.30	.42	6.50E+19	3.754	2.77	1.244
		1.30E+20	6.753	4.99	2.212
		1.43E+20	7.291	5.39	2.382
		1.90E+20	9.100	6.73	2.944
		2.60E+20	11.483	8.49	3.662
		2.86E+20	12.292	9.09	3.899
		3.25E+20	13.441	9.93	4.231
		3.90E+20	15.211	11.24	4.730
		5.20E+20	18.320	13.54	5.569
		6.50E+20	21.003	15.52	6.257
.50	.71	6.50E+19	5.816	4.30	1.147
		1.30E+20	10.047	7.43	1.934
		1.43E+20	10.780	7.97	2.066
		1.90E+20	13.202	9.76	2.488
		2.60E+20	16.304	12.05	3.002
		2.86E+20	17.338	12.81	3.167
		3.25E+20	18.793	13.89	3.394
		3.90E+20	21.003	15.52	3.727
		5.20E+20	24.811	18.34	4.270
		6.50E+20	28.025	20.71	4.699
.70	.99	6.50E+19	7.640	5.65	1.065

		1.30E+20	12.812	9.47	1.727
		1.43E+20	13.687	10.12	1.834
		1.90E+20	16.547	12.23	2.169
		2.60E+20	20.148	14.89	2.567
		2.86E+20	21.335	15.77	2.692
		3.25E+20	22.995	17.00	2.862
		3.90E+20	25.495	18.84	3.109
		5.20E+20	29.740	21.98	3.504
		6.50E+20	33.261	24.58	3.808
1.00	1.41	6.50E+19	10.047	7.43	.966
		1.30E+20	16.304	12.05	1.498
		1.43E+20	17.338	12.81	1.580
		1.90E+20	20.678	15.28	1.834
		2.60E+20	24.811	18.34	2.127
		2.86E+20	26.157	19.33	2.218
		3.25E+20	28.025	20.71	2.340
		3.90E+20	30.809	22.77	2.515
		5.20E+20	35.449	26.20	2.786
		6.50E+20	39.211	28.98	2.984
1.50	2.12	6.50E+19	13.441	9.93	.841
		1.30E+20	21.003	15.52	1.238
		1.43E+20	22.221	16.42	1.297
		1.90E+20	26.106	19.30	1.475
		2.60E+20	30.809	22.77	1.675
		2.86E+20	32.315	23.88	1.736
		3.25E+20	34.385	25.41	1.816
		3.90E+20	37.420	27.66	1.926
		5.20E+20	42.352	31.30	2.085
		6.50E+20	46.228	34.17	2.188
2.00	2.83	6.50E+19	16.304	12.05	.749
		1.30E+20	24.811	18.34	1.063
		1.43E+20	26.157	19.33	1.108
		1.90E+20	30.404	22.47	1.244
		2.60E+20	35.449	26.20	1.391
		2.86E+20	37.042	27.38	1.434
		3.25E+20	39.211	28.98	1.490
		3.90E+20	42.352	31.30	1.563
		5.20E+20	47.347	34.99	1.659
		6.50E+20	51.176	37.82	1.711
3.00	4.24	6.50E+19	21.003	15.52	.619
		1.30E+20	30.809	22.77	.837
		1.43E+20	32.315	23.88	.867
		1.90E+20	36.983	27.33	.955
		2.60E+20	42.352	31.30	1.042
		2.86E+20	44.006	32.53	1.065
		3.25E+20	46.228	34.17	1.093
		3.90E+20	49.378	36.50	1.126
		5.20E+20	54.225	40.08	1.156
		6.50E+20	57.802	42.72	1.158

* *

Nd:YAG

	RANGE (nm)
SOLAR SPECTRUM	115.0 - 1000000.0
ABSORPTION SPECTRUM OF LASANT	300.0 - 900.0
INCIDENT ANGLE (in degree) =	45

* *

INTEGRATED SOLAR INTENSITY (mW/cm^2) = 135.3

ROD DIA. (cm)	PUMPING LENGTH (cm)	DOPING DENSITY (ions/cm^3)	ABSORBED SOLAR INTENSITY (mW/cm^2)	RATIO (Abs. S.I./ Integ. S.I.)(%)	ABSORBED POWER AT CENTER dia=1mm,(mW/cm^2)
.10	.14	1.30E+20	2.594	1.92	2.594
		1.43E+20	2.829	2.09	2.829
		1.95E+20	3.734	2.76	3.734
		2.60E+20	4.793	3.54	4.793
		3.90E+20	6.714	4.96	6.714
.20	.28	1.30E+20	4.793	3.54	2.378
		1.43E+20	5.197	3.84	2.574
		1.95E+20	6.714	4.96	3.308
		2.60E+20	8.429	6.23	4.121
		3.90E+20	11.407	8.43	5.490
.30	.42	1.30E+20	6.714	4.96	2.199
		1.43E+20	7.248	5.36	2.368
		1.95E+20	9.224	6.82	2.981
		2.60E+20	11.407	8.43	3.636
		3.90E+20	15.099	11.16	4.693
.50	.71	1.30E+20	9.983	7.38	1.922
		1.43E+20	10.710	7.92	2.052
		1.95E+20	13.348	9.87	2.510
		2.60E+20	16.181	11.96	2.978
		3.90E+20	20.826	15.39	3.692
.70	.99	1.30E+20	12.724	9.40	1.715
		1.43E+20	13.591	10.05	1.820
		1.95E+20	16.700	12.34	2.183
		2.60E+20	19.982	14.77	2.543
		3.90E+20	25.259	18.67	3.076

* *

Nd:YLF (PHI_POLARIZED)

	RANGE (nm)
SOLAR SPECTRUM	115.0 - 1000000.0
ABSORPTION SPECTRUM OF LASANT	300.0 - 900.0

INCIDENT ANGLE (in degree) = 45

* *

INTEGRATED SOLAR INTENSITY (mW/cm^2) = 135.3

ROD DIA. (cm)	PUMPING LENGTH (cm)	DOPING DENSITY (ions/cm^3)	ABSORBED SOLAR INTENSITY (mW/cm^2)	RATIO (Abs. S.I./ Integ. S.I.)(%)	ABSORBED POWER AT CENTER dia=1mm,(mW/cm^2)
.10	.14	1.30E+20	1.647	1.22	1.647
		2.60E+20	3.165	2.34	3.165
.20	.28	1.30E+20	3.165	2.34	1.580
		2.60E+20	5.869	4.34	2.921
.30	.42	1.30E+20	4.568	3.38	1.518
		2.60E+20	8.208	6.07	2.705
.50	.71	1.30E+20	7.080	5.23	1.403
		2.60E+20	12.053	8.91	2.338
.70	.99	1.30E+20	9.262	6.85	1.301
		2.60E+20	15.095	11.16	2.043
1.00	1.41	1.30E+20	12.053	8.91	1.168
		2.60E+20	18.662	13.79	1.698
1.50	2.12	1.30E+20	15.761	11.65	.988
		2.60E+20	22.992	16.99	1.300
2.00	2.83	1.30E+20	18.662	13.79	.849
		2.60E+20	26.165	19.34	1.039
3.00	4.24	1.30E+20	22.992	16.99	.650
		2.60E+20	30.733	22.71	.728

* *

Nd:YLF (SIGMA_POLARIZED)

	RANGE (nm)
SOLAR SPECTRUM	115.0 - 1000000.0
ABSORPTION SPECTRUM OF LASANT	300.0 - 900.0

INCIDENT ANGLE (in degree) = 45

* *

INTEGRATED SOLAR INTENSITY (mW/cm^2) = 135.3

ROD DIA. (cm)	PUMPING LENGTH (cm)	DOPING DENSITY (ions/cm^3)	ABSORBED SOLAR INTENSITY (mW/cm^2)	RATIO (Abs. S.I./ Integ. S.I.)(%)	ABSORBED POWER AT CENTER dia=1mm,(mW/cm^2)
.10	.14	6.50E+19	.618	.46	.618
		1.30E+20	1.216	.90	1.216
		1.95E+20	1.794	1.33	1.794
		2.60E+20	2.355	1.74	2.355
		2.86E+20	2.574	1.90	2.574
		3.25E+20	2.897	2.14	2.897
		3.90E+20	3.423	2.53	3.423
		5.20E+20	4.427	3.27	4.427
		6.50E+20	5.372	3.97	5.372
.20	.28	6.50E+19	1.216	.90	.608
		1.30E+20	2.355	1.74	1.176
		1.95E+20	3.423	2.53	1.709
		2.60E+20	4.427	3.27	2.207
		2.86E+20	4.811	3.56	2.397
		3.25E+20	5.372	3.97	2.674
		3.90E+20	6.263	4.63	3.112
		5.20E+20	7.900	5.84	3.908
		6.50E+20	9.371	6.93	4.611
.30	.42	6.50E+19	1.794	1.33	.598
		1.30E+20	3.423	2.53	1.139
		1.95E+20	4.906	3.63	1.628
		2.60E+20	6.263	4.63	2.072
		2.86E+20	6.773	5.01	2.238
		3.25E+20	7.508	5.55	2.474
		3.90E+20	8.655	6.40	2.840
		5.20E+20	10.700	7.91	3.474
		6.50E+20	12.473	9.22	4.000
.50	.71	6.50E+19	2.897	2.14	.579
		1.30E+20	5.372	3.97	1.068
		1.95E+20	7.508	5.55	1.483
		2.60E+20	9.371	6.93	1.836
		2.86E+20	10.052	7.43	1.962
		3.25E+20	11.013	8.14	2.136
		3.90E+20	12.473	9.22	2.392
		5.20E+20	14.969	11.06	2.800
		6.50E+20	17.043	12.60	3.102
.70	.99	6.50E+19	3.932	2.91	.560
		1.30E+20	7.104	5.25	1.004
		1.95E+20	9.716	7.18	1.356
		2.60E+20	11.909	8.80	1.638
		2.86E+20	12.692	9.38	1.734
		3.25E+20	13.784	10.19	1.863
		3.90E+20	15.413	11.39	2.045
		5.20E+20	18.135	13.40	2.314

		6.50E+20	20.354	15.04	2.496
1.00	1.41	6.50E+19	5.372	3.97	.534
		1.30E+20	9.371	6.93	.917
		1.95E+20	12.473	9.22	1.195
		2.60E+20	14.969	11.06	1.397
		2.86E+20	15.842	11.71	1.462
		3.25E+20	17.043	12.60	1.547
		3.90E+20	18.811	13.90	1.659
		5.20E+20	21.723	16.06	1.812
		6.50E+20	24.079	17.80	1.909
1.50	2.12	6.50E+19	7.508	5.55	.494
		1.30E+20	12.473	9.22	.796
		1.95E+20	16.050	11.86	.984
		2.60E+20	18.811	13.90	1.105
		2.86E+20	19.760	14.60	1.141
		3.25E+20	21.057	15.56	1.186
		3.90E+20	22.956	16.97	1.242
		5.20E+20	26.071	19.27	1.317
		6.50E+20	28.598	21.14	1.369
2.00	2.83	6.50E+19	9.371	6.93	.459
		1.30E+20	14.969	11.06	.698
		1.95E+20	18.811	13.90	.829
		2.60E+20	21.723	16.06	.905
		2.86E+20	22.719	16.79	.926
		3.25E+20	24.079	17.80	.953
		3.90E+20	26.071	19.27	.988
		5.20E+20	29.348	21.69	1.037
		6.50E+20	32.012	23.66	1.077
3.00	4.24	6.50E+19	12.473	9.22	.398
		1.30E+20	18.811	13.90	.552
		1.95E+20	22.956	16.97	.621
		2.60E+20	26.071	19.27	.658
		2.86E+20	27.138	20.06	.669
		3.25E+20	28.598	21.14	.684
		3.90E+20	30.740	22.72	.705
		5.20E+20	34.274	25.33	.740
		6.50E+20	37.156	27.46	.770

* *

Nd:GLASS

		RANGE (nm)
SOLAR SPECTRUM		115.0 - 1000000.0
ABSORPTION SPECTRUM OF LASANT		300.0 - 900.0

INCIDENT ANGLE (in degree) = 45

GLASS COMPOSITION : SiO_2 = 66 wt %, Nd_2O_3 = 5 wt %
Na_2O = 16 wt %, BaO = 5 wt %
Al_2O_3= 2 wt %, Sb_2O_3 = 1 wt %

* *

INTEGRATED SOLAR INTENSITY (mW/cm^2) = 135.3

ROD DIAMETER (cm)	PUMPING LENGTH (cm)	DOPING DENSITY (wt % Nd2O3)	ABSORBED SOLAR INTENSITY (mW/cm^2)	RATIO (Abs. S. I. / Integ. S.I.)(%)	ABSORBED POWER AT CENTER dia=1mm,(mW/cm^2)
.10	.14	1.00	1.300	.961	1.300
		2.00	2.534	1.87	2.534
		3.00	3.703	2.74	3.708
		5.00	5.891	4.35	5.891
		7.00	7.877	5.82	7.877
		9.00	9.692	7.16	9.692
		10.00	10.542	7.79	10.542
.20	.28	1.00	2.534	1.873	1.267
		2.00	4.826	3.57	2.409
		3.00	6.907	5.10	3.440
		5.00	10.542	7.79	5.217
		7.00	13.612	10.06	6.680
		9.00	16.244	12.01	7.890
		10.00	17.426	12.88	8.416
.30	.42	1.00	3.708	2.741	1.235
		2.00	6.907	5.10	2.292
		3.00	9.692	7.16	3.199
		5.00	14.307	10.57	4.651
		7.00	17.988	13.30	5.735
		9.00	21.012	15.53	6.552
		10.00	22.337	16.51	6.884
.50	.71	1.00	5.891	4.354	1.174
		2.00	10.542	7.79	2.081
		3.00	14.307	10.57	2.785
		5.00	20.065	14.83	3.765
		7.00	24.325	17.98	4.376
		9.00	27.669	20.45	4.768
		10.00	29.100	21.51	4.911
.70	.99	1.00	7.877	5.822	1.118
		2.00	13.612	10.06	1.898
		3.00	17.988	13.30	2.447
		5.00	24.325	17.98	3.119
		7.00	28.825	21.30	3.478
		9.00	32.285	23.86	3.682
		10.00	33.751	24.95	3.751
1.00	1.41	1.00	10.542	7.792	1.040
		2.00	17.426	12.88	1.665
		3.00	22.337	16.51	2.047
		5.00	29.100	21.51	2.443
		7.00	33.751	24.95	2.620

		9.00	37.268	27.54	2.710
		10.00	38.744	28.64	2.738
1.50	2.12	1.00	14.307	10.574	.927
		2.00	22.337	16.51	1.364
		3.00	27.669	20.45	1.581
		5.00	34.715	25.66	1.763
		7.00	39.427	29.14	1.830
		9.00	42.927	31.73	1.860
		10.00	44.380	32.80	1.867
2.00	2.83	1.00	17.426	12.880	.832
		2.00	26.088	19.28	1.143
		3.00	31.608	23.36	1.272
		5.00	38.744	28.64	1.366
		7.00	43.430	32.10	1.396
		9.00	46.864	34.64	1.403
		10.00	48.278	35.68	1.402

* *

Nd:Cr:GSGG

	RANGE (nm)
SOLAR SPECTRUM	115.0 - 1000000.0
ABSORPTION SPECTRUM OF LASANT	300.0 - 920.0
INCIDENT ANGLE (in degree) =	45

DOPING DENSITY (ions/cm^3): Cr = 1.E+20
Nd = 2.E+20

* *

INTEGRATED SOLAR INTENSITY (mW/cm^2) = 135.3

ROD DIA. (cm)	PUMPING LENGTH (cm)	DOPING DENSITY (ions/cm^3)	ABSORBED SOLAR INTENSITY (mW/cm^2)	RATIO (Abs. S.I./ Integ. S.I.)(%)	ABSORBED POWER AT CENTER dia=1mm,(mW/cm^2)
.30	.42	1.00E+00	34.282	25.34	10.774

* *

Nd:Cr:GSGG

	RANGE (nm)
SOLAR SPECTRUM	115.0 - 1000000.0
ABSORPTION SPECTRUM OF LASANT	300.0 - 900.0
INCIDENT ANGLE (in degree) =	45

DOPING DENSITY (ions/cm^3): Cr = 1.E+20
Nd = 2.E+20

* *

INTEGRATED SOLAR INTENSITY (mW/cm^2) = 135.3

ROD DIA. (cm)	PUMPING LENGTH (cm)	DOPING DENSITY (ions/cm^3)	ABSORBED SOLAR INTENSITY (mW/cm^2)	RATIO (Abs. S.I./ Integ. S.I.)(%)	ABSORBED POWER AT CENTER dia=1mm,(mW/cm^2)
.30	.42	1.00E+00	34.236	25.30	10.758

* *

Appendix B. Temperature distribution in various laser crystals.

```
CRYSTAL * * * * * *
   CRYSTAL =                                              Nd:YAG
   ROD DIAMETER (cm) =                                     .32
   ROD LENGTH (cm) =                                       7.5
   EFFECTIVE PUMPING LENGTH (cm) =                         7
   THERMAL CONDUCTIVITY (W/cm/degree C) =                  .14

PUMPING SOURCE * * * * * *
   TOTAL ABSORBED SOLAR INTENSITY (W/cm^2) =               .006753
   SOLAR CONSTANT =                                        4000
   SURFACE ABSORPTION FACTOR =                             .8

COOLING SYSTEM * * * * * *
   NAME OF COOLANT =                                      WATER
   THERMAL CONDUCTIVITY (W/cm/degree C) =                  .0569
   VOLUMETRIC THERMAL EXPANSION COEFF.(1/degree            6.43E-5
   SPECIFIC HEAT (Cal/g/degree C) =                        1
                 (J/g/degree C)   =                        4.186
   DENSITY ( g/cm^3) =                                     1
   VISCOSITY ( g/cm/sec) =                                 .01
   DIAMETER OF WATER JACKET (cm) =                         1.308
   ENTERING TEMPERATURE OF COOLANT (degree C) =            20
COOLANT MASS FLOW-RATE(Gal/min)=     .5    (=   31.6 cm^3/sec)
```

```
RATE OF TOTAL HEAT DESSIPATION BY THE ROD (W/cm^2) =          152.07037576
RATE OF HEAT GENERATION PER UNIT VOLUME IN THE CRYSTAL (W/cm^2) =       270.12

Prandtl Number =      .735676625659
Granshof Number without Temperature Term =          607.726091598
Reynold Number =      1480.49291043
COOLANT MASS FLOW-RATE(Gal/min)=      .3    (=   18.9 cm^3/sec)

LAMINAR FLOW * * * * *
   HEAT TRANSFER COEFFICIENT = 2.61334646526
   ROD TEMPERATURE AT THE COOLANT ENTRANCE (degree C) =       27.4775901055

AXIAL TEMPERATURE GRADIANT OF ROD & COOLANT =       1.91908751961

* * * * * * * * * * * * * * * * * * * * * * * * * * * * * * * * * * *
RADIAL TEMPERATURE DISTRIBUTION OF CRYSTAL
                @ DISTANCE FROM ENTRANCE(cm)       3.75

RADIAL DISTANCE FROM     TEMPERATURE
ROD CENTER (mm)          (degree C)
  0.000                  40.7854767224
   .160                  40.6619932939
   .320                  40.2915430081
   .480                  39.6741258653
   .640                  38.8097418653
   .800                  37.6983910081
   .960                  36.3400732939
  1.120                  34.7347887224
  1.280                  32.8825372939
  1.440                  30.7833190081
  1.600                  28.4371338653
* * * * * * * * * * * * * * * * * * * * * * * * * * * * * * * * * * *

RATE OF TOTAL HEAT DESSIPATION BY THE ROD (W/cm^2) =          152.07037576
RATE OF HEAT GENERATION PER UNIT VOLUME IN THE CRYSTAL (W/cm^2) =       270.12

Prandtl Number =      .735676625659
Granshof Number without Temperature Term =          607.726091598
Reynold Number =      12337.4409203
COOLANT MASS FLOW-RATE(Gal/min)=     2.5    (=  157.8 cm^3/sec)

TURBURANT FLOW * * * *
   HEAT TRANSFER COEFFICIENT = 4.11570935606
   ROD TEMPERATURE AT THE COOLANT ENTRANCE (degree C) =       25.2505165284

AXIAL TEMPERATURE GRADIANT OF ROD & COOLANT =       .230290502353

* * * * * * * * * * * * * * * * * * * * * * * * * * * * * * * * * * *
RADIAL TEMPERATURE DISTRIBUTION OF CRYSTAL
                @ DISTANCE FROM ENTRANCE(cm)       3.75

RADIAL DISTANCE FROM     TEMPERATURE
ROD CENTER (mm)          (degree C)
  0.000                  37.7140046367
   .160                  37.5905212081
   .320                  37.2200709224
   .480                  36.6026537796
   .640                  35.7382697796
   .800                  34.6269189224
   .960                  33.2686012081
  1.120                  31.6633166367
  1.280                  29.8110652081
```

```
  1.440                 27.7118469224
  1.600                 25.3656617796
* * * * * * * * * * * * * * * * * * * * * * * * * * * * * * * *

RATE OF TOTAL HEAT DESSIPATION BY THE ROD (W/cm^2) =          152.07037576
RATE OF HEAT GENERATION PER UNIT VOLUME IN THE CRYSTAL (W/cm^2) =      270.12

Prandtl Number =      .735676625659
Granshof Number without Temperature Term =          607.726091598
Reynold Number =      2467.48818405
COOLANT MASS FLOW-RATE(Gal/min)=      .5    (=   31.6 cm^3/sec)

BOUNDARY Between LAMINAR and TURBULENT flows * * * *
   HEAT TRANSFER COEFF. (using LAMINAR flow equation) =      3.28873535843
   ROD TEMPERATURE at COOLANT ENTRANCE (degree C) =          26.0073594604

   HEAT TRANSFER COEFF. (using TURBULENT flow equation) =    1.1357132553
   ROD TEMPERATURE at COOLENT ENTRANCE (degree C) =          39.0273380179

AXIAL TEMPERATURE GRADIANT OF ROD @ COOLANT =      1.15145251177

* * * * * * * * * * * * * * * * * * * * * * * * * * * * * * * *
RADIAL TEMPERATURE DISTRIBUTION OF CRYSTAL
                @ DISTANCE FROM ENTRANCE(cm)      3.75

RADIAL DISTANCE FROM    TEMPERATURE
ROD CENTER (mm)         (degree C)
  0.000                 40.024069113
   .160                 39.9005856845
   .320                 39.5301353987
   .480                 38.9127182559
   .640                 38.0483342559
   .800                 36.9369833987
   .960                 35.5786656845
  1.120                 33.973381113
  1.280                 32.1211296845
  1.440                 30.0219113987
  1.600                 27.6757262559
* * * * * * * * * * * * * * * * * * * * * * * * * * * * * * * *

* * * * * * * * * * * * * * * * * * * * * * * * * * * * * * * *
TEMPERATURE DISTRIBUTION ALONG THE LENGTH OF THE CRYSTAL
              AT CYSTAL SURFACE

DISTANCE FROM       TEMPERATURE
ENTRANCE (cm)       (degree C)

  0.000             27.1
   .750             27.2151452512
  1.500             27.3302905024
  2.250             27.4454357535
  3.000             27.5605810047
  3.750             27.6757262559
  4.500             27.7908715071
  5.250             27.9060167582
  6.000             28.0211620094
  6.750             28.1363072606
  7.500             28.2514525118
* * * * * * * * * * * * * * * * * * * * * * * * * * * * * * * *
```

```
CRYSTAL * * * * * *
   CRYSTAL =                                          Nd:YLF (1 at % Nd)
   ROD DIAMETER (cm) =                                 .32
   ROD LENGTH (cm) =                                   7.5
   EFFECTIVE PUMPING LENGTH (cm) =                     7
   THERMAL CONDUCTIVITY (W/cm/degree C) =              .06

PUMPING SOURCE * * * * * *
   TOTAL ABSORBED SOLAR INTENSITY (W/cm^2) =           .003996
   SOLAR CONSTANT =                                    4000
   SURFACE ABSORPTION FACTOR =                         .8

COOLING SYSTEM * * * * * *
   NAME OF COOLANT =                                  WATER
   THERMAL CONDUCTIVITY (W/cm/degree C) =              .0569
   VOLUMETRIC THERMAL EXPANSION COEFF.(1/degree        6.43E-5
   SPECIFIC HEAT (Cal/g/degree C) =                    1
                 (J/g/degree C)   =                    4.186
   DENSITY ( g/cm^3) =                                 1
   VISCOSITY ( g/cm/sec) =                             .01
   DIAMETER OF WATER JACKET (cm) =                     1.308
   ENTERING TEMPERATURE OF COOLANT (degree C) =        20
COOLANT MASS FLOW-RATE(Gal/min)=     .5    (=   31.6 cm^3/sec)
```

```
RATE OF TOTAL HEAT DESSIPATION BY THE ROD (W/cm^2) =          89.9856688192
RATE OF HEAT GENERATION PER UNIT VOLUME IN THE CRYSTAL (W/cm^2) =       159.84

Prandtl Number =      .735676625659
Granshof Number without Temperature Term =          607.726091598
Reynold Number =      1480.49291043
COOLANT MASS FLOW-RATE(Gal/min)=      .3    (=    18.9 cm^3/sec)

LAMINAR FLOW * * * * *
   HEAT TRANSFER COEFFICIENT = 2.61334646526
   ROD TEMPERATURE AT THE COOLANT ENTRANCE (degree C) =       24.5367139586

AXIAL TEMPERATURE GRADIANT OF ROD & COOLANT =       1.13559510267

* * * * * * * * * * * * * * * * * * * * * * * * * * * * * * * * * * *
RADIAL TEMPERATURE DISTRIBUTION OF CRYSTAL
                @ DISTANCE FROM ENTRANCE(cm)       3.75

RADIAL DISTANCE FROM     TEMPERATURE
ROD CENTER (mm)          (degree C)
  0.000                  42.15411151
   .160                  41.98361551
   .320                  41.47212751
   .480                  40.61964751
   .640                  39.42617551
   .800                  37.89171151
   .960                  36.01625551
  1.120                  33.79980751
  1.280                  31.24236751
  1.440                  28.34393551
  1.600                  25.10451151
* * * * * * * * * * * * * * * * * * * * * * * * * * * * * * * * * * *

RATE OF TOTAL HEAT DESSIPATION BY THE ROD (W/cm^2) =          89.9856688192
RATE OF HEAT GENERATION PER UNIT VOLUME IN THE CRYSTAL (W/cm^2) =       159.84

Prandtl Number =      .735676625659
Granshof Number without Temperature Term =          607.726091598
Reynold Number =      12337.4409203
COOLANT MASS FLOW-RATE(Gal/min)=     2.5    (=   157.8 cm^3/sec)

TURBURANT FLOW * * * * *
   HEAT TRANSFER COEFFICIENT = 4.11570935606
   ROD TEMPERATURE AT THE COOLANT ENTRANCE (degree C) =       23.1069249293

AXIAL TEMPERATURE GRADIANT OF ROD & COOLANT =       .136271412321

* * * * * * * * * * * * * * * * * * * * * * * * * * * * * * * * * * *
RADIAL TEMPERATURE DISTRIBUTION OF CRYSTAL
                @ DISTANCE FROM ENTRANCE(cm)       3.75

RADIAL DISTANCE FROM     TEMPERATURE
ROD CENTER (mm)          (degree C)
  0.000                  40.2246606354
   .160                  40.0541646354
   .320                  39.5426766354
   .480                  38.6901966354
   .640                  37.4967246354
   .800                  35.9622606354
   .960                  34.0868046354
  1.120                  31.8703566354
  1.280                  29.3129166354
```

```
  1.440                 26.4144846354
  1.600                 23.1750606354
* * * * * * * * * * * * * * * * * * * * * * * * * * * * * * * * * * *

RATE OF TOTAL HEAT DESSIPATION BY THE ROD (W/cm^2) =          89.9856688192
RATE OF HEAT GENERATION PER UNIT VOLUME IN THE CRYSTAL (W/cm^2) =       159.84

Prandtl Number =      .735676625659
Granshof Number without Temperature Term =          607.726091598
Reynold Number =      2467.48818405
COOLANT MASS FLOW-RATE(Gal/min)=      .5    (=    31.6 cm^3/sec)

BOUNDARY Between LAMINAR and TURBULENT flows * * * *
   HEAT TRANSFER COEFF. (using LAMINAR flow equation) =      3.28873535843
   ROD TEMPERATURE at COOLANT ENTRANCE (degree C) =          23.644713221

   HEAT TRANSFER COEFF. (using TURBULENT flow equation) =    1.1357132553
   ROD TEMPERATURE at COOLENT ENTRANCE (degree C) =          31.2591800266

AXIAL TEMPERATURE GRADIANT OF ROD & COOLANT =       .681357061605

* * * * * * * * * * * * * * * * * * * * * * * * * * * * * * * * * * *
RADIAL TEMPERATURE DISTRIBUTION OF CRYSTAL
                @ DISTANCE FROM ENTRANCE(cm)      3.75

RADIAL DISTANCE FROM    TEMPERATURE
ROD CENTER (mm)         (degree C)
  0.000                 41.7902785308
   .160                 41.6197825308
   .320                 41.1082945308
   .480                 40.2558145308
   .640                 39.0623425308
   .800                 37.5278785308
   .960                 35.6524225308
  1.120                 33.4359745308
  1.280                 30.8785345308
  1.440                 27.9801025308
  1.600                 24.7406785308
* * * * * * * * * * * * * * * * * * * * * * * * * * * * * * * * * * *

* * * * * * * * * * * * * * * * * * * * * * * * * * * * * * * * * * *
TEMPERATURE DISTRIBUTION ALONG THE LENGTH OF THE CRYSTAL
               AT CYSTAL SURFACE

DISTANCE FROM       TEMPERATURE
ENTRANCE (cm)       (degree C)

  0.000             24.4
   .750             24.4681357062
  1.500             24.5362714123
  2.250             24.6044071185
  3.000             24.6725428246
  3.750             24.7406785308
  4.500             24.808814237
  5.250             24.8769499431
  6.000             24.9450856493
  6.750             25.0132213554
  7.500             25.0813570616
* * * * * * * * * * * * * * * * * * * * * * * * * * * * * * * * * * *
```

```
CRYSTAL * * * * * *
   CRYSTAL =                                          Nd:GLASS (ABOUT 1.3 wt %)
   ROD DIAMETER (cm) =                                 .32
   ROD LENGTH (cm) =                                   7.5
   EFFECTIVE PUMPING LENGTH (cm) =                     7
   THERMAL CONDUCTIVITY (W/cm/degree C) =              .0135

PUMPING SOURCE * * * * * *
   TOTAL ABSORBED SOLAR INTENSITY (W/cm^2) =           .0045
   SOLAR CONSTANT =                                    4000
   SURFACE ABSORPTION FACTOR =                         .8

COOLING SYSTEM * * * * * *
   NAME OF COOLANT =                                  WATER
   THERMAL CONDUCTIVITY (W/cm/degree C) =              .0569
   VOLUMETRIC THERMAL EXPANSION COEFF.(1/degree        6.43E-5
   SPECIFIC HEAT (Cal/g/degree C) =                    1
                 (J/g/degree C)    =                   4.186
   DENSITY ( g/cm^3) =                                 1
   VISCOSITY ( g/cm/sec) =                             .01
   DIAMETER OF WATER JACKET (cm) =                     1.308
   ENTERING TEMPERATURE OF COOLANT (degree C) =        20
COOLANT MASS FLOW-RATE(Gal/min)=     .3    (=   18.9 cm^3/sec)


RATE OF TOTAL HEAT DESSIPATION BY THE ROD (W/cm^2) =          101.335212634
RATE OF HEAT GENERATION PER UNIT VOLUME IN THE CRYSTAL (W/cm^2) =       180

Prandtl Number =      .735676625659
Granshof Number without Temperature Term =          607.726091598
Reynold Number =      1480.49291043
COOLANT MASS FLOW-RATE(Gal/min)=     .3    (=   18.9 cm^3/sec)

LAMINAR FLOW * * * * *
   HEAT TRANSFER COEFFICIENT = 2.61334646526
   ROD TEMPERATURE AT THE COOLANT ENTRANCE (degree C) =       25.0800958497

AXIAL TEMPERATURE GRADIANT OF ROD & COOLANT =       1.27882331382

* * * * * * * * * * * * * * * * * * * * * * * * * * * * * * * * * * *
RADIAL TEMPERATURE DISTRIBUTION OF CRYSTAL
                @ DISTANCE FROM ENTRANCE(cm)       3.75

RADIAL DISTANCE FROM     TEMPERATURE
ROD CENTER (mm)          (degree C)
  0.000                  111.05284084
   .160                  110.199507507
   .320                  107.639507507
   .480                  103.37284084
   .640                  97.3995075066
   .800                  89.7195075066
   .960                  80.3328408399
  1.120                  69.2395075066
  1.280                  56.4395075066
  1.440                  41.9328408399
  1.600                  25.7195075066
* * * * * * * * * * * * * * * * * * * * * * * * * * * * * * * * * * *
```

```
RATE OF TOTAL HEAT DESSIPATION BY THE ROD (W/cm^2) =          101.335212634
RATE OF HEAT GENERATION PER UNIT VOLUME IN THE CRYSTAL (W/cm^2) =       180

Prandtl Number =      .735676625659
Granshof Number without Temperature Term =          607.726091598
Reynold Number =      12337.4409203
COOLANT MASS FLOW-RATE(Gal/min)=    2.5    (=  157.8 cm^3/sec)

TURBURANT FLOW * * * *
   HEAT TRANSFER COEFFICIENT = 4.11570935606
   ROD TEMPERATURE AT THE COOLANT ENTRANCE (degree C) =       23.4987893348

AXIAL TEMPERATURE GRADIANT OF ROD & COOLANT =       .153458797659

* * * * * * * * * * * * * * * * * * * * * * * * * * * * * * * * * * *
RADIAL TEMPERATURE DISTRIBUTION OF CRYSTAL
                @ DISTANCE FROM ENTRANCE(cm)       3.75

RADIAL DISTANCE FROM    TEMPERATURE
ROD CENTER (mm)         (degree C)
  0.000                 108.908852067
   .160                 108.055518734
   .320                 105.495518734
   .480                 101.228852067
   .640                 95.2555187336
   .800                 87.5755187336
   .960                 78.1888520669
  1.120                 67.0955187336
  1.280                 54.2955187336
  1.440                 39.7888520669
  1.600                 23.5755187336
* * * * * * * * * * * * * * * * * * * * * * * * * * * * * * * * * * *
```

```
RATE OF TOTAL HEAT DESSIPATION BY THE ROD (W/cm^2) =          101.335212634
RATE OF HEAT GENERATION PER UNIT VOLUME IN THE CRYSTAL (W/cm^2) =       180

Prandtl Number =      .735676625659
Granshof Number without Temperature Term =          607.726091598
Reynold Number =      2467.48818405
COOLANT MASS FLOW-RATE(Gal/min)=      .5    (=   31.6 cm^3/sec)

BOUNDARY Between LAMINAR and TURBULENT flows * * * *
   HEAT TRANSFER COEFF. (using LAMINAR flow equation) =      3.28873535843
   ROD TEMPERATURE at COOLANT ENTRANCE (degree C) =          24.0812563181

   HEAT TRANSFER COEFF. (using TURBULENT flow equation) =    1.1357132553
   ROD TEMPERATURE at COOLENT ENTRANCE (degree C) =          32.6792567867

AXIAL TEMPERATURE GRADIANT OF ROD & COOLANT =       .767293988294

* * * * * * * * * * * * * * * * * * * * * * * * * * * * * * * * * * *
RADIAL TEMPERATURE DISTRIBUTION OF CRYSTAL
                @ DISTANCE FROM ENTRANCE(cm)      3.75

RADIAL DISTANCE FROM     TEMPERATURE
ROD CENTER (mm)          (degree C)
  0.000                  110.616980327
   .160                  109.763646994
   .320                  107.203646994
   .480                  102.936980327
   .640                  96.9636469941
   .800                  89.2836469941
   .960                  79.8969803275
  1.120                  68.8036469941
  1.280                  56.0036469941
  1.440                  41.4969803275
  1.600                  25.2836469941
* * * * * * * * * * * * * * * * * * * * * * * * * * * * * * * * * * *

* * * * * * * * * * * * * * * * * * * * * * * * * * * * * * * * * * *
TEMPERATURE DISTRIBUTION ALONG THE LENGTH OF THE CRYSTAL
               AT CYSTAL SURFACE

DISTANCE FROM        TEMPERATURE
ENTRANCE (cm)        (degree C)

  0.000              24.9
   .750              24.9767293988
  1.500              25.0534587977
  2.250              25.1301881965
  3.000              25.2069175953
  3.750              25.2836469941
  4.500              25.360376393
  5.250              25.4371057918
  6.000              25.5138351906
  6.750              25.5905645895
  7.500              25.6672939883
* * * * * * * * * * * * * * * * * * * * * * * * * * * * * * * * * * *
```

```
CRYSTAL * * * * * *
   CRYSTAL =                                          Nd:Cr:GSGG (Nd=2E20)
   ROD DIAMETER (cm) =                                 .32
   ROD LENGTH (cm) =                                   7.5
   EFFECTIVE PUMPING LENGTH (cm) =                     7
   THERMAL CONDUCTIVITY (W/cm/degree C) =              .08

PUMPING SOURCE * * * * * *
   TOTAL ABSORBED SOLAR INTENSITY (W/cm^2) =           .034282
   SOLAR CONSTANT =                                    4000
   SURFACE ABSORPTION FACTOR =                         .8

COOLING SYSTEM * * * * * *
   NAME OF COOLANT =                                  WATER
   THERMAL CONDUCTIVITY (W/cm/degree C) =              .0569
   VOLUMETRIC THERMAL EXPANSION COEFF.(1/degree        6.43E-5
   SPECIFIC HEAT (Cal/g/degree C) =                    1
                 (J/g/degree C)   =                    4.186
   DENSITY ( g/cm^3) =                                 1
   VISCOSITY ( g/cm/sec) =                             .01
   DIAMETER OF WATER JACKET (cm) =                     1.308
   ENTERING TEMPERATURE OF COOLANT (degree C) =        20
COOLANT MASS FLOW-RATE(Gal/min)=    2.5    (=  157.8 cm^3/sec)
```

```
RATE OF TOTAL HEAT DESSIPATION BY THE ROD (W/cm^2) =          771.994168783
RATE OF HEAT GENERATION PER UNIT VOLUME IN THE CRYSTAL (W/cm^2) =      1371.28

Prandtl Number =      .735676625659
Granshof Number without Temperature Term =          607.726091598
Reynold Number =      1480.49291043
COOLANT MASS FLOW-RATE(Gal/min)=      .3    (=    18.9 cm^3/sec)

LAMINAR FLOW * * * * *
   HEAT TRANSFER COEFFICIENT = 2.61334646526
   ROD TEMPERATURE AT THE COOLANT ENTRANCE (degree C) =      55.134397703

AXIAL TEMPERATURE GRADIANT OF ROD & COOLANT =      9.74236018766

* * * * * * * * * * * * * * * * * * * * * * * * * * * * * * * * * *
RADIAL TEMPERATURE DISTRIBUTION OF CRYSTAL
                @ DISTANCE FROM ENTRANCE(cm)      3.75

RADIAL DISTANCE FROM     TEMPERATURE
ROD CENTER (mm)          (degree C)
  0.000                  169.707977797
   .160                  168.610953797
   .320                  165.319881797
   .480                  159.834761797
   .640                  152.155593797
   .800                  142.282377797
   .960                  130.215113797
  1.120                  115.953801797
  1.280                  99.4984417968
  1.440                  80.8490337968
  1.600                  60.0055777968
* * * * * * * * * * * * * * * * * * * * * * * * * * * * * * * * * *

RATE OF TOTAL HEAT DESSIPATION BY THE ROD (W/cm^2) =          771.994168783
RATE OF HEAT GENERATION PER UNIT VOLUME IN THE CRYSTAL (W/cm^2) =      1371.28

Prandtl Number =      .735676625659
Granshof Number without Temperature Term =          607.726091598
Reynold Number =      12337.4409203
COOLANT MASS FLOW-RATE(Gal/min)=    2.5    (=  157.8 cm^3/sec)

TURBURANT FLOW * * * *
   HEAT TRANSFER COEFFICIENT = 4.11570935606
   ROD TEMPERATURE AT THE COOLANT ENTRANCE (degree C) =      46.654554661

AXIAL TEMPERATURE GRADIANT OF ROD & COOLANT =      1.16908322252

* * * * * * * * * * * * * * * * * * * * * * * * * * * * * * * * * *
RADIAL TEMPERATURE DISTRIBUTION OF CRYSTAL
                @ DISTANCE FROM ENTRANCE(cm)      3.75

RADIAL DISTANCE FROM     TEMPERATURE
ROD CENTER (mm)          (degree C)
  0.000                  156.941496272
   .160                  155.844472272
   .320                  152.553400272
   .480                  147.068280272
   .640                  139.389112272
   .800                  129.515896272
   .960                  117.448632272
  1.120                  103.187320272
  1.280                  86.7319602723
```

RATE OF TOTAL HEAT DESSIPATION BY THE ROD (W/cm^2) = 771.994168783
RATE OF HEAT GENERATION PER UNIT VOLUME IN THE CRYSTAL (W/cm^2) = 1371.28

Prandtl Number = .735676625659
Granshof Number without Temperature Term = 607.726091598
Reynold Number = 2467.48818405
COOLANT MASS FLOW-RATE(Gal/min)= .5 (= 31.6 cm^3/sec)

BOUNDARY Between LAMINAR and TURBULENT flows * * * *
HEAT TRANSFER COEFF. (using LAMINAR flow equation) = 3.28873535843
ROD TEMPERATURE at COOLANT ENTRANCE (degree C) = 48.2263340796

HEAT TRANSFER COEFF. (using TURBULENT flow equation) = 1.1357132553
ROD TEMPERATURE at COOLENT ENTRANCE (degree C) = 116.593395813

AXIAL TEMPERATURE GRADIANT OF ROD & COOLANT = 5.8454161126

* *
RADIAL TEMPERATURE DISTRIBUTION OF CRYSTAL
@ DISTANCE FROM ENTRANCE(cm) 3.75

RADIAL DISTANCE FROM ROD CENTER (mm)	TEMPERATURE (degree C)
0.000	167.025108056
.160	165.928084056
.320	162.637012056
.480	157.151892056
.640	149.472724056
.800	139.599508056
.960	127.532244056
1.120	113.270932056
1.280	96.8155720563
1.440	78.1661640563
1.600	57.3227080563

* *

* *
TEMPERATURE DISTRIBUTION ALONG THE LENGTH OF THE CRYSTAL
AT CYSTAL SURFACE

DISTANCE FROM ENTRANCE (cm)	TEMPERATURE (degree C)
0.000	54.4
.750	54.9845416113
1.500	55.5690832225
2.250	56.1536248338
3.000	56.738166445
3.750	57.3227080563
4.500	57.9072496676
5.250	58.4917912788
6.000	59.0763328901
6.750	59.6608745013
7.500	60.2454161126

* *

J. References

1. Z.J. Kiss, H.R. Lewis, and R.C. Duncan, Jr. "Sun Pumped Continuous Optical Lasers" Appl. Phys. Lett. 2(5), 93 (1963).

2. G.R. Simpson, "Continuous Sun-Pumped Room Temperature Glass Laser Operation" Appl. Optics, 3(6), 783 (1964).

3. G.W. Reno, "Solar-Pumped Modulated Laser", RCA Review, pp. 149, March 1966.

4. C.G. Young, "A Sun-Pumped cw One-Watt Laser" Appl. Optics, 5(6), 993 (1966).

5. L. Huff, "Sun-Pumped Laser" Final Report, AFAL-TR-72-310, Sept. 1972.

6. J. Falk, L. Huff, and J.D. Taynai, "Solar-Pumped, Mode-Locked, Frequency Doubled Nd:YAG Laser" Appl. Optics, 15(6), 1383 (1976).

7. D. Radeck, E. Reed, and C. Chadwick, "Sun-Pump and Lamp-Pump Nd:YAG Lasers for Space Communications" SPIE Vol. 150, Laser & Fiber Optics Communications, 23 (1978).

8. V.M. Batenin, A.L. Golger, and I.I. Klimovskii, "Feasibility of a solar-radiation-pumped color-center crystal laser" Sov. J. Quantum Electronics, 11(3), 382 (1981).

9. H. Arashi, Y. Oka, and N. Sasahara, "A solar-pumped cw 18 W Nd:YAG laser" Jap. J. Appl. Phys. 23, 1051 (1984).

10. M. Weksler, J. Shawrtz, and Weizmann, "Solar-pumped Nd:YAG Laser Produces High Output" Laser Focus/Electro-optics, 22(10), 46 (1986).

11. L. Zapata, private communications (1986).

12. W. Koechner, "Solid State Laser Engineering" Springer-Verlag, New York, 1976.

13. J.C. McCathy, M.G. Knights, and E.P. Chicklis "Laser Performance of Nd:YLF" Proceedings of SPIE VOl. 335, Advanced Laser Technology and Applications, Arlington, VA, May 6-7 (1982) pp. 2.

14. J.E. Murray, "Pulsed Gain and Thermal Lensing of Nd:YLF_4" IEEE J. Quantum Electronics, QE-19(4), 488 (1983).

15. E.J. Sharp, D.J. Horowitz, and J.E. Miller, "High-Efficiency Nd^{3+}:L_iYF_4 Laser" J. Appl. Phys., 44(12), 5399 (1973).

16. D. LeGoff, A. Bettinger, and A. Labadens, "ETUDE D'UN OSCILLATEUR A BLOCAGE DE MODES UTILISANT UN CRYSTAL DE $LiYF_4$ DOPE AU NEODYME" Optics Comm. 26(1), 108 (1978).

17. T.M. Pollak, W.F. Wing, R.J. Grasso, E.P. Chicklis, and H.P. Jensen, "CW Laser Operation of Nd:YLF" IEEE J. Quantum Electronics, QE-18(2), 159 (1982).

18. M.D. Thomas, M.G. Knight, and E.P. Chicklis, "High Gain Nd:YLF Amplifier" Proc. of SPIE Vol. 622, High Power and Solid State Lasers, Los Angeles, CA, Jan. 23-24 (1986), pp. 142.

19. A. L. Harmer, A. Linz and D. R. Gabbe, "Fluorescence of Nd^{3+} in Lithium Yttrium Fluoride" J. Phys. Chem. Solids, 30, 148 (1969).

20. T. Y. Fan, G. J. Dixon, and R. L. Byer, "Efficient GaAlAs diode-laser-pumped operation of Nd:YLF at 1.047 um with intracavity doubling to 523.6nm" Optics Lett. 11 (4), 204 (1986).

21. G. A. Rines, M. D. Thomas, M. G. Knights, and E. P. Chicklis, "Laser Performance of Nd:YLF at 1.3um" Conference on Laser and electro-Optics (CLEO), Baltimore, Md, May 21-24 (1985) Session WJ2.

22. H. P Jesson, D. R. Gabbe, A. Linz, and C. S. Naiman, "Spectral Diversity Crystalline Fluoride Lasers" Proc. of the International Conf. on Laser '81, New Orleans, Luisiana, Dec. 14-18, 1981.

23. T. Duvillier, J. Luce and A Diard, "Simple Numerical Control Loop for Stabilizing Nd:YLF Single-Mode Oscillators" Optics Comm., 59 (2), 127 (1986).

24. D. Pruss, G. Huber, A. Beioivski, V. V. Lapter, I. A. Shcherbakov, and Y. V. Zharikov, "Efficient Cr^{3+} Sensitized Nd^{3+} :GdScGa-Garnet Laser at 1.06um" Appl. Phys. B. 28, 355 (1982).

25. E. Reed, "A Flashlamp-Pumped, Q-switched Cr:Nd:GSGG Laser" IEEE J. of Quantum Electronics, QE-21 (10), 1625 (1985).

26. E. V. Zharikov, N. N. Ilichev, V. V. Laptev, A. A. Maylutin, V. G. Ostroumov, P. P. Pashinin, A. S. Pimenov, V. A. Smirnov, and I. A. Shcherbakov, "Spectral, luminescence, and lasing properties of gadolinium garnet crystals activated with neodymium and chromium ions" Sov. J. Quantum Electronics, 13 (1), 82 (1983).

27. Laporta, V. Magni, and O. Svelto, "Comparative Study of the Optical Pumping Efficiency in Solid-State Lasers" IEEE. J. of Quantum Electronics QE-21 (8), 122 (1985).

28. S. Stokowski, J. Caird, M. Shinn, L. Smith, and R. Wilder, "GSGG Crystal Growth and Quality: A Status Report" Optical Science and Engineering Series 6. AIP. Conf. Proc. 146 New York (1986), Editors: W. C. Stwally and M. Lapp.

29 W. F. Krupke, "Modern Solid State Laser Materials" Report UCID-20119 (1984) Order No. DE 85003665.

30. E. V. Zharikov, et. al, "Output characterizaiton of a gadolinium scandium gallium garnet laser operating in the pulse-periodic regime" Sov. J. Quantum Electronics 13 (10), 1306 (1983).

31. J. Buchort, and R. R. Afano, "Emerald-A New Gem Laser Material" Laser Focus Electro-Optics, pp.117 Sept. (1983).

32. A. Budgor, "Overview of Chromium Doped Tunable Vibronic Lasers" Proc. SPIE. Vol. 461 New Lasers for Analytical and Industrial Chemistry pp.62 (1984).

33. J. C. Walling, O. G. Peterson, H. P. Jessen, R. C. Morris, and E. W. O'Dell, "Tunable Alaxandrite Lasers" IEEE. J. of Quantum Electronics, QE-16 (12), 1303 (1980).

34. M. L. Shand and S. T. Lai, "CW Laser Pumped Emerald laser" IEEE J. of Quantum Electronics, QE-20 (2), 105 (1984).

35. S. T. Lai, "Review of Spectroscopic and Laser Properties of Emerald" SPIE Vol. 622 High Power and Solid State Lasers, 146 (1986).

36. D. D. Venable and L. Brown in Hampton University, by Private Communications (1987).

37. W. Koechner, "Absorbed Pump Power, Thermal Profile and Stresses in CW Pumped Nd:YAG Crystal" Appl. Optics, 9 (6) 1429 (1970).

38. J. H. Lee and W. R. Weaver, "A Solar Simulator-Pumped Atomic Iodine Laser" Appl.. Phys. Lett. 39 (2), 137 (1981).

III. Kinetic Modeling of Solar-Pumped Iodine Laser

This report relates the work performed during the period of Sept. 1, 1986 through February 28, 1987. During this time, the work to construct a kinetic model algorithm which predicts the output parameters of a solar-pumped iodine laser (lasing time, time to threshold, and pulse energy) has progressed. To this date the kinetic model has improved such that there is good agreement between the theoretical model and the experimental data for the system, defined in the previous progress report as flashlamp-pumped iodine laser oscillator system (characterized by a cylindrical resonator cavity and pumping times of about one millisecond). The three experimental data sets given graphically in Fig. 1, 2, and 3 are for three iodides i-C_3F_7I, n-C_4F_9I, and t-C_4F_9I used as lasants in this experimental setup. The subsequent kinetic rates found for the different gases are given in Table I. These kinetic rates are important to establish scalability for space to space power transmission. By introducing the heat equation, a diffusion time constant, the pumping rates, and the photodissociation cross-section for the three iodides (May 1986 Progress Report) into the kinetic model (NASA TP-2241); the model has been modified to incorporate a cylindrical laser cavity.

Of the three lasants the rate coefficients have been best identified for i - C_3F_7I; and as reported previously with in experimentally found bounds for these coefficients, a best fit is found for the data given by this experiment. To find the best fit to the experimental data by the theoretical model an initial I_2 density is introduced as a function of fill pressure (Oct. 1986 Progress Report) for the three lasants. In Fig. 2 and 3 for the gases n - C_4F_9I and t - C_4F_9I, the initial I_2 density is retained and C_3, C_4, and Q_2 (Table I) are kept constant in the theoretical model, thereby a best fit to the data using the information known about the two iodides is found by adjusting the rate coefficients. Therefore, the reaction rates are identified in the same system with similar initial conditionsgiving the comparative reaction rates which are tabulated in Table I.

Of the three iodides the least is known about the rate coefficients for n - C_4F_9I. In spite of this, very good agreement has been obtained between the theoretical predictions and the experimental data (Fig. 2) for this gas. The predicted lasing times are shorter than that given by experiment, but Fig. 7, 8, and 9 show good agreement with the theoretical power output and the

experimental data for the power output, except very late in the pulse. The difference very late in the pulse implies a pumping mechanism which remains to be included in the model, wall effects are being investigated.

The iodide t - C_4F_9I has been identified as the preferable lasant material. As the reaction rates demonstrate (Table I), this lasant recycles easier since the recombination rate to the parent molecule is higher and the formation of the radical dymer is relatively small. In Fig. 3 the time to threshold predicted by the model is later than that of the experimental data for the gas t - C_4F_9I. This implies that there is an omission in theoretical model using the rate coefficients found thus far. On ther hand, as shown in Fig. 10, 11 and 12, the power output as a function of time agrees with the experimental data as the pulse decays. This problem is being investigated and will be reported later. (Probably initial I_2 density is too large since the system maybe cleaner.)

To identify the relative contribution of a specific reaction upon the gain in the medium, the derivative of the inversion density as a functionof pulse duration divided by the sum of the photodissociation rates is given in Fig. 13 through 21 for the three gases and or different fill pressure. For instance, for the reaction

$$I^* + R \xrightarrow{k_1} RI$$

$$d\,I/dt = -K_1\,[I^*]\,[R]$$

Where the negative sign indicates a loss of inversion density, where as, a positive sign would have indicated a pumping reaction. The relative peak value for each rate is given in the key along with the reaction's sign (+ or -). If the contribution is bleow 10^{-5}, it is omitted from the graph. Also shown is the theoretical prediction for the power output normalized to one and given in the key is the peak power (W/cm^2). These graphs show explicitly that quenching by I_2 turns off the laser - a reaction that increases at higher pressures. Furthermore, the graphs give the relative size of the contribution of each of the reactions to the inversion density.

Upon examination of Fig. 1, 2 and 3, it can be seen that by adjusting the rate coefficients within the known bounds as reported previously in literature good agreement is found for the theoretical prediction of experimental data.

Therefore, a comparison of the important rate coefficients is accomplished (Tabel I) for these three iodides in the experiment design stated above. In addition, the theoretical model as found is used to indicate graphically the individual contribution by each of the chemical reactions to the inversion density of the lasant, showing the relative magnitudes and times the reaction contributes to the output power of the laser.

It remains to simulate multiple pumping pulses using the same gas fill for different pressures and comparing the theoretical results to the experimental data. This would further characterize the I_2 diffusion and the wall reactions in addition to be her understanding the kinetics. After this is accomplished and using the information about the kinetic rates, the model will be modified to predict data for other experimental systems. This will further define the reaction kinetics of three iodides (i - C_3F_7I, t - C_4F_9I, and n - C_4F_9I) and allow the establishment of scalability of the solar-pumped iodine laser for space-power applications.

Table I- Reaction rate coefficients found by fitting the data shown in figure 1, 2, and 3. The reaction rates found are within previously published values.

Symbol	Reaction	Reaction rate coefficient, $(cm^3)^n/sec$		
		$R = i\text{-}C_3F_7$	$R = n\text{-}C_4F_9$	$R = t\text{-}C_4F_9$
K_1	$R + I^* = RI$	3.48×10^{-12}	7.75×10^{-14}	1.66×10^{-12}
K_2	$R + I = RI$	1.38×10^{-11}	2.88×10^{-11}	1.49×10^{-11}
K_3	$R + R = R_2$	4.15×10^{-12}	6.05×10^{-12}	3.56×10^{-14}
K_4	$R + RI = R_2 + I$	7.66×10^{-17}	7.76×10^{-17}	7.58×10^{-17}
K_5	$I_2 + R = RI + I$	6.27×10^{-13}	1.94×10^{-13}	2.34×10^{-12}
C_1	$I^* + I + RI = I_2 + RI$	1.09×10^{-33}	1.11×10^{-33}	1.09×10^{-33}
C_2	$I + I + RI = I_2 + RI$	2.42×10^{-32}	2.76×10^{-32}	2.28×10^{-32}
C_3	$I^* + I + I_2 = I_2 + I_2$	8×10^{-32}	8×10^{-32}	8×10^{-32}
C_4	$I + I + I_2 = I_2 + I_2$	3.8×10^{-30}	3.8×10^{-30}	3.8×10^{-30}
Q_1	$I^* + RI = I + RI$	1.08×10^{-16}	1.17×10^{-15}	8.45×10^{-16}
Q_2	$I^* + I_2 = I + I_2$	4.96×10^{-11}	4.96×10^{-11}	4.96×10^{-11}

List of Figures

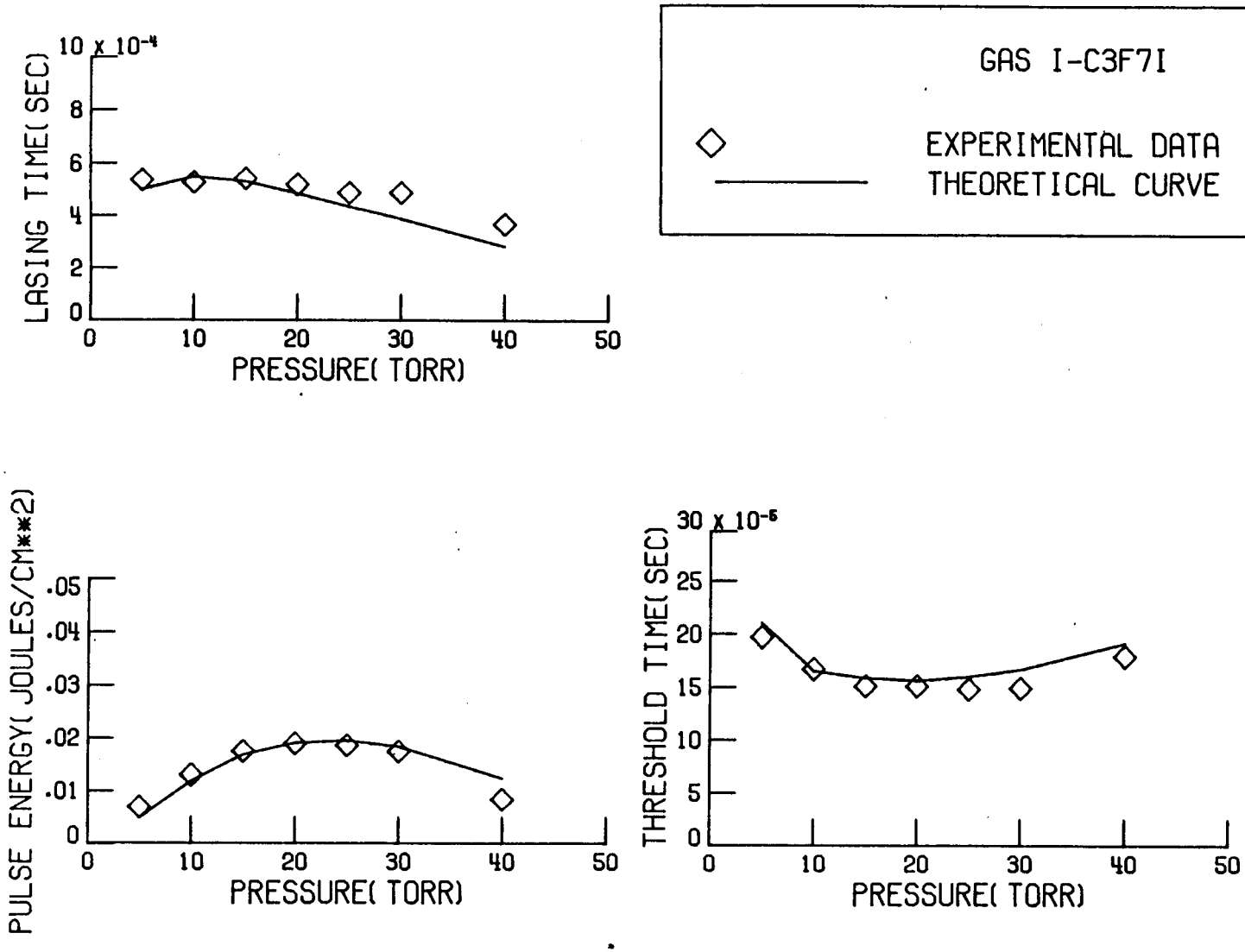
GAS I-C3F7I
EXPERIMENTAL DATA
THEORETICAL CURVE
LASING TIME(SEC)
10 x 10⁻⁴
8
6
4
2
0
0
10
20
30
40
50
PRESSURE(TORR)
PULSE ENERGY(JOULES/CM**2)
.05
.04
.03
.02
.01
0
PRESSURE(TORR)
THRESHOLD TIME(SEC)
30 x 10⁻⁵
25
20
15
10
5
0
PRESSURE(TORR)

Figure 1

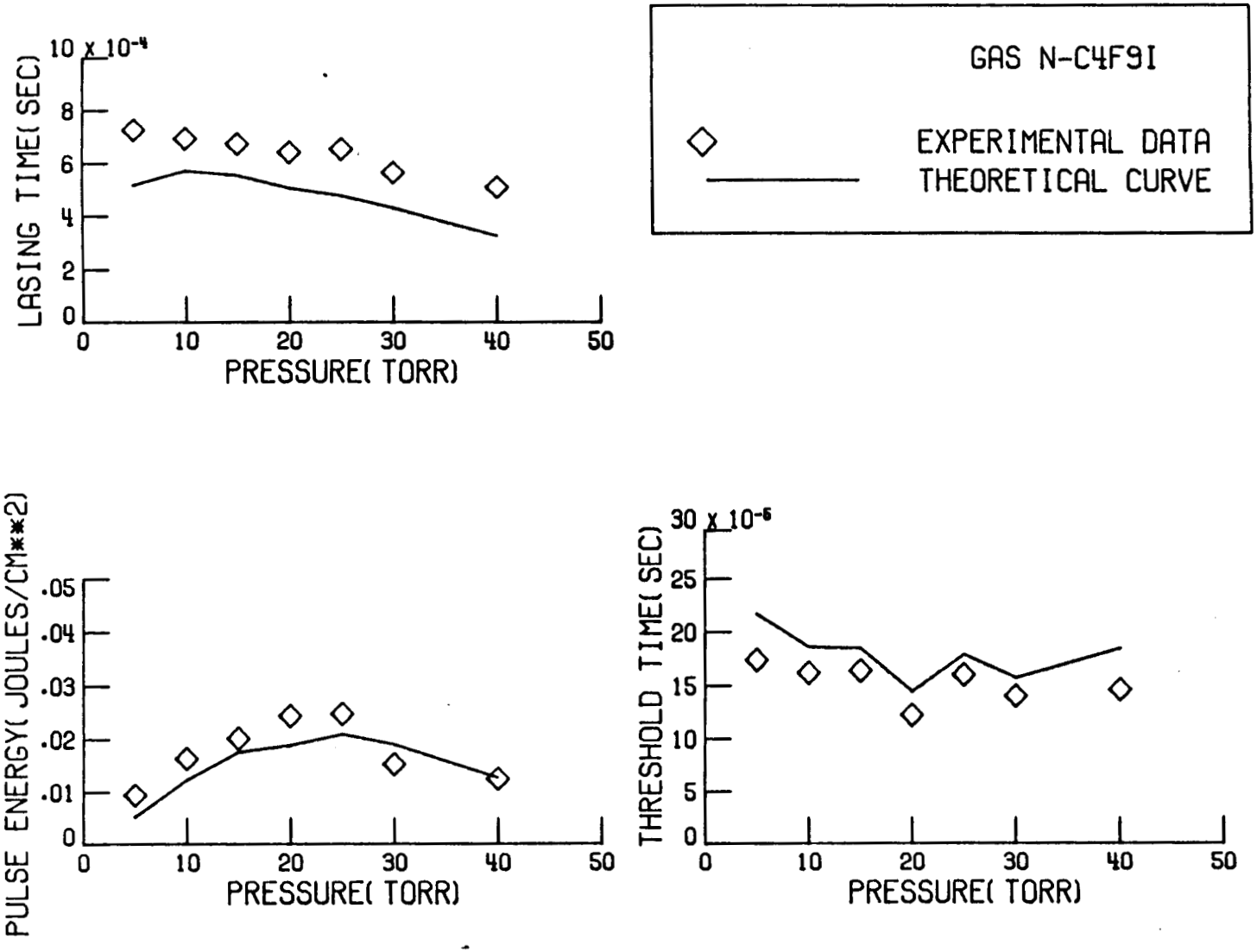
GAS N-C4F9I
EXPERIMENTAL DATA
THEORETICAL CURVE
LASING TIME(SEC)
10 X 10⁻⁴
8
6
4
2
0
0
10
20
30
40
50
PRESSURE(TORR)
PULSE ENERGY(JOULES/CM**2)
.05
.04
.03
.02
.01
0
PRESSURE(TORR)
THRESHOLD TIME(SEC)
30 X 10⁻⁶
25
20
15
10
5
0
PRESSURE(TORR)

Figure 2

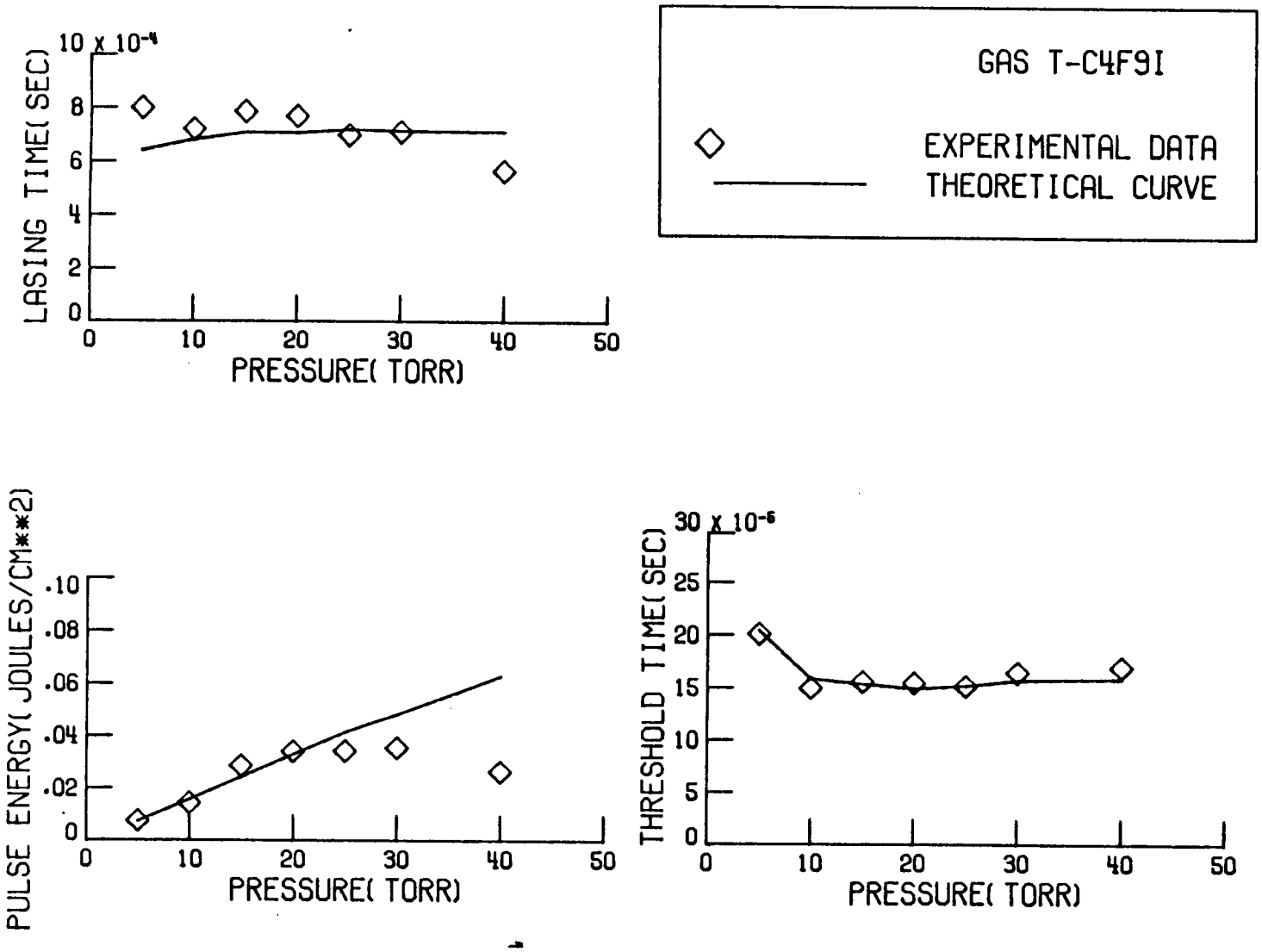
GAS T-C4F9I
EXPERIMENTAL DATA
THEORETICAL CURVE
LASING TIME(SEC)
10 X 10⁻⁶
PRESSURE(TORR)
PULSE ENERGY(JOULES/CM**2)
THRESHOLD TIME(SEC)
30 X 10⁻⁶

Figure 3

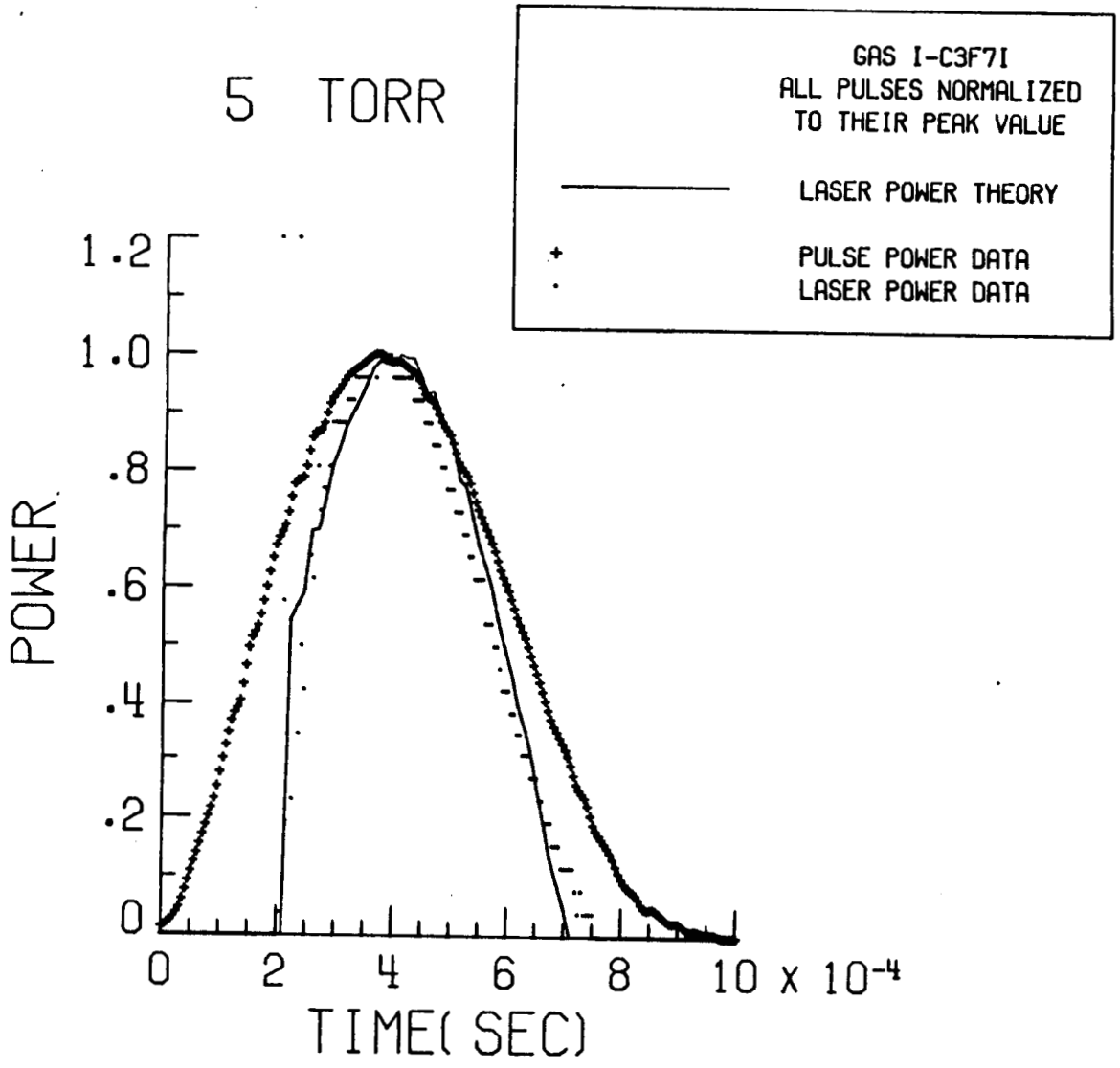
5 TORR
GAS I-C3F7I
ALL PULSES NORMALIZED
TO THEIR PEAK VALUE
LASER POWER THEORY
PULSE POWER DATA
LASER POWER DATA
POWER
1.2
1.0
.8
.6
.4
.2
0
0
2
4
6
8
10 X 10-4
TIME(SEC)

Figure 4

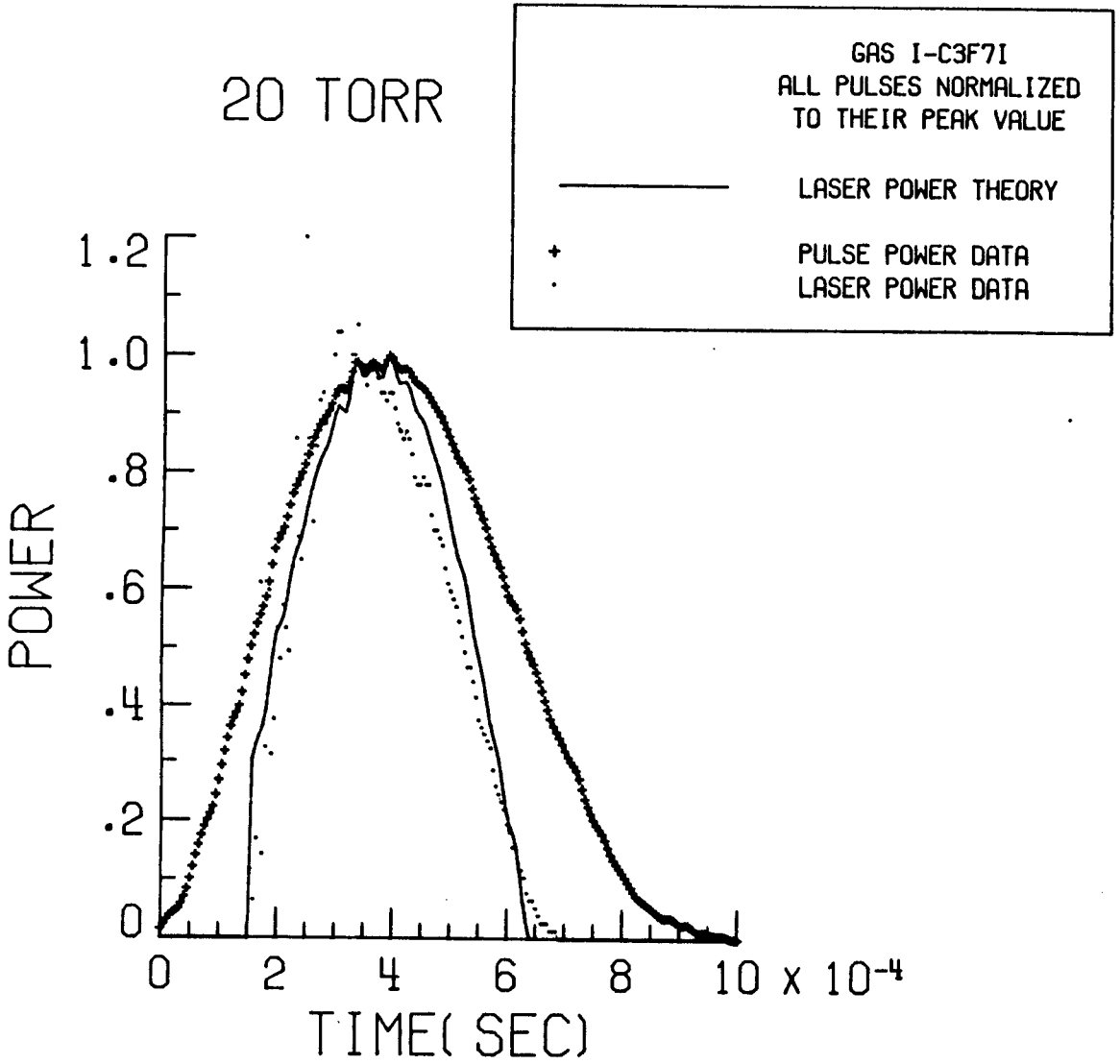
20 TORR
GAS I-C3F7I
ALL PULSES NORMALIZED
TO THEIR PEAK VALUE
LASER POWER THEORY
PULSE POWER DATA
LASER POWER DATA
POWER
1.2
1.0
.8
.6
.4
.2
0
0
2
4
6
8
10 X 10-4
TIME(SEC)

Figure 5

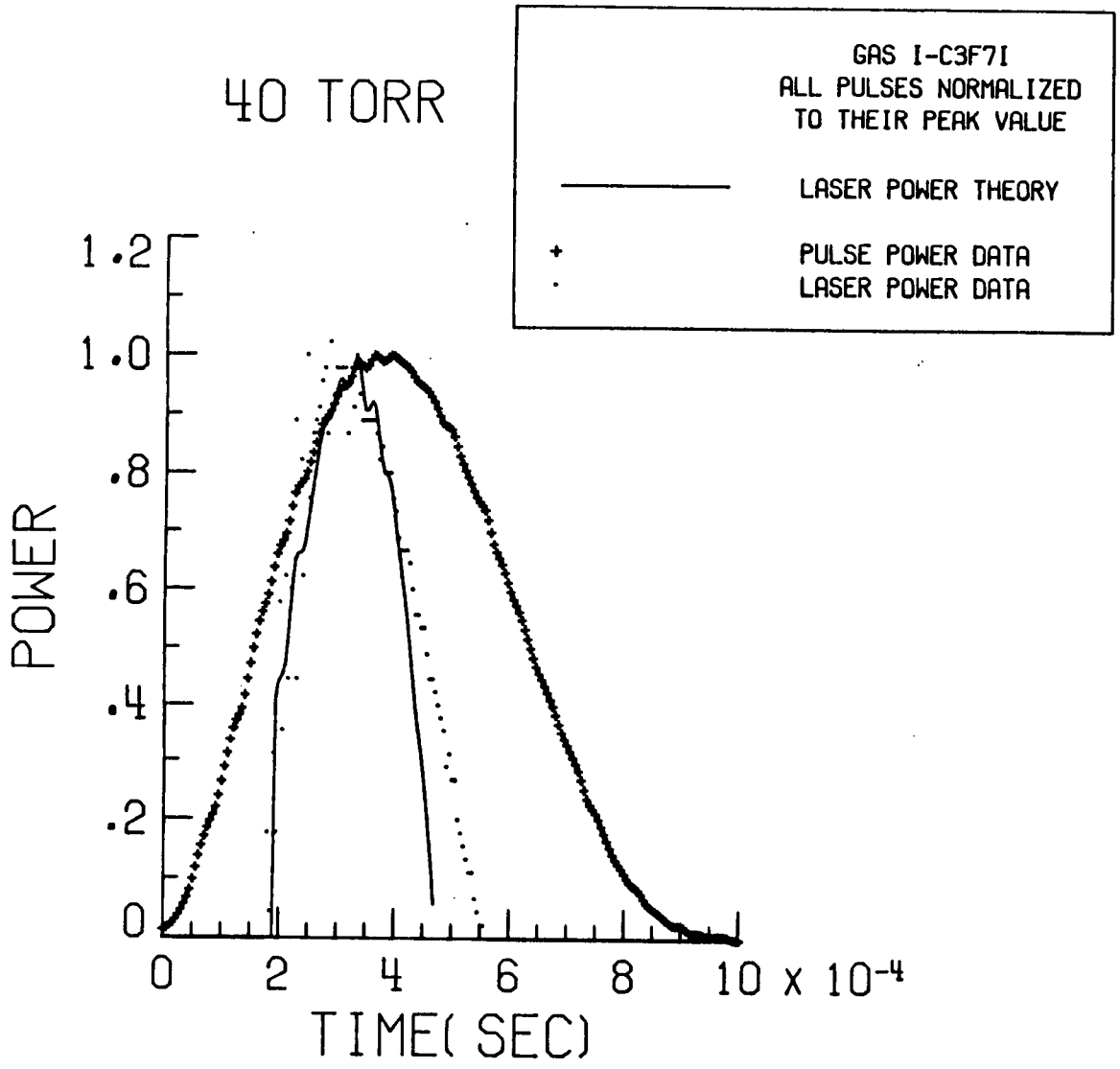
40 TORR
GAS I-C3F7I
ALL PULSES NORMALIZED
TO THEIR PEAK VALUE
LASER POWER THEORY
PULSE POWER DATA
LASER POWER DATA
POWER
1.2
1.0
.8
.6
.4
.2
0
0
2
4
6
8
10 X 10-4
TIME(SEC)

Figure 6

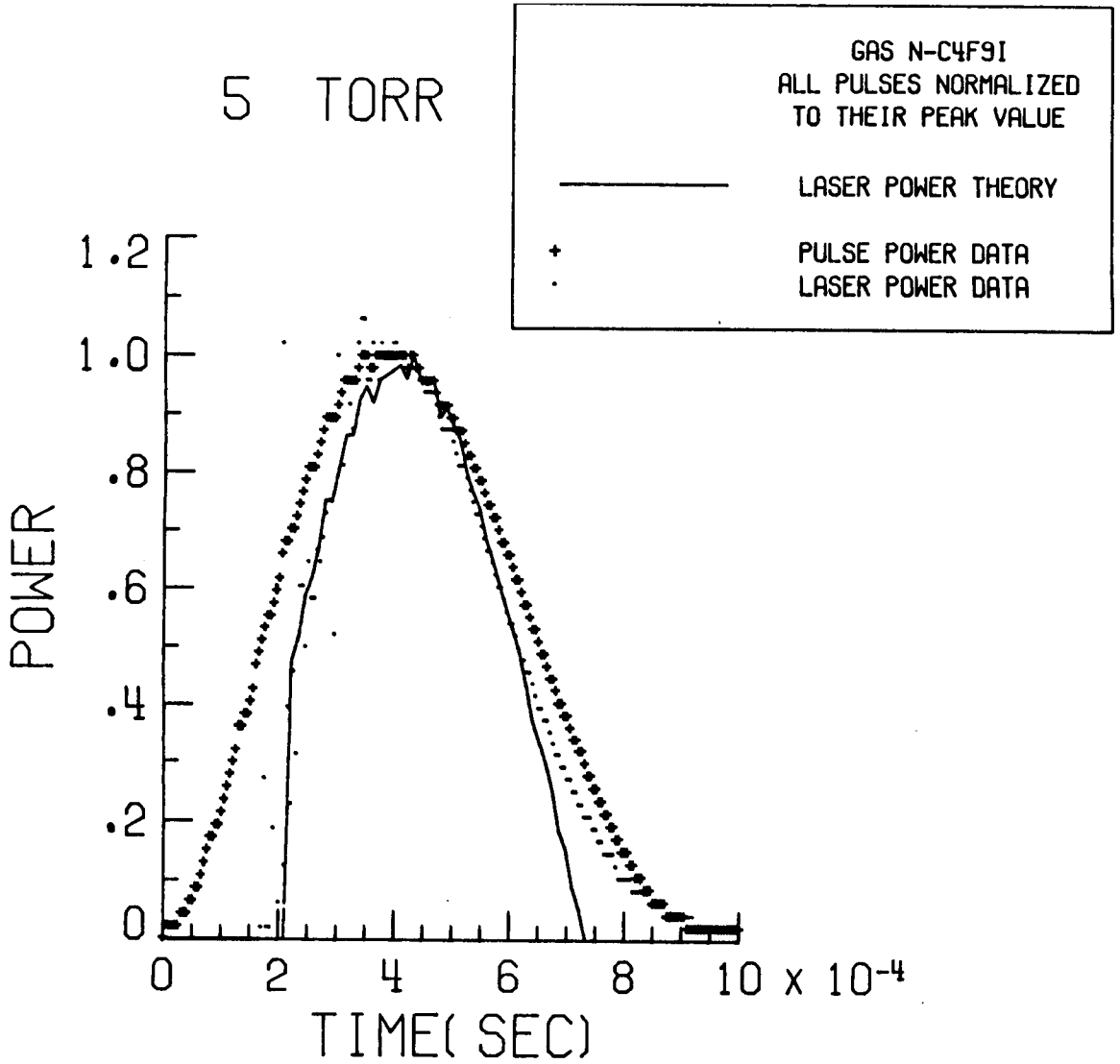
5 TORR
GAS N-C4F9I
ALL PULSES NORMALIZED
TO THEIR PEAK VALUE
LASER POWER THEORY
PULSE POWER DATA
LASER POWER DATA
POWER
1.2
1.0
.8
.6
.4
.2
0
0
2
4
6
8
10 X 10-4
TIME(SEC)

Figure 7

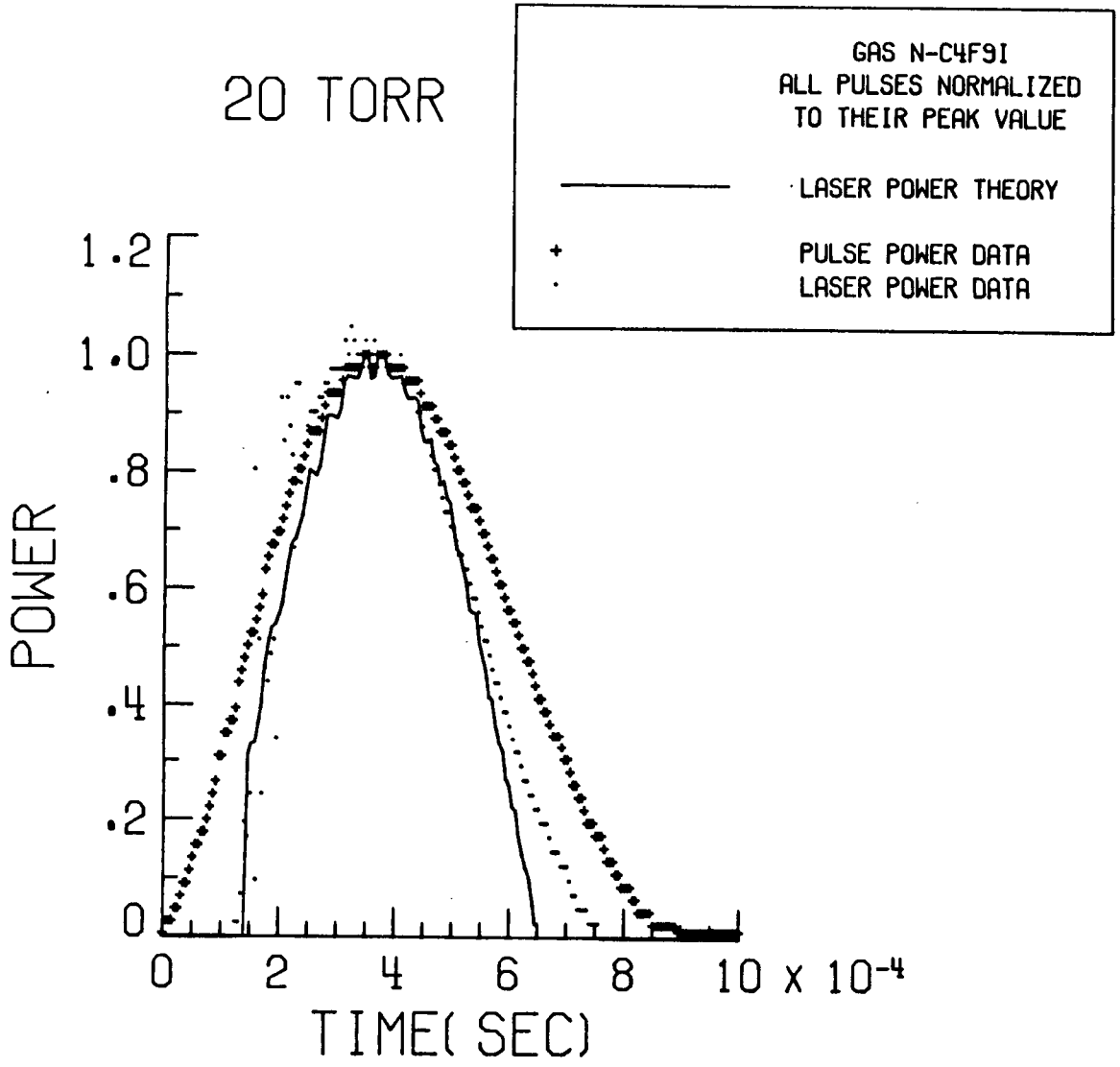
20 TORR
GAS N-C4F9I
ALL PULSES NORMALIZED
TO THEIR PEAK VALUE
LASER POWER THEORY
PULSE POWER DATA
LASER POWER DATA
POWER
1.2
1.0
.8
.6
.4
.2
0
0
2
4
6
8
10 X 10-4
TIME(SEC)

Figure 8

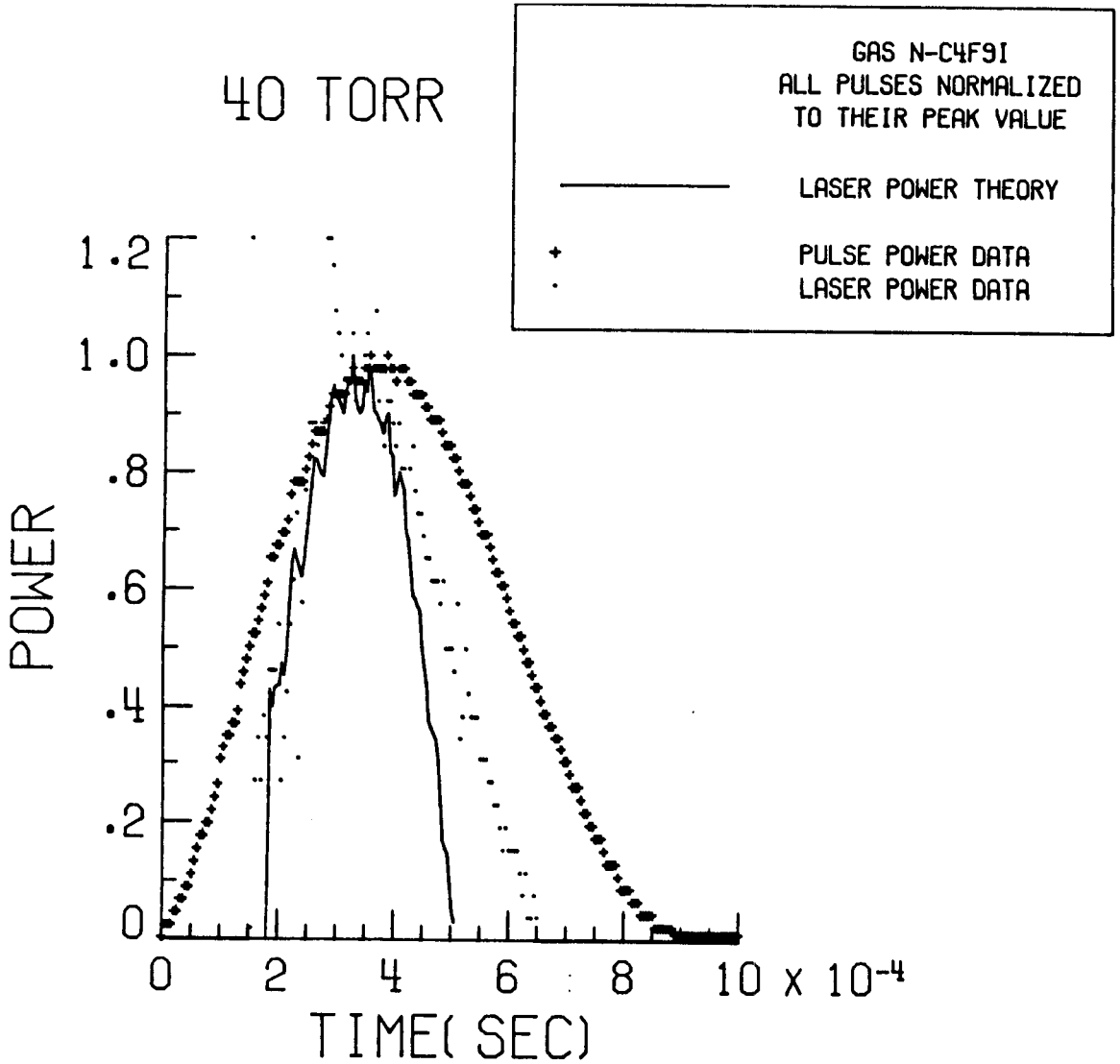
40 TORR
GAS N-C4F9I
ALL PULSES NORMALIZED
TO THEIR PEAK VALUE
LASER POWER THEORY
PULSE POWER DATA
LASER POWER DATA
POWER
1.2
1.0
.8
.6
.4
.2
0
0
2
4
6
8
10 X 10-4
TIME(SEC)

Figure 9

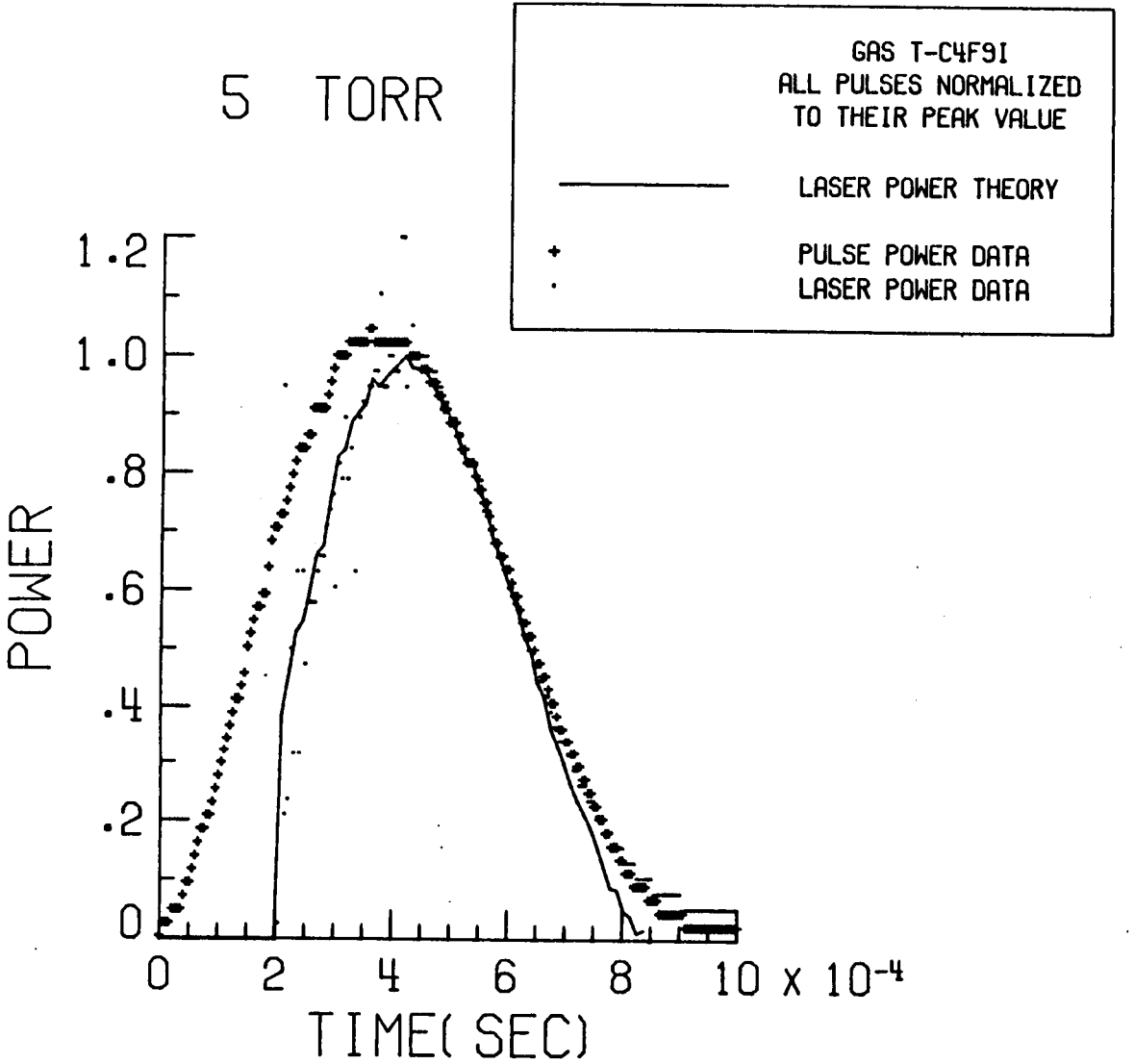
5 TORR
GAS T-C4F9I
ALL PULSES NORMALIZED
TO THEIR PEAK VALUE
LASER POWER THEORY
PULSE POWER DATA
LASER POWER DATA
POWER
1.2
1.0
.8
.6
.4
.2
0
0
2
4
6
8
10 X 10-4
TIME(SEC)

Figure 10

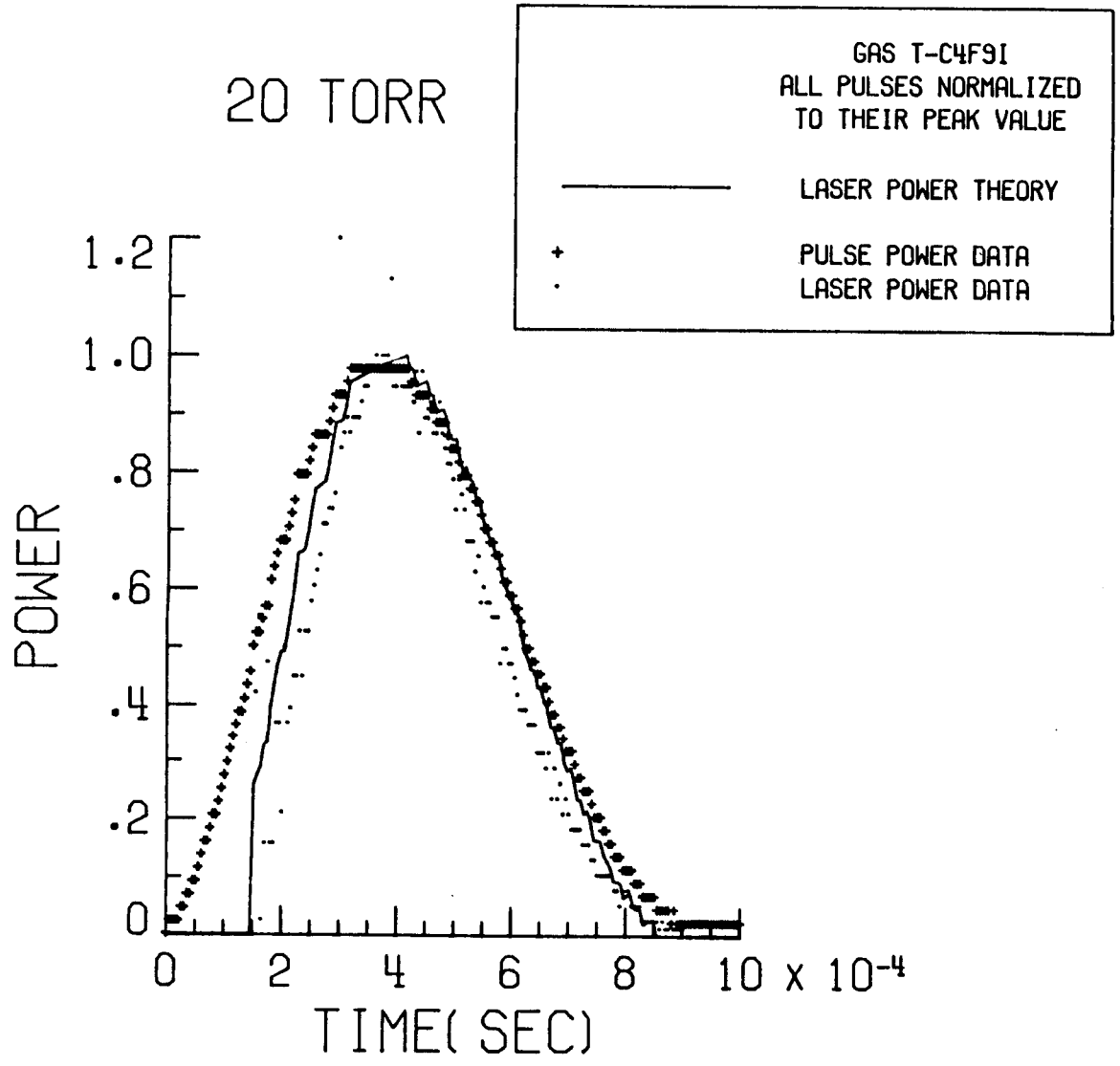
20 TORR
GAS T-C4F9I
ALL PULSES NORMALIZED
TO THEIR PEAK VALUE
LASER POWER THEORY
PULSE POWER DATA
LASER POWER DATA
POWER
1.2
1.0
.8
.6
.4
.2
0
0
2
4
6
8
10 X 10-4
TIME(SEC)

Figure 11

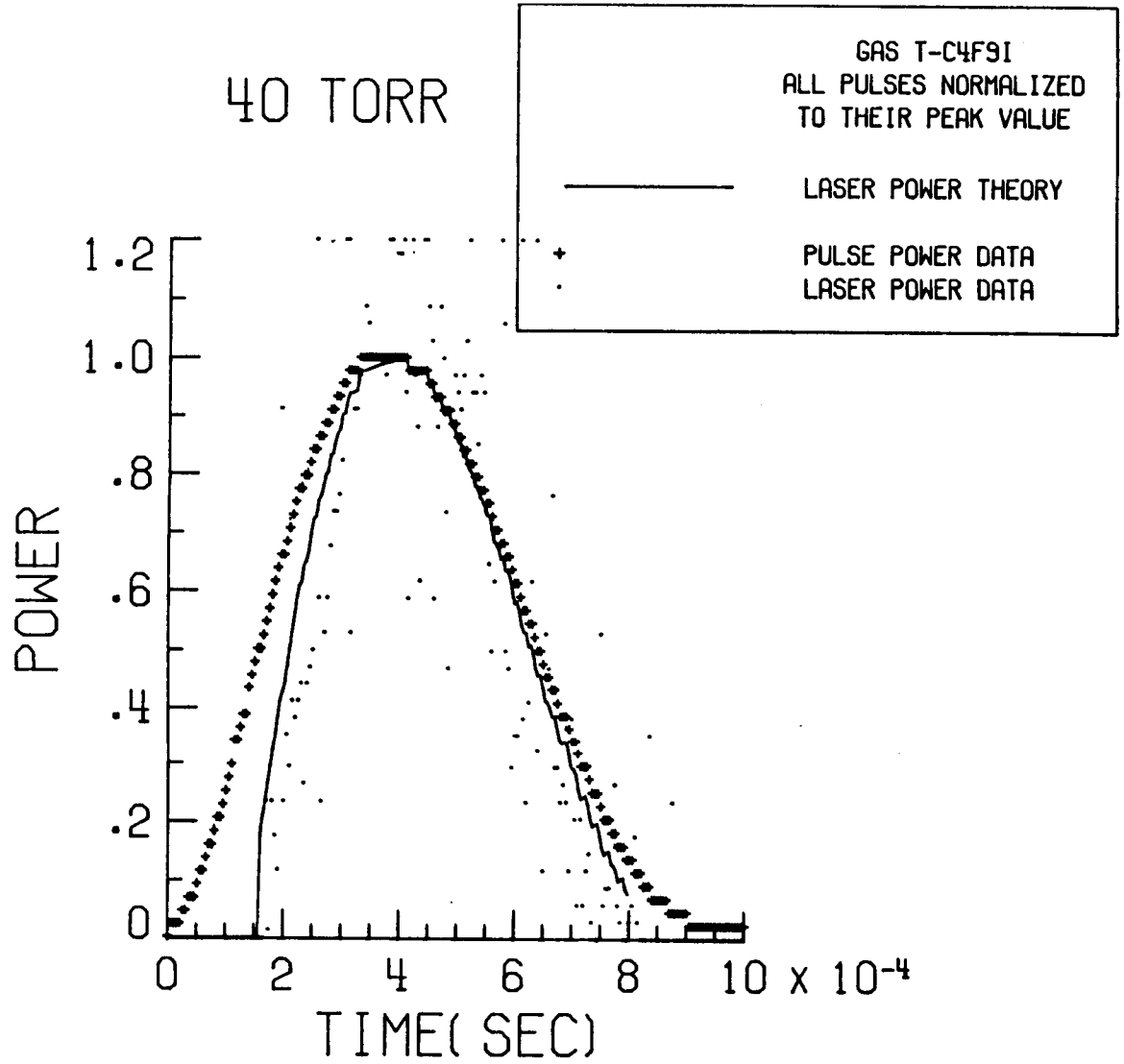
40 TORR
GAS T-C4F9I
ALL PULSES NORMALIZED
TO THEIR PEAK VALUE
LASER POWER THEORY
PULSE POWER DATA
LASER POWER DATA
POWER
1.2
1.0
.8
.6
.4
.2
0
0
2
4
6
8
10 X 10-4
TIME(SEC)

Figure 12

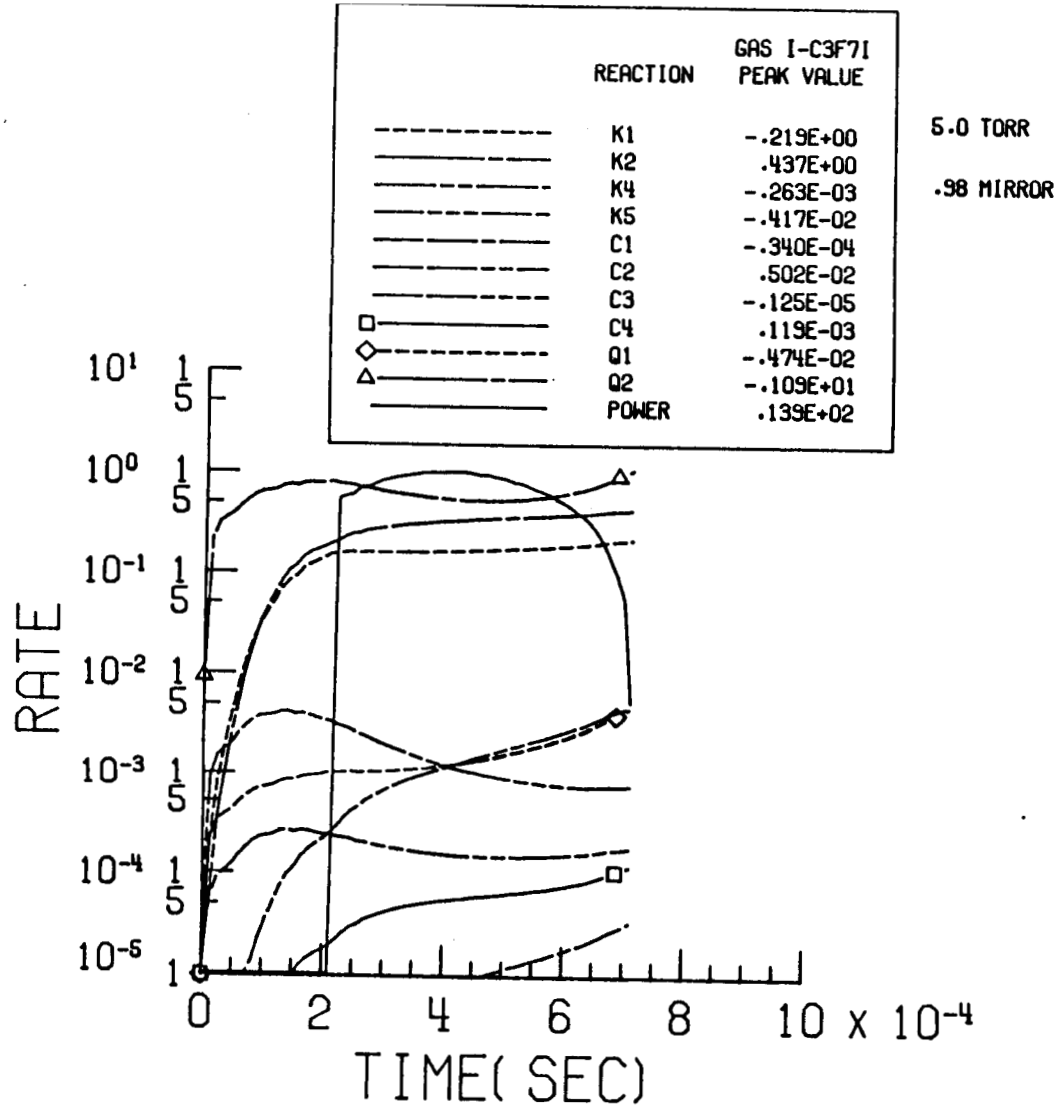
REACTION
GAS I-C3F7I
PEAK VALUE
K1 -.219E+00
K2 .437E+00
K4 -.263E-03
K5 -.417E-02
C1 -.340E-04
C2 .502E-02
C3 -.125E-05
C4 .119E-03
Q1 -.474E-02
Q2 -.109E+01
POWER .139E+02
5.0 TORR
.98 MIRROR
RATE
10^{1}
10^{0}
10^{-1}
10^{-2}
10^{-3}
10^{-4}
10^{-5}
1/5
0
2
4
6
8
10 x 10^{-4}
TIME(SEC)

Figure 13

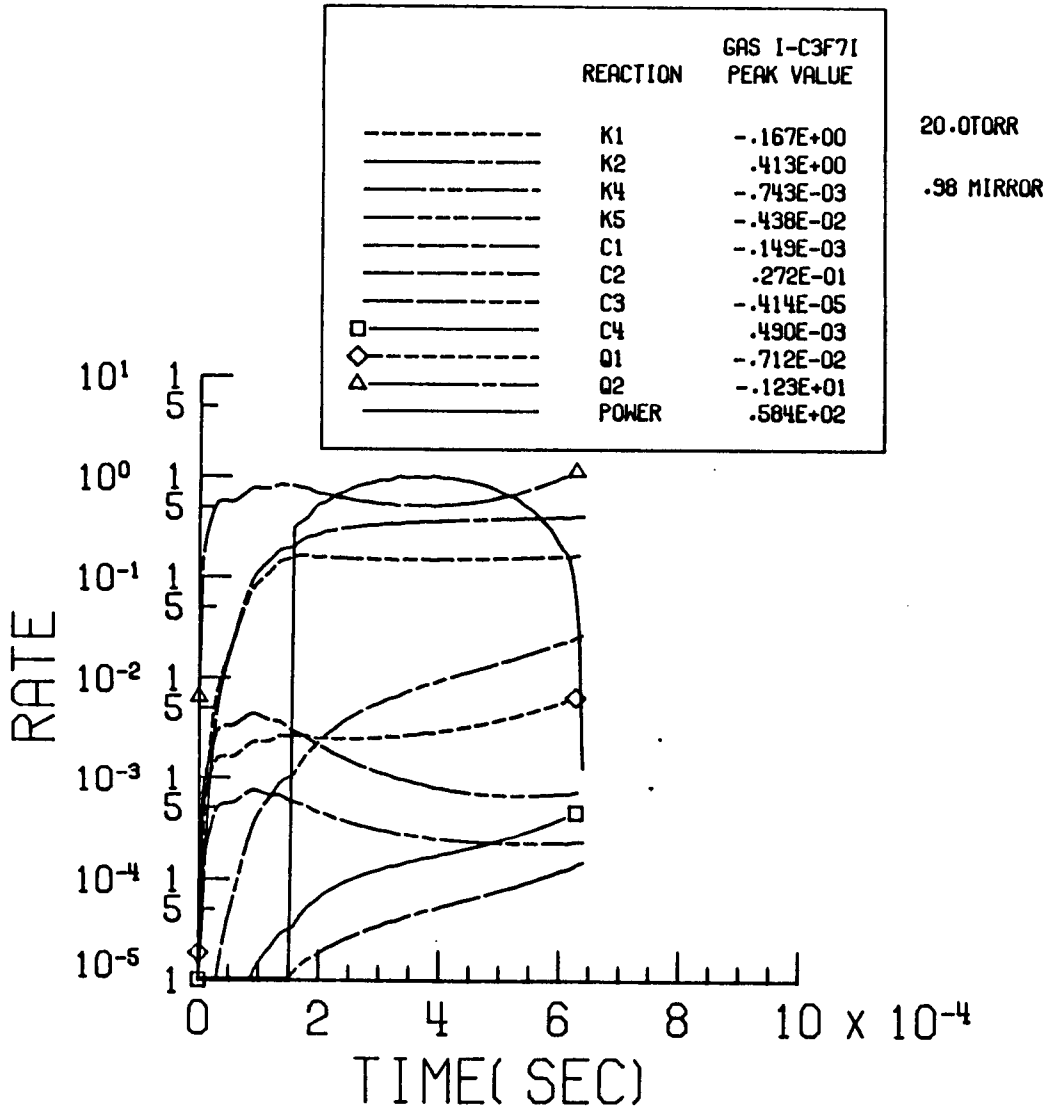
REACTION
GAS I-C3F7I PEAK VALUE
K1 -.167E+00
K2 .413E+00
K4 -.743E-03
K5 -.438E-02
C1 -.149E-03
C2 .272E-01
C3 -.414E-05
C4 .490E-03
Q1 -.712E-02
Q2 -.123E+01
POWER .584E+02
20.0TORR
.98 MIRROR
RATE
10^{1}
10^{0}
10^{-1}
10^{-2}
10^{-3}
10^{-4}
10^{-5}
1/5
0 2 4 6 8 10 x 10^{-4}
TIME(SEC)

Figure 14

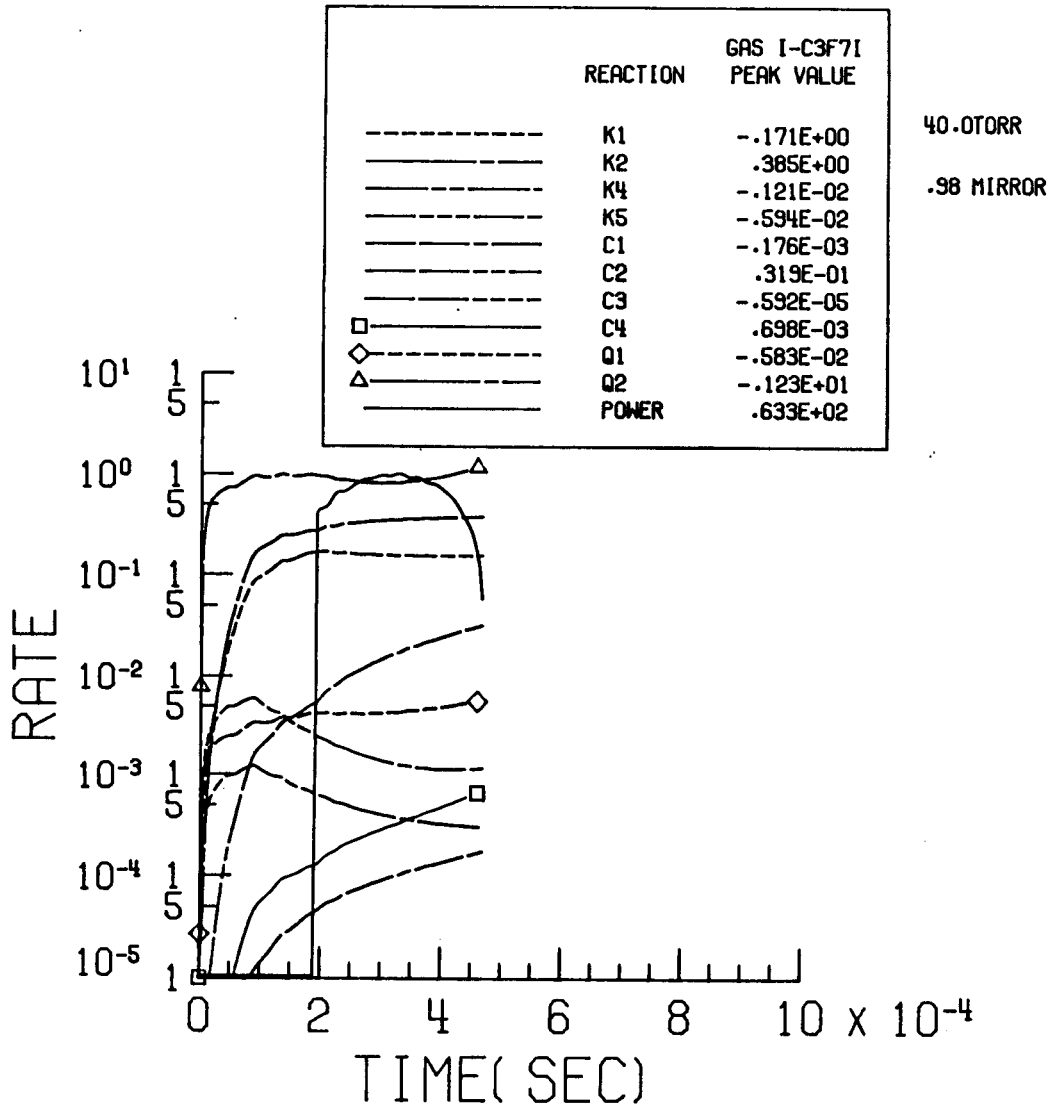
GAS I-C3F7I
REACTION
PEAK VALUE
K1 -.171E+00
K2 .385E+00
K4 -.121E-02
K5 -.594E-02
C1 -.176E-03
C2 .319E-01
C3 -.592E-05
C4 .698E-03
Q1 -.583E-02
Q2 -.123E+01
POWER .633E+02
40.0TORR
.98 MIRROR
RATE
10^{1} 10^{0} 10^{-1} 10^{-2} 10^{-3} 10^{-4} 10^{-5}
1/5
1
0 2 4 6 8 10 x 10^{-4}
TIME(SEC)

Figure 15

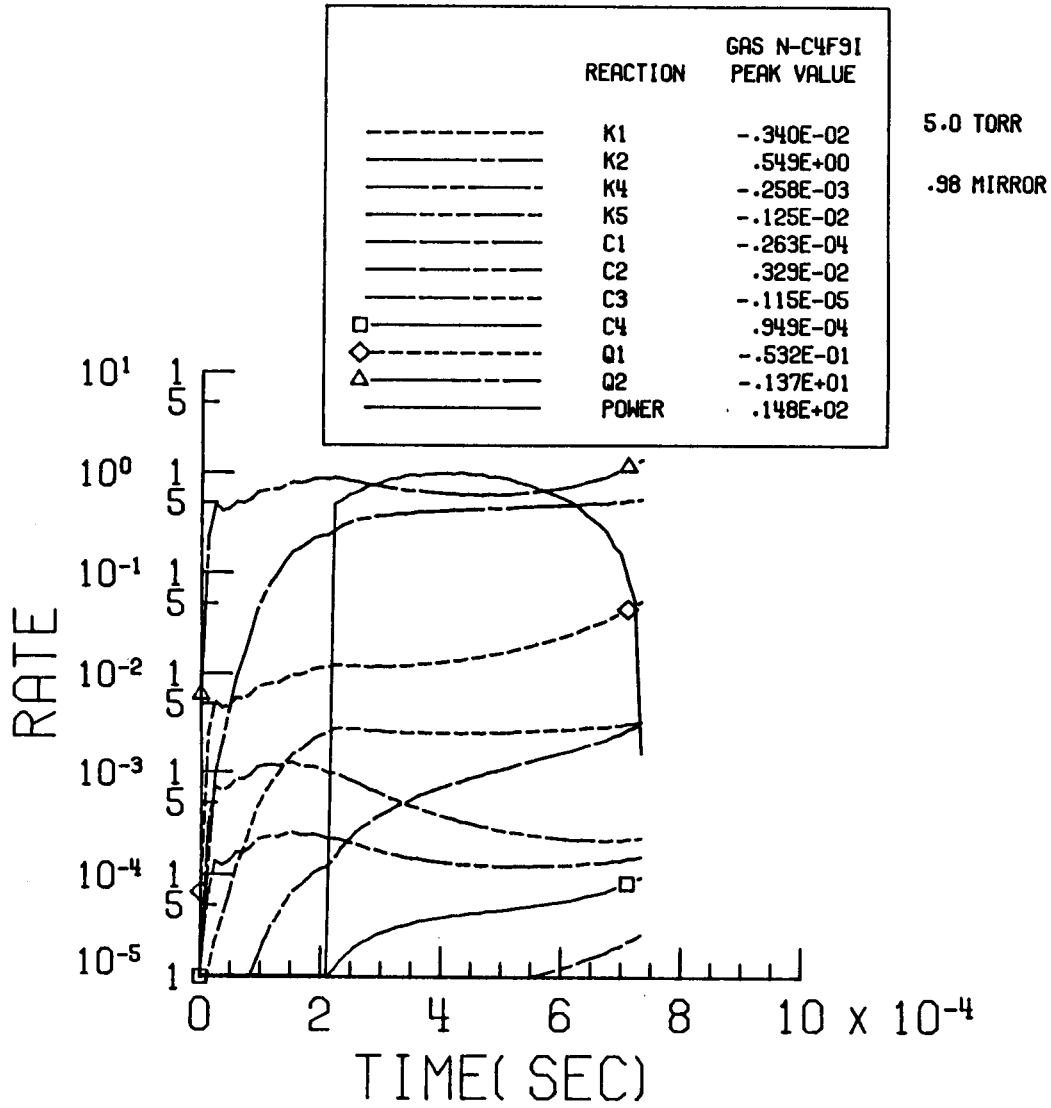
REACTION
GAS N-C4F9I PEAK VALUE
K1 -.340E-02
K2 .549E+00
K4 -.258E-03
K5 -.125E-02
C1 -.263E-04
C2 .329E-02
C3 -.115E-05
C4 .949E-04
Q1 -.532E-01
Q2 -.137E+01
POWER .148E+02
5.0 TORR
.98 MIRROR
RATE
10^{1}
10^{0}
10^{-1}
10^{-2}
10^{-3}
10^{-4}
10^{-5}
1/5
1
0 2 4 6 8 10 x 10^{-4}
TIME(SEC)

Figure 16

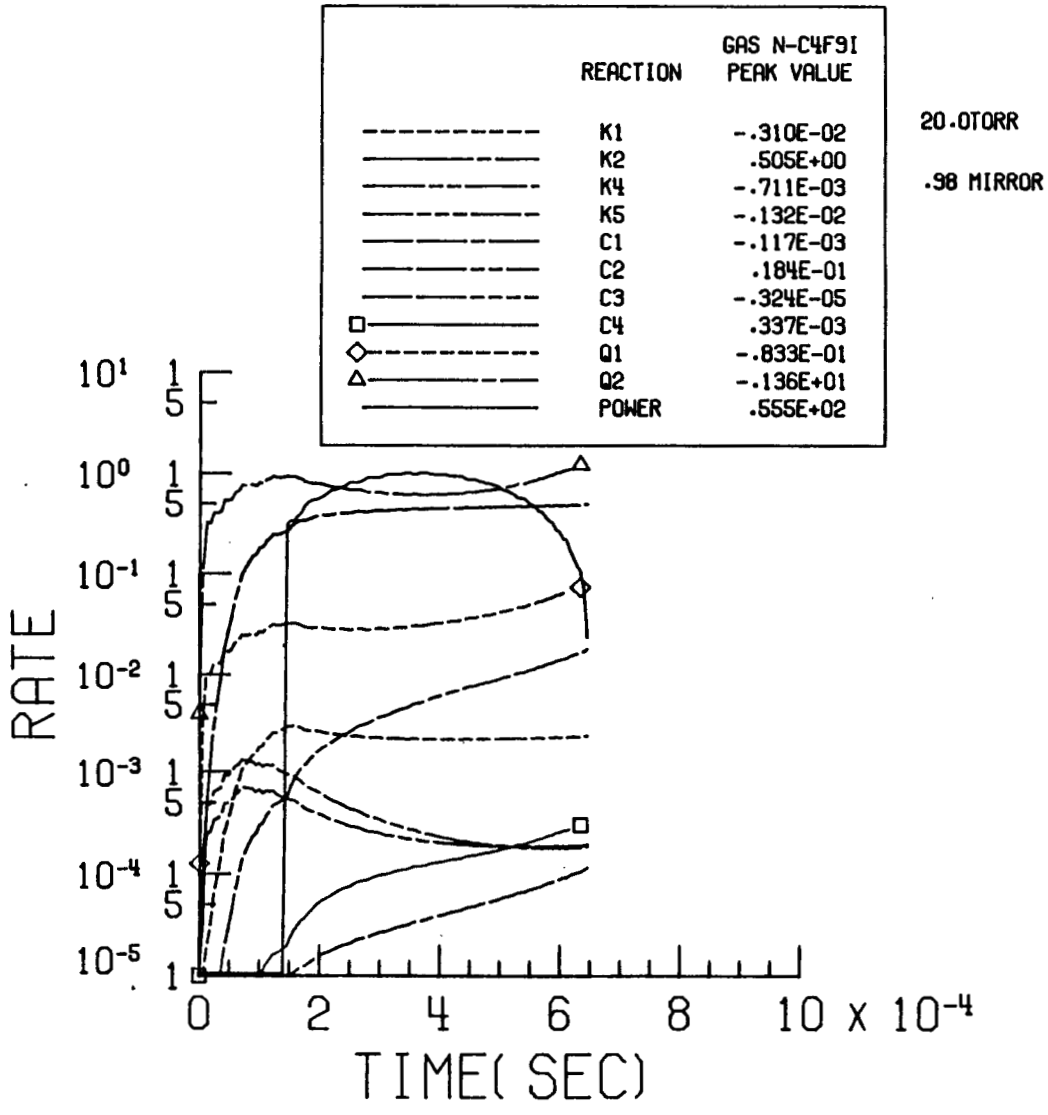
REACTION
GAS N-C4F9I PEAK VALUE
K1 -.310E-02
K2 .505E+00
K4 -.711E-03
K5 -.132E-02
C1 -.117E-03
C2 .184E-01
C3 -.324E-05
C4 .337E-03
Q1 -.833E-01
Q2 -.136E+01
POWER .555E+02
20.0TORR
.98 MIRROR
RATE
TIME(SEC)
0 2 4 6 8 10 X 10-4

Figure 17

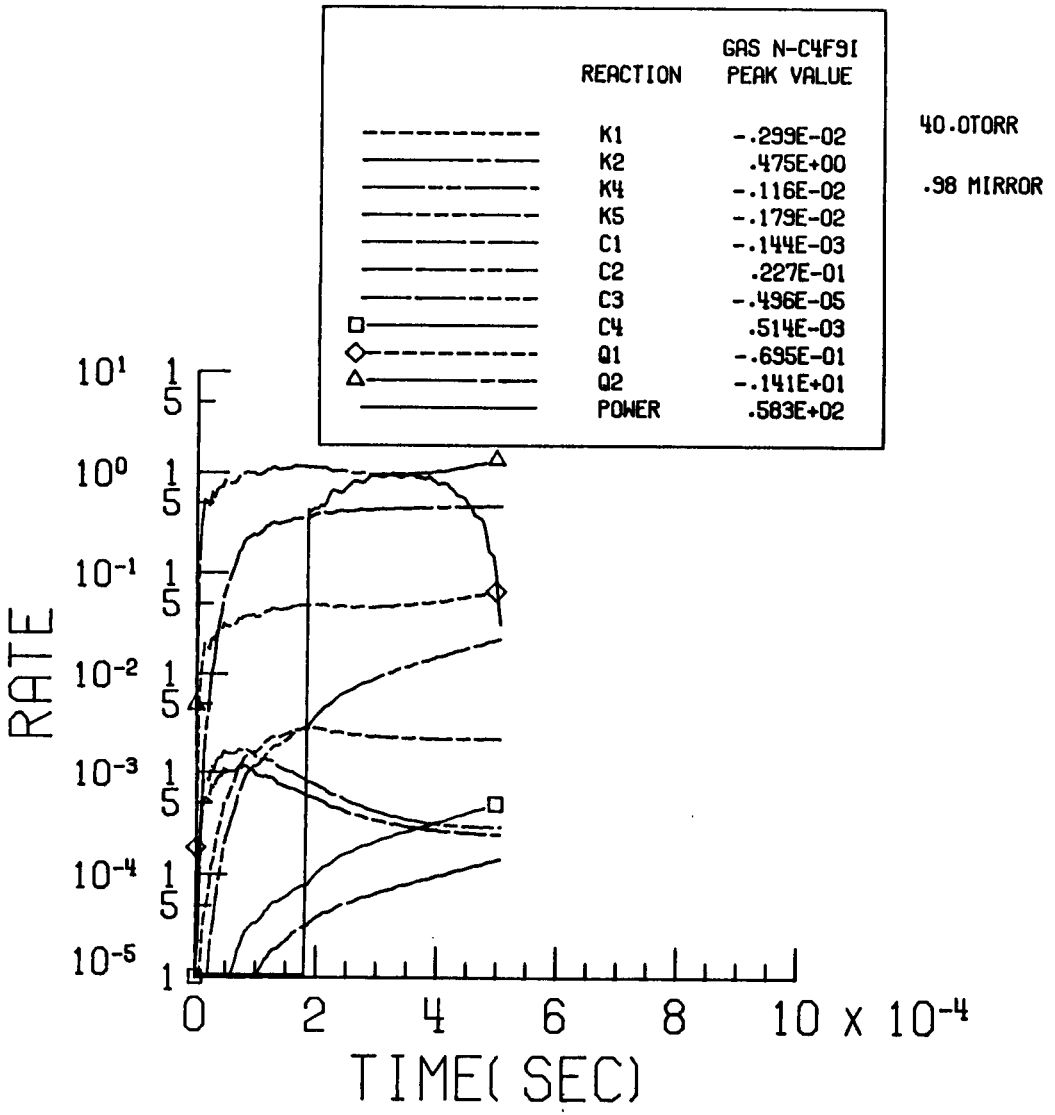
GAS N-C4F9I
REACTION
PEAK VALUE
K1 -.299E-02
K2 .475E+00
K4 -.116E-02
K5 -.179E-02
C1 -.144E-03
C2 .227E-01
C3 -.496E-05
C4 .514E-03
Q1 -.695E-01
Q2 -.141E+01
POWER .583E+02
40.0TORR
.98 MIRROR
RATE
TIME(SEC)
10 X 10-4

Figure 18

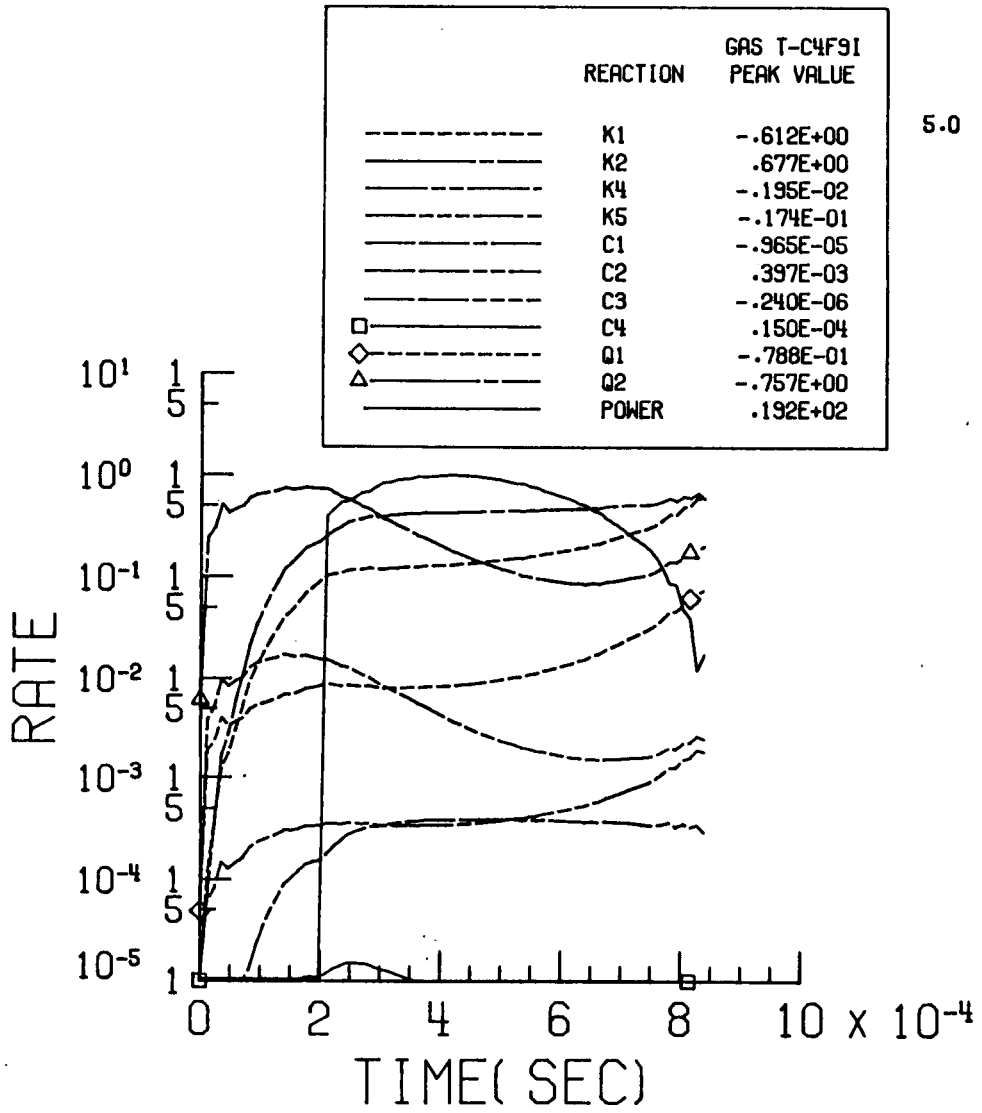
REACTION
GAS T-C4F9I PEAK VALUE
K1 -.612E+00
K2 .677E+00
K4 -.195E-02
K5 -.174E-01
C1 -.965E-05
C2 .397E-03
C3 -.240E-06
C4 .150E-04
Q1 -.788E-01
Q2 -.757E+00
POWER .192E+02
5.0 TORR
RATE
TIME(SEC)
0 2 4 6 8 10 x 10-4

Figure 19

END

DATE

OCT. 6, 1987

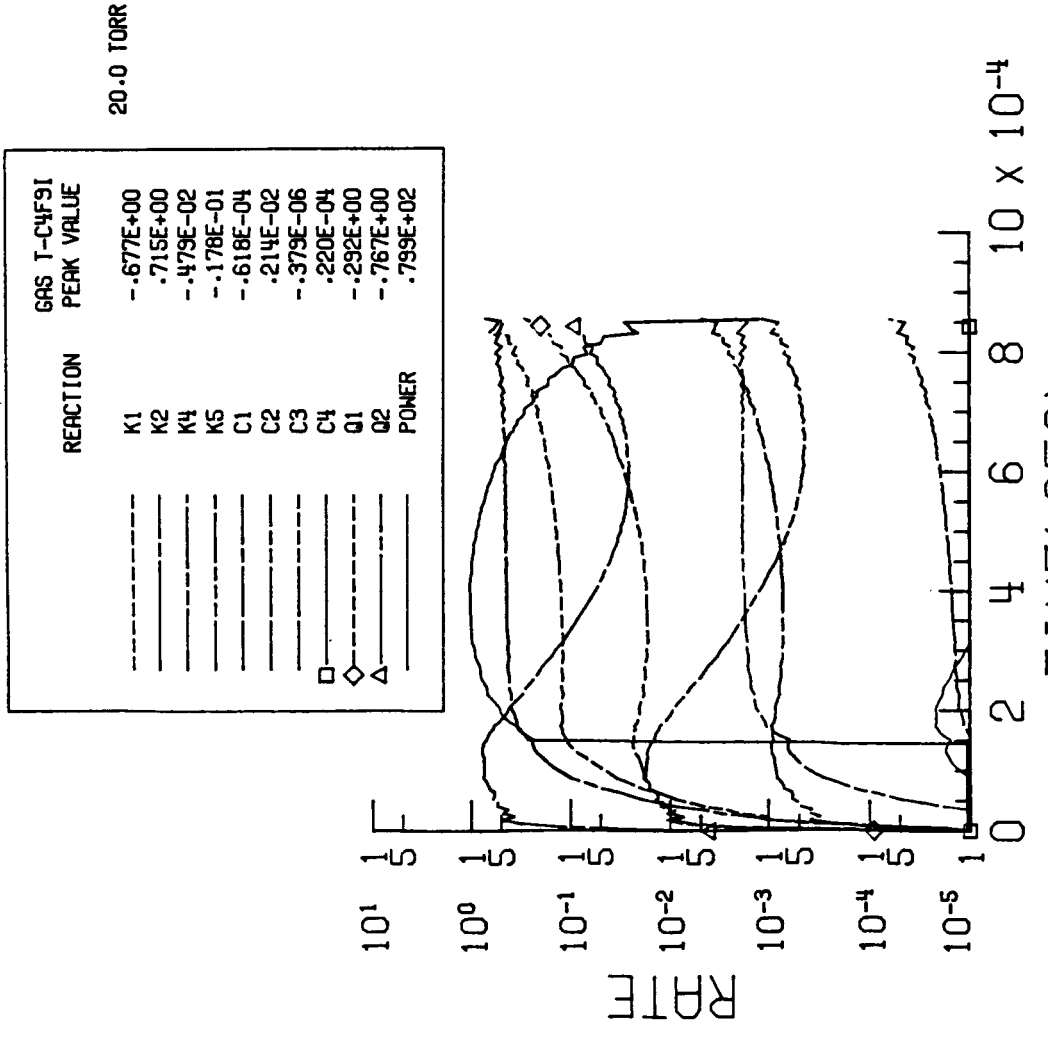

Figure 20

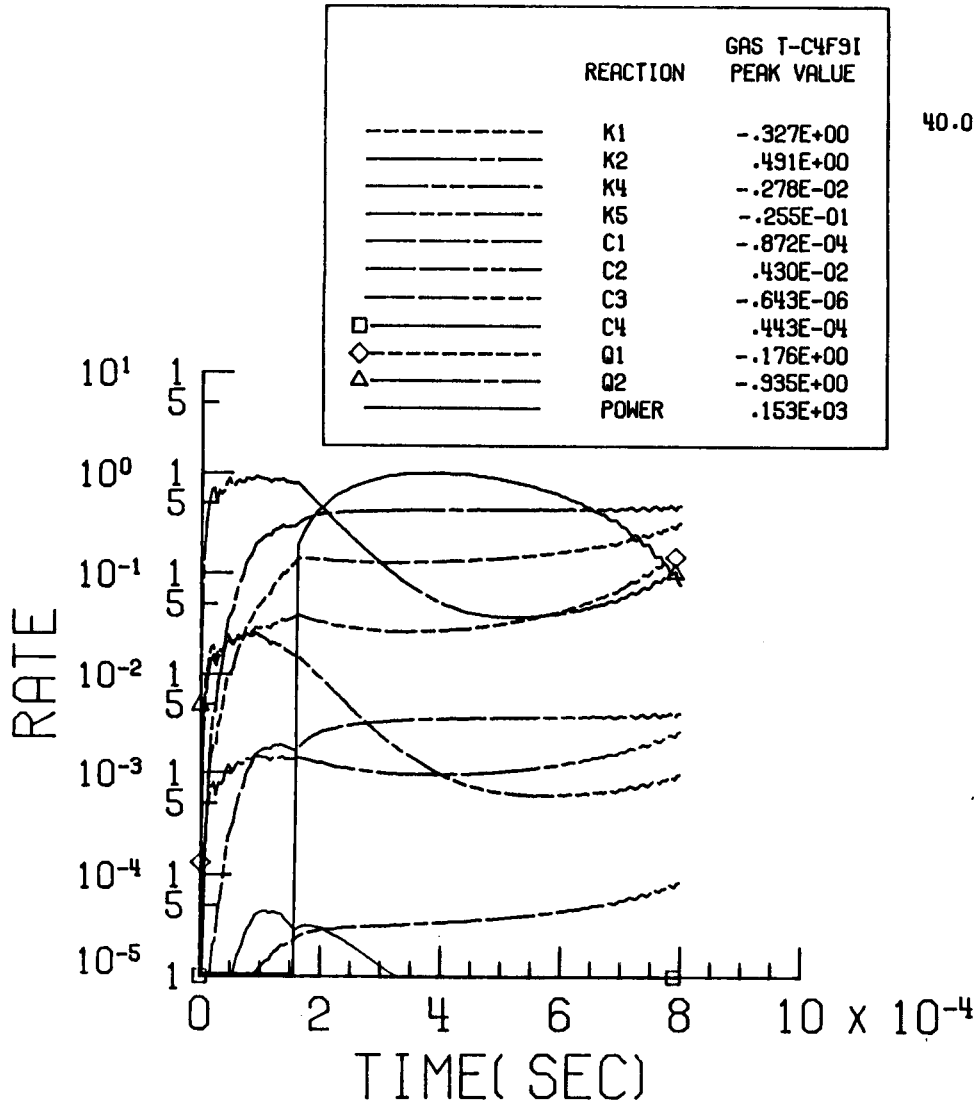
REACTION
GAS T-C4F9I PEAK VALUE
K1 -.327E+00
K2 .491E+00
K4 -.278E-02
K5 -.255E-01
C1 -.872E-04
C2 .430E-02
C3 -.643E-06
C4 .443E-04
Q1 -.176E+00
Q2 -.935E+00
POWER .153E+03
40.0 TORR
RATE
TIME(SEC)
10 X 10-4

Figure 21